Doctorate Dissertation

博士論文

Shortcuts to Adiabaticity Applied to Many-Body Systems
(多体系における断熱時間発展の加速)

Takuya Hatomura

鳩村 拓矢

Abstract

Adiabatic control of given systems is often utilized in a wide range of operation processes. It is known that such control can be robust with respect to various noises and errors. However, adiabatic control requires a long operation time and it often suffers from decoherence. Recently much attention has been paid to shortcuts to adiabaticity, which enable us to speedup adiabatic time evolution with keeping some robustness. In this thesis, we study application of shortcuts to adiabaticity to many-body systems. In particular, we consider two many-body systems, i.e., classical spin systems and bosonic Josephson junctions.

For generic classical spin systems, we show that shortcuts can be constructed without knowing their details. This is a significant feature of our method because knowledge of equal energy surfaces in phase space is usually required in shortcuts to adiabaticity for classical systems, which makes difficult to construct shortcuts in generic, or even specific, classical many-body systems. Counter-diabatic terms of generic classical spin systems are given by additional time-dependent external fields whose amplitude and directions are determined by their Hamiltonians. Our method can also be used as a method to systematically construct classical-approximate counter-diabatic terms for quantum spin systems and it could work well in semi-classical regimes. This feature is also significant because knowledge of energy eigenstates is usually required in shortcuts to adiabaticity for quantum systems and thus it is non-trivial to construct even approximate shortcuts. We demonstrate our method in a simple model and show fast stationary state tracking and influence of first order transitions and criticality. We also consider to apply our method to a classical model of quantum annealing.

On the other hand, for bosonic Josephson junctions, we propose an approximate shortcut. We adopt the Holstein-Primakoff transformation with $1/N$ expansion and the harmonic approximation. We construct counter-diabatic terms for bosonic Josephson junctions by using the counter-diabatic terms for a harmonic oscillator. The form of our approximate counter-diabatic terms is nothing but the two-axis counter-twisting Hamiltonian. We apply our approximate counter-diabatic terms to create a cat state in a bosonic Josephson junction. We show that some of diabatic changes during a generation process are suppressed and a cat state can be generated in a bosonic Josephson junction within a short time.

Acknowledgment

Publication list

Chapter 3 was mostly published in

- Takuya Hatomura and Takashi Mori: Shortcuts to adiabatic classical spin dynamics mimicking quantum annealing, *Physical Review E* **98** 032136 (2018).

Chapter 5 was mostly published in

- Takuya Hatomura: Shortcuts to adiabatic cat-state generation in bosonic Josephson junctions, *New Journal of Physics* **20** 015010 (2018); Invited paper for the special issue "Focus on Shortcuts to Adiabaticity".

Both of Chapter 3 and Chapter 5 were partly published in

- Takuya Hatomura: Shortcuts to Adiabaticity in the Infinite-Range Ising Model by Mean-Field Counter-Diabatic Driving, *Journal of the Physical Society of Japan* **86** 094002 (2017).

Contents

Chapter 1

Introduction

In this chapter, we introduce shortcuts to adiabaticity and associated concepts. First we review a current situation of quantum science and technologies and context of shortcuts to adiabaticity in Sec. 1.1. The scope and the structure of this thesis are also summarized. In Sec. 1.2, we introduce the concept of adiabaticity. We discuss counter-diabatic driving and Lewis-Riesenfeld invariant-based inverse engineering, which are representative methods of shortcuts to adiabaticity, in Sec. 1.3. Simple examples of shortcuts to adiabaticity, which are relevant to the present thesis, are demonstrated in Sec. 1.4.

1.1 Overview

1.1.1 Quantum science and technologies

Recently, much attention has been paid to quantum science and technologies stimulated by development of experimental techniques in these decades [1,2]. This movement toward developing quantum technologies has spread over from academias to industry and government. Their interest is not only in quantum computation but also in quantum simulation, quantum sensing and metrology, and other technologies benefiting by quantumness [1]. However, current status of quantum science and technologies is not close to the ideal, i.e., there are a lot of obstacles to benefit by quantumness. Therefore, our near term goal is to show evidence for advantage of quantumness by using noisy intermediate-scale quantum devices [2]. It is also important to clarify what we can do by using classical devices.

One of the most prominent commercial quantum technologies would be quantum annealers first developed by D-Wave Systems [3,4], which is one of the quantum simulators emulating quantum annealing [5]. They can be used to heuristically solve combinatorial optimization problems, which often appear when we consider practical social problems, and thus they fascinate a wide range of communities. Indeed, quantum annealers have already been applied to solve social problems, for example, job-shop scheduling [6], traffic flow optimization [7], air traffic control [8], and so on. However, it should be noted that it has been still unclear if quantum annealers really utilize quantumness effectively. It is also of great interest to utilize them as programmable quantum simulators for condensed matter physics [9,10]. In this direction, it might be possible to show advantage of quantumness with respect to classical technologies.

Another upcoming quantum technology would be quantum sensing and metrology [11–13]. Recent significant manufacturing technique enables us to design even atomic-scale devices. Such high precision manufacturing requires significantly accurate sensors. In quantum sensing and metrology, we seek for quantum-enhanced sensors overwhelming classical sensors. The limitation of accuracy to estimate unknown parameters by using classical sensors is known as the standard quantum limit, and thus quantum-enhanced sensors should overcome this limit [14–16]. Such high performance sensors can be realized in highly entangled probe states.

Among these quantum science and technologies, adiabaticity in quantum mechanics plays an important role. In particular, the theory of quantum annealing is mainly based on the adiabatic theorem [17], which ensures that a system remains to be adiabatic when parameters of the system vary slowly enough. Not

only that, but also adiabatic control of quantum states has a lot of benefits in other quantum science and technologies. In adiabatic control of quantum states, systems are confined around classical fixed points, which can be understood as bottoms of potential energy. Such control can lead to precise tailoring of quantum states in desired ways and also can be robust with respect to various errors. However, in contrast to stability against errors, adiabatic control often suffers from decoherence. This is because adiabatic control requires a long time in order to achieve target processing. As mentioned in the next section, shortcuts to adaibaticity [18] could be one of the candidates to overcome this drawback.

1.1.2 Shortcuts to adiabaticity

Shortcuts to adiabaticity offer strategies to speedup adiabatic time evolution, and thus those enable us to overcome a drawback of adiabatic control. Counter-diabatic driving, which is one of the methods of shortcuts to adiabaticity, was independently developed by Demirplak and Rice in 2003 [19, 20] and by Berry in 2009 [21]. In counter-diabatic driving, additional terms in Hamiltonians called counter-diabatic terms cancel diabatic transitions out, and thus systems behave as adiabatic, while they are actually non-adiabatic. In order to construct counter-diabatic terms, knowledge of energy spectra is usually required, and thus counter-diabatic driving was first applied to simple systems [18], for example, two- and three-level systems [19–22] and harmonic oscillators [23]. One of the breakthroughs in counter-diabatic driving was an extension to many-body systems. In particular, the counter-diabatic terms for quasi-free fermion systems, which include a wide range of quantum many-body systems, were found by del Campo *et al.* in 2012 [24]. Not only that but also effectiveness of truncating counter-diabatic terms, i.e., that of approximations in counter-diabatic terms, was shown. A systematic construction of approximate counter-diabatic terms for many-body systems without knowing their energy spectra was proposed by Sels and Polkovnikov in 2017 [25]. Counter-diabatic driving in classical systems and their relation to quantum cases are also of great interest. In scale-invariant systems, counter-diabatic terms for both classical and quantum cases can be obtained within an unified framework [26–28]. It is also possible to construct counter-diabatic terms for quantum many-body systems by using the knowledge of classical non-linear integrable systems [29]. Recently, counter-diabatic driving was extended to classical many-body spin systems by the present author Hatomura and Mori in 2018 [30], which can be also understood as the consequence of the mean-field approximation in quantum many-body spin systems, whereas the counter-diabatic terms are exact for classical many-body spin systems. It should be noted that the essence of the theoretical framework of counter-diabatic driving can be found in past literatures [31–33]. In particular, quantal and classical parallel transport discussed by Jarzynski in 1995 [31] actually produce adiabatic time evolution although their constructions are non-trivial. In other words, counter-diabatic driving is nothing but a systematic construction of Hamiltonians that generate quantal and classical parallel transport.

There are other approaches in shortcuts to adiabaticity. Another representative method is Lewis-Riesenfeld invariant-based inverse engineering developed by Chen *et al.* in 2010 [34], in which the Lewis-Riesenfeld theory of quantum mechanics plays an important role [35]. In Lewis-Riesenfeld invariant-based inverse engineering, populations in the eigenvectors of the Lewis-Riesenfeld invariants are conserved during time evolution, whereas populations in the eigenstates of the reference Hamiltonians are always conserved in counter-diabatic driving. We inversely design Hamiltonians in order to obtain desired results at the end. In other words, duration of time evolution in Lewis-Riesenfeld invariant-based inverse engineering is not identical to adiabatic time evolution, but the final result is identical to that of adiabatic time evolution. Nevertheless duration of time evolution and constructions are completely different, similarities (and also differences) between Lewis-Riesenfeld invariant-based inverse engineering and counter-diabatic driving have been pointed out [36].

Here we briefly review other approaches in shortcuts to adiabaticity, which are not discussed in this thesis. Fast forward scaling developed by Masuda and Nakamura in 2008 [37] is a method to accelerate any time evolution including adiabatic time evolution [38–40]. Fast forward scaling is realized by adding fast forward potentials, which are constructed by rescaling wave functions. Quantum adiabatic brachistochrone developed by Rezakhani *et al.* in 2009 [41, 42], which is an adiabatic version of a time optimizing brachistochrone approach [43, 44], is a method to suppress unwanted non-adiabatic transi-

tions. Such suppression is realized by optimizing a conditional expression of the adiabatic condition. Conventional optimal control theory [45] could also be viewed as a method of shortcuts to adiabaticity.

It is of great interest to apply these methods to quantum science and technologies. Indeed, a lot of such applications have been proposed and reported in this decade. A simple example would be to control internal states of small systems [46–53], which for example enables us to quickly and precisely manipulate each qubit [53]. Decompress (compress) of potentials trapping atoms without excitations would be also a simple and nice example [34, 54–64]. This application enables us to cool down (heat up) atomic systems without changing populations, and thus we could apply it to quantum heat engines [65–70]. Indeed, a large number of works on quantum heat engines associated with shortcuts to adiabaticity have been reported [55, 71–73]. Transport of trapped atomic gases with keeping populations was also considered [74–78], which could be used in order to connect two different processes. Another interesting example is fast wave-packet splitting without excitations [62, 79] because it could be applied to entanglement generation. Indeed, beyond the mean-field description, generation of entanglement via wave-packet splitting was proposed [80–82]. One would expect if shortcuts to adiabaticity can be applied to adiabatic quantum computation or quantum annealing. Indeed, some challenges have been done both in adiabatic quantum computation and quantum annealing. For adiabatic quantum computation, acceleration of some algorithms were proposed [83, 84]. In addition, fast implementation of gate operations and primitive quantum information processing were proposed [85–88]. For quantum annealing, some proposals have also been presented [30, 89–91].

Besides a number of works enumerated above, there are still a lot of follow-up concerning applications, fundamental frameworks, and methods combining some approaches [92–108].

1.1.3 Scope of this thesis

In this thesis, we study acceleration of adiabatic time evolution of many-body systems by using shortcuts to adiabaticity. In particular, we focus on two many-body systems, i.e., classical spin systems and bosonic Josephson junctions. In the former case, we show that the exact counter-diabatic terms for arbitrary classical spin systems, which enable us to track instantaneous stationary states within an arbitrary time, can be easily constructed without knowing tracked stationary states. We point out that this method can also be applied to solve combinatorial optimization problems by considering a classical model of quantum annealing. In the latter case, we show a construction of approximate counter-diabatic terms for bosonic Josephson junctions. We demonstrate that this approximate method can successfully suppress some of diabatic transitions to highly excited states and it can be used to generate macroscopically entangled states.

Structure of this thesis

In the rest of the present chapter, in Chapter 1, we introduce the concept of adiabaticity and two representative methods of shortcuts to adiabaticity, i.e., counter-diabatic driving and Lewis-Riesenfeld invariant-based inverse engineering. We also show some basic examples of shortcuts to adiabaticity, which are relevant to the present thesis.

Chapter 2 is devoted to a review of quantum annealing, which is one of the applications based on adiabatic time evolution. After introducing the theory of quantum annealing, we discuss classical algorithms, which enable us to implement quantum annealing by using classical computers. We also discuss the previous work concerning shortcuts to adiabaticity for quantum annealing.

In Chapter 3, based on the papers by the present author [30, 109], we discuss shortcuts to adiabaticity for classical spin systems. We introduce classical spin dynamics and the concept of stationary states and criticality. We construct counter-diabatic terms for classical spin systems and explain how to track stationary states without knowing them. We demonstrate our method in a simple model and apply it to a classical model of quantum annealing.

In Chapter 4, we introduce the concept of macroscopic entanglement. We discuss macroscopic entanglement in collective spin systems, and as an example of collective spin systems, we introduce bosonic Josephson junctions. We mention how to generate a macroscopically entangled state in bosonic Josephson junctions. We also introduce counter-diabatic terms for bosonic Josephson junctions developed in

the previous work.

In Chapter 5, based on the papers by the present author [82,109], we discuss shortcuts to adiabaticity for bosonic Josephson junctions. In order to cross the critical point, we consider finite-size corrections in counter-diabatic terms. We discuss acceleration of adiabatic generation of macroscopic entanglement in bosonic Josephson junctions.

In Chapter 6, we summarize this thesis and discuss perspectives.

Here we show the flowchart of this thesis in Fig. 1.1. Each solid arrow represents a flow of discussion and the dashed arrow indicates inessential relationship.
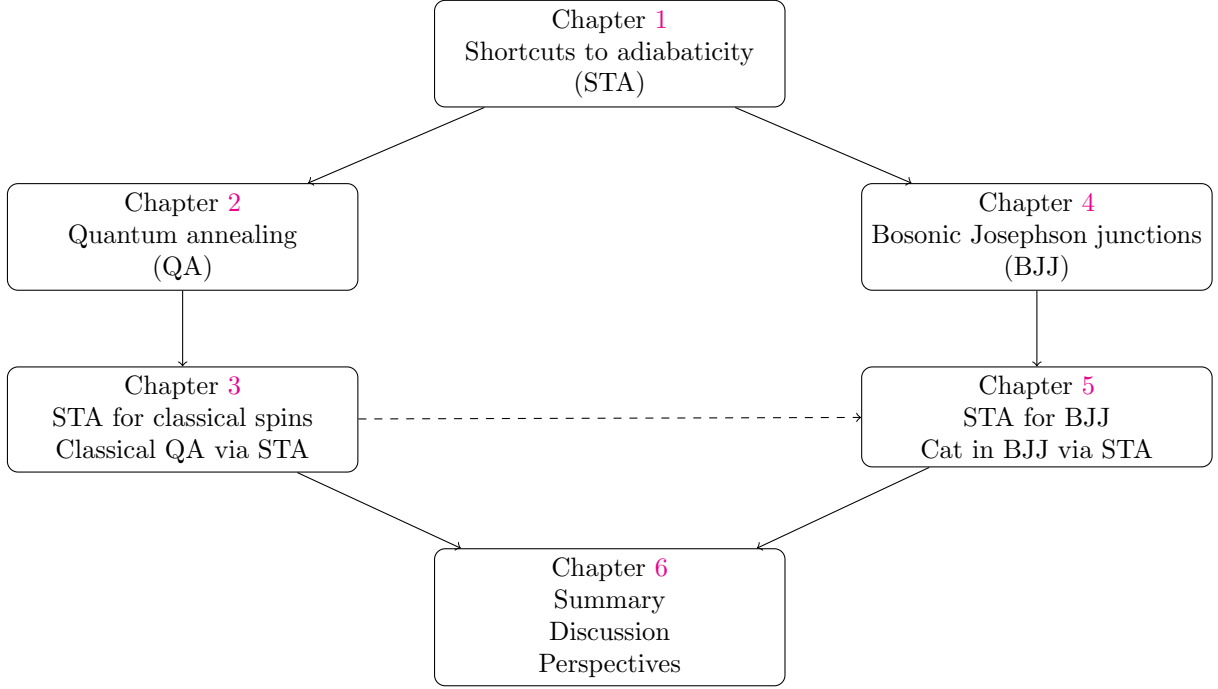
Figure1.1   Flowchart of this thesis.

1.2 Adiabaticity

1.2.1 Adiabatic time evolution

In this section, we introduce basic concepts of adiabaticity in quantum mechanics. In particular, we introduce the dynamical transformation, which corresponds to usual unitary time evolution, and the adiabatic transformation, which corresponds to adiabatic time evolution. We mention that these two transformations are bridged by the adiabatic theorem and the adiabatic condition.

We consider a state $|\psi(t)\rangle$ under a time-dependent Hamiltonian $\hat{\mathcal{H}}(\boldsymbol{\lambda};t)$. Here, $\boldsymbol{\lambda}(t) = (\lambda_1, \lambda_2, \cdots ;t)$ specifies a point in parameter space at time t and the Hamiltonian $\hat{\mathcal{H}}(\boldsymbol{\lambda};t)$ depends on time through the parameter $\boldsymbol{\lambda}(t)$. Time evolution of this system is governed by the Schrödinger equation

$$i\hbar\frac{\partial}{\partial t}|\psi(t)\rangle = \hat{\mathcal{H}}(\boldsymbol{\lambda};t)|\psi(t)\rangle. \tag{1.1}$$

We introduce a time evolution operator

$$\hat{U}_D(t) = \mathcal{T}\exp\left[-\frac{i}{\hbar}\int_0^t dt'\hat{\mathcal{H}}(\boldsymbol{\lambda};t')\right], \tag{1.2}$$

which generates the Schrödinger dynamics

$$|\psi(t)\rangle = \hat{U}_D(t)|\psi(0)\rangle. \tag{1.3}$$

We call this time evolution operator $\hat{U}_D(t)$ the dynamical transformation.

Next, we consider the spectrum decomposition of the Hamiltonian

$$\hat{\mathcal{H}}(\boldsymbol{\lambda};t) = \sum_n E_n(\boldsymbol{\lambda};t)\hat{P}_n(\boldsymbol{\lambda};t), \tag{1.4}$$

where $E_n(\boldsymbol{\lambda};t)$ is the nth energy eigenvalue and $\hat{P}_n(\boldsymbol{\lambda};t)$ is the projection operator onto the associated energy eigenspace. Here, $\hat{P}_n(\boldsymbol{\lambda};t)$ satisfies the complete orthonormal condition

$$\hat{P}_n(\boldsymbol{\lambda};t)\hat{P}_m(\boldsymbol{\lambda};t) = \delta_{nm}\hat{P}_n(\boldsymbol{\lambda};t), \quad \sum_n \hat{P}_n(\boldsymbol{\lambda};t) = \hat{1}. \tag{1.5}$$

We introduce a time evolution operator $\hat{U}_A(t)$ that isometrically transforms the projection operators

$$\hat{P}_n(\boldsymbol{\lambda};t) = \hat{U}_A(t)\hat{P}_n(\boldsymbol{\lambda};0)\hat{U}_A^\dagger(t). \tag{1.6}$$

Time evolution operator $\hat{U}_A(t)$ generates adiabatic time evolution

$$|\psi_{\mathrm{ad}}(t)\rangle = \hat{U}_A(t)|\psi(0)\rangle, \tag{1.7}$$

which conserves the probability distribution of the energy eigenstates

$$\langle\psi_{\mathrm{ad}}(t)|\hat{P}_n(\boldsymbol{\lambda};t)|\psi_{\mathrm{ad}}(t)\rangle = \langle\psi(0)|\hat{P}_n(\boldsymbol{\lambda};0)|\psi(0)\rangle, \tag{1.8}$$

and thus we call this time evolution operator $\hat{U}_A(t)$ the adiabatic transformation (see Appendix A.1 for details).

The adiabatic theorem [17] implies that the dynamical transformation $\hat{U}_D(t)$ and the adiabatic transformation $\hat{U}_A(t)$ coincide when change of the Hamiltonian in time, $||(d/dt)\hat{\mathcal{H}}(\boldsymbol{\lambda};t)|| = ||(d\boldsymbol{\lambda}/dt)\cdot\partial_{\boldsymbol{\lambda}}\hat{\mathcal{H}}(\boldsymbol{\lambda};t)||$, is sufficiently small. Indeed, we can show the relation

$$|\psi(t)\rangle - |\psi_{\mathrm{ad}}(t)\rangle = [\hat{U}_D(t) - \hat{U}_A(t)]|\psi(0)\rangle = \mathcal{O}(d\boldsymbol{\lambda}/dt), \tag{1.9}$$

and thus they coincide except for phase factors when $|d\boldsymbol{\lambda}/dt| \ll 1$ (see Appendix A.2 for a proof). We can regard the dynamical transformation as the adiabatic transformation if the following adiabatic condition

$$\hbar\left|\frac{d\boldsymbol{\lambda}}{dt} \cdot \frac{\langle n(\boldsymbol{\lambda};t)|\partial_{\boldsymbol{\lambda}}m(\boldsymbol{\lambda};t)\rangle}{E_m(\boldsymbol{\lambda};t) - E_n(\boldsymbol{\lambda};t)}\right| \ll 1, \tag{1.10}$$

or equivalently,

$$\hbar\left|\frac{d\boldsymbol{\lambda}}{dt} \cdot \frac{\langle n(\boldsymbol{\lambda};t)|(\partial_{\boldsymbol{\lambda}}\hat{\mathcal{H}}(\boldsymbol{\lambda};t))|m(\boldsymbol{\lambda};t)\rangle}{(E_m(\boldsymbol{\lambda};t) - E_n(\boldsymbol{\lambda};t))^2}\right| \ll 1, \tag{1.11}$$

holds [110] (see Appendix A.3 for details).

1.2.2 Geometric phases accompanying adiabatic time evolution

In Sec. 1.2.1, we introduced adiabatic time evolution, but it still leaves room for discussion about a phase factor during adiabatic time evolution. Here we introduce the Berry phase that accompanies adiabatic time evolution [111, 112]. First, we assume that a time-dependent Hamiltonian $\hat{\mathcal{H}}(\boldsymbol{\lambda};t)$ has no degeneracy during time evolution, but later we will extend to a time-dependent Hamiltonian $\hat{\mathcal{H}}(\boldsymbol{\lambda};t)$ that has degeneracies but no level crossing [113].

Suppose that the initial state is given by the nth energy eigenstate $|n(\boldsymbol{\lambda};t)\rangle$ of a Hamiltonian $\hat{\mathcal{H}}(\boldsymbol{\lambda};t)$ at time $t = 0$. If the Hamiltonian varies slowly in time and the adiabatic condition is satisfied, the adiabatic theorem implies that the state is proportional to $|n(\boldsymbol{\lambda};t)\rangle$ at time t. We assume that the state at time t is given by

$$|\psi(t)\rangle = \exp\left[-\frac{i}{\hbar}\int_0^t dt' E_n(\boldsymbol{\lambda};t')\right]\exp[i\gamma_n(t)]|n(\boldsymbol{\lambda};t)\rangle, \tag{1.12}$$

where the first phase factor is the dynamical phase, which can be intuitively understood from the Schrödinger equation, and the second phase factor $\gamma_n(t)$ is an additional phase factor, which we will discuss in this section. Time evolution of the state is governed by the Schrödinger equation, and thus $\gamma_n(t)$ should satisfy the following differential equation

$$\frac{d\gamma_n}{dt} = i\frac{d\boldsymbol{\lambda}}{dt} \cdot \langle n(\boldsymbol{\lambda};t)|\partial_{\boldsymbol{\lambda}}n(\boldsymbol{\lambda};t)\rangle, \tag{1.13}$$

i.e., $\gamma_n(t)$ is given by

$$\gamma_n(t) = i\int_{\mathcal{C}}\langle n(\boldsymbol{\lambda};t)|\partial_{\boldsymbol{\lambda}}n(\boldsymbol{\lambda};t)\rangle \cdot d\boldsymbol{\lambda}, \tag{1.14}$$

where $\mathcal{C}$ is a path in parameter space. Note that this phase factor does not make sense unless a given path $\mathcal{C}$ is a closed loop. This is because gauge transformation

$$|n(\boldsymbol{\lambda};t)\rangle \rightarrow \exp[i\mu_n(\boldsymbol{\lambda};t)]|n(\boldsymbol{\lambda};t)\rangle, \tag{1.15}$$

leads the integrand of Eq. (1.14) to

$$\langle n(\boldsymbol{\lambda};t)|\partial_{\boldsymbol{\lambda}}n(\boldsymbol{\lambda};t)\rangle \rightarrow \langle n(\boldsymbol{\lambda};t)|\partial_{\boldsymbol{\lambda}}n(\boldsymbol{\lambda};t)\rangle + i\frac{\partial}{\partial\boldsymbol{\lambda}}\mu_n(\boldsymbol{\lambda};t), \tag{1.16}$$

and thus $\gamma_n(t)$ has gauge degree of freedom. In contrast, gauge-dependence of $\gamma_n(t)$ disappears when a given path $\mathcal{C}$ is a closed loop, and then $\gamma_n(t)$ reflects geometric properties of a state on parameter space. Hereafter we consider open paths in the parameter space, and thus we can arbitrarily choose a phase factor.

Now we extend above discussion to a system that has degeneracies but no level crossing. The nth energy eigenstate is expressed as $|n, \mu(\boldsymbol{\lambda};t)\rangle$, where an additional index μ represents degeneracies. Suppose that the initial state is given by a state in the nth energy subspace, i.e., $\sum_{\mu} c_{\mu}^{(n)}(t)|n, \mu(\lambda;t)\rangle$ at time $t = 0$, where $c_{\mu}^{(n)}(t)$ gives a distribution of energy eigenstates. If change of the Hamiltonian in time is slow enough, then the state at time t is given by

$$|\psi(t)\rangle = \exp\left[-\frac{i}{\hbar}\int_0^t dt' E_n(\boldsymbol{\lambda};t')\right]\sum_{\mu} c_{\mu}^{(n)}(t)|n, \mu(\boldsymbol{\lambda};t)\rangle. \tag{1.17}$$

Here, we expect that the coefficient $c_{\mu}^{(n)}(t)$ has a similar phase factor to the Berry phase. Because this state obeys the Schrödinger equation, $c_{\nu}^{(n)}(t)$ satisfies the following differential equation

$$\frac{d}{dt}c_{\mu}^{(n)}(t) + \frac{d\boldsymbol{\lambda}}{dt} \cdot \sum_{\nu} c_{\nu}^{(n)}(t)\langle n, \mu(\boldsymbol{\lambda};t)|\partial_{\boldsymbol{\lambda}}n, \nu(\boldsymbol{\lambda};t)\rangle = 0, \tag{1.18}$$

and thus it can be formally solved as

$$c_{\mu}^{(n)}(t) = \sum_{\nu} U_{\mu\nu}^{(n)}(t)c_{\nu}^{(n)}(0), \tag{1.19}$$

where $U_{\mu\nu}^{(n)}(t)$ is the matrix element of

$$\hat{U}^{(n)}(t) = \mathcal{T}\exp\left[\frac{i}{\hbar}\int_0^t dt' \hat{A}^{(n)}(t')\right]. \tag{1.20}$$

Here, $\hat{A}^{(n)}(t)$ is a non-Abelian gauge field, which is generalization of the Berry phase, and its matrix element is given by

$$A_{\mu\nu}^{(n)}(t) = i\hbar \frac{d\boldsymbol{\lambda}}{dt} \cdot \langle n, \mu(\boldsymbol{\lambda}; t)|\partial_{\boldsymbol{\lambda}} n, \nu(\boldsymbol{\lambda}; t)\rangle. \tag{1.21}$$

This non-Abelian gauge field also shows similar properties to the Berry phase.

1.2.3 Generator of adiabatic time evolution

In this section, we introduce the concept of the generator of adiabatic time evolution according to Jarzynski [31].

We consider a generator $\hat{\boldsymbol{\xi}}(\boldsymbol{\lambda}; t)$ that generates small displacement of the adiabatic transformation $|\delta\psi_{\mathrm{ad}}(t)\rangle$ associated with small displacement of a parameter $\delta\boldsymbol{\lambda}$, i.e., the following equation

$$i\hbar|\delta\psi_{\mathrm{ad}}(t)\rangle = \delta\boldsymbol{\lambda} \cdot \hat{\boldsymbol{\xi}}(\boldsymbol{\lambda}; t)|\psi_{\mathrm{ad}}(t)\rangle, \tag{1.22}$$

or equivalently

$$i\hbar\frac{\partial}{\partial t}|\psi_{\mathrm{ad}}(t)\rangle = \frac{d\boldsymbol{\lambda}}{dt} \cdot \hat{\boldsymbol{\xi}}(\boldsymbol{\lambda}; t)|\psi_{\mathrm{ad}}(t)\rangle, \tag{1.23}$$

holds. Now we assume that $|\psi_{\mathrm{ad}}(t)\rangle$ is given by a single energy eigenstate $|n(\boldsymbol{\lambda}; t)\rangle$. By differentiating the equality

$$\hat{\mathcal{H}}(\boldsymbol{\lambda}; t)|n(\boldsymbol{\lambda}; t)\rangle = E_n(\boldsymbol{\lambda}; t)|n(\boldsymbol{\lambda}; t)\rangle, \tag{1.24}$$

by $\boldsymbol{\lambda}$, we obtain

$$i\hbar\frac{\partial}{\partial\boldsymbol{\lambda}}(\hat{\mathcal{H}}(\boldsymbol{\lambda}; t)|n(\boldsymbol{\lambda}; t)\rangle) = i\hbar\left(\frac{\partial}{\partial\boldsymbol{\lambda}}\hat{\mathcal{H}}(\boldsymbol{\lambda}; t)\right)|n(\boldsymbol{\lambda}; t)\rangle + \hat{\mathcal{H}}(\boldsymbol{\lambda}; t)\hat{\boldsymbol{\xi}}(\boldsymbol{\lambda}; t)|n(\boldsymbol{\lambda}; t)\rangle, \tag{1.25}$$

from the left-hand side and

$$i\hbar\frac{\partial}{\partial\boldsymbol{\lambda}}(E_n(\boldsymbol{\lambda}; t)|n(\boldsymbol{\lambda}; t)\rangle) = i\hbar\left(\frac{\partial}{\partial\boldsymbol{\lambda}}E_n(\boldsymbol{\lambda}; t)\right)|n(\boldsymbol{\lambda}; t)\rangle + \hat{\boldsymbol{\xi}}(\boldsymbol{\lambda}; t)\hat{\mathcal{H}}(\boldsymbol{\lambda}; t)|n(\boldsymbol{\lambda}; t)\rangle, \tag{1.26}$$

from the right-hand side. Therefore, we obtain the commutation relation between the Hamiltonian $\hat{\mathcal{H}}(\boldsymbol{\lambda}; t)$ and the generator $\hat{\boldsymbol{\xi}}(\boldsymbol{\lambda}; t)$ as

$$[\hat{\boldsymbol{\xi}}(\boldsymbol{\lambda}; t), \hat{\mathcal{H}}(\boldsymbol{\lambda}; t)] = i\hbar\left(\frac{\partial}{\partial\boldsymbol{\lambda}}\hat{\mathcal{H}}(\boldsymbol{\lambda}; t) - \hat{\boldsymbol{D}}(\boldsymbol{\lambda}; t)\right), \tag{1.27}$$

where $\hat{\boldsymbol{D}}(\boldsymbol{\lambda}; t)$ is the diagonal matrix of $[\partial_{\boldsymbol{\lambda}}\hat{\mathcal{H}}(\boldsymbol{\lambda}; t)]$, i.e., it satisfies

$$\langle m(\boldsymbol{\lambda}; t)|\hat{\boldsymbol{D}}(\boldsymbol{\lambda}; t)|n(\boldsymbol{\lambda}; t)\rangle = \langle m(\boldsymbol{\lambda}; t)|(\partial_{\boldsymbol{\lambda}}\hat{\mathcal{H}}(\boldsymbol{\lambda}; t))|n(\boldsymbol{\lambda}; t)\rangle\delta_{mn}. \tag{1.28}$$

From these equations, we could find the generator of adiabatic time evolution in principle. Note that we call this generation of adiabatic time evolution the quantal parallel transport.

1.2.4 Adiabaticity in classical mechanics

In order to discuss adiabaticity in quantum mechanics, the energy spectrum of a given Hamiltonian are of importance as seen in Sec. 1.2.1. In contrast, energy in classical mechanics can take a continuous value, and thus we cannot apply the discussion in Sec. 1.2.1 to classical systems. In this section, we introduce adiabaticity in classical mechanics by analogy of discussion in Sec. 1.2.3 according to Jarzynski [31].

A classical state is given by a point in phase space

$$z(\boldsymbol{\lambda}; t) = (\{q_i(\boldsymbol{\lambda}; t), p_i(\boldsymbol{\lambda}; t)\}), \tag{1.29}$$

where $\{q_i(\boldsymbol{\lambda}; t), p_i(\boldsymbol{\lambda}; t)\}$ is a set of canonical variables depending on a temporal parameter $\boldsymbol{\lambda}(t)$. By analogy of Eq. (1.23), a classical generator $\boldsymbol{\xi_\lambda}(z)$ would define adiabatic time evolution in classical mechanics as

$$\frac{dz_{\mathrm{ad}}}{dt} = \frac{d\boldsymbol{\lambda}}{dt} \cdot \{z_{\mathrm{ad}}(\boldsymbol{\lambda}; t), \boldsymbol{\xi_\lambda}(z_{\mathrm{ad}})\}, \tag{1.30}$$

where $z_{\mathrm{ad}}(\boldsymbol{\lambda}; t)$ is adiabatic time evolution in classical mechanics and $\{\cdot, \cdot\}$ is the Poisson bracket. This classical generator should satisfy classical counterpart of Eq. (1.27), i.e., by introducing the classical Hamiltonian $\mathcal{H_\lambda}(z)$, it should satisfy

$$\{\boldsymbol{\xi_\lambda}(z_{\mathrm{ad}}), \mathcal{H_\lambda}(z_{\mathrm{ad}})\} = \partial_{\boldsymbol{\lambda}}\mathcal{H_\lambda}(z_{\mathrm{ad}}) - \langle\partial_{\boldsymbol{\lambda}}\mathcal{H_\lambda}(z)\rangle_{\mathcal{H_\lambda}(z_{\mathrm{ad}})}. \tag{1.31}$$

Here, $\langle\cdot\rangle_E$ is an expectation value averaged over an equal energy surface

$$\langle\cdot\rangle_E = \left(\frac{\partial\Omega_{\boldsymbol{\lambda}}}{\partial E}\right)^{-1} \int dz \cdot \delta(E - \mathcal{H_\lambda}(z)), \tag{1.32}$$

where $\Omega_{\boldsymbol{\lambda}}$ is volume of phase space enclosed by an equal energy surface

$$\Omega_{\boldsymbol{\lambda}}(E) = \int dz\theta(E - \mathcal{H_\lambda}(z)). \tag{1.33}$$

In order to characterize this time evolution z_{ad}, and also to show that this is actually classical adiabatic time evolution, we introduce the adiabatic invariant

$$\omega_{\boldsymbol{\lambda}}(z) = \Omega_{\boldsymbol{\lambda}}(\mathcal{H_\lambda}) = \int dz'\theta(\mathcal{H_\lambda}(z) - \mathcal{H_\lambda}(z')) \tag{1.34}$$

which is conserved during adiabatic time evolution, i.e., it should satisfy

$$\frac{d}{dt}\omega_{\boldsymbol{\lambda}}(z_{\mathrm{ad}}) = 0. \tag{1.35}$$

Indeed, we can show it as follows. First, by differentiating the adiabatic invariant $\omega_{\boldsymbol{\lambda}}(z)$ by a temporal parameter $\boldsymbol{\lambda}$, we obtain

$$\begin{aligned}\partial_{\boldsymbol{\lambda}}\omega_{\boldsymbol{\lambda}}(z) &= \int dz'(\partial_{\boldsymbol{\lambda}}\mathcal{H_\lambda}(z) - \partial_{\boldsymbol{\lambda}}\mathcal{H_\lambda}(z'))\delta(\mathcal{H_\lambda}(z) - \mathcal{H_\lambda}(z')) \\ &= \left(\frac{\partial\Omega_{\boldsymbol{\lambda}}}{\partial\mathcal{H_\lambda}}\right)(\partial_{\boldsymbol{\lambda}}\mathcal{H_\lambda}(z) - \langle\partial_{\boldsymbol{\lambda}}\mathcal{H_\lambda}(z')\rangle_{\mathcal{H_\lambda}(z)}).\end{aligned} \tag{1.36}$$

We also calculate the following Poisson bracket as

$$\begin{aligned}\{\boldsymbol{\xi_\lambda}(z), \omega_{\boldsymbol{\lambda}}(z)\} &= \{\boldsymbol{\xi_\lambda}(z), \Omega_{\boldsymbol{\lambda}}(\mathcal{H_\lambda})\} \\ &= \left(\frac{\partial\Omega_{\boldsymbol{\lambda}}}{\partial\mathcal{H_\lambda}}\right)\{\boldsymbol{\xi_\lambda}(z), \mathcal{H_\lambda}(z)\}.\end{aligned} \tag{1.37}$$

Then, from Eq. (1.31), Eqs. (1.36) and (1.37) lead to

$$\{\boldsymbol{\xi_\lambda}(z_{\mathrm{ad}}), \omega_{\boldsymbol{\lambda}}(z_{\mathrm{ad}})\} = \partial_{\boldsymbol{\lambda}}\omega_{\boldsymbol{\lambda}}(z_{\mathrm{ad}}). \tag{1.38}$$

Besides, Eq. (1.30) implies

$$\begin{cases}\dfrac{dq_{\mathrm{ad}}}{dt} = \dfrac{d\boldsymbol{\lambda}}{dt} \cdot \dfrac{\partial\boldsymbol{\xi_\lambda}(z_{\mathrm{ad}})}{\partial p_{\mathrm{ad}}}, \\[2mm] \dfrac{dp_{\mathrm{ad}}}{dt} = -\dfrac{d\boldsymbol{\lambda}}{dt} \cdot \dfrac{\partial\boldsymbol{\xi_\lambda}(z_{\mathrm{ad}})}{\partial q_{\mathrm{ad}}},\end{cases} \tag{1.39}$$

where $z_{\mathrm{ad}} = (q_{\mathrm{ad}}, p_{\mathrm{ad}})$, and thus we have

$$\frac{\partial \omega_{\boldsymbol{\lambda}}(z_{\mathrm{ad}})}{\partial z_{\mathrm{ad}}} \frac{dz_{\mathrm{ad}}}{dt} = \frac{d\boldsymbol{\lambda}}{dt} \cdot \{\omega_{\boldsymbol{\lambda}}(z_{\mathrm{ad}}), \boldsymbol{\xi}_{\boldsymbol{\lambda}}(z_{\mathrm{ad}})\}. \tag{1.40}$$

Therefore, from Eqs. (1.38) and (1.40), we obtain

$$\begin{aligned} \frac{d}{dt}\omega_{\boldsymbol{\lambda}}(z_{\mathrm{ad}}) =& \frac{d\boldsymbol{\lambda}}{dt} \cdot \partial_{\boldsymbol{\lambda}}\omega_{\boldsymbol{\lambda}}(z_{\mathrm{ad}}) + \frac{\partial \omega_{\boldsymbol{\lambda}}(z_{\mathrm{ad}})}{\partial z_{\mathrm{ad}}} \frac{dz_{\mathrm{ad}}}{dt} \\ =& \frac{d\boldsymbol{\lambda}}{dt} \cdot [\{\boldsymbol{\xi}_{\boldsymbol{\lambda}}(z_{\mathrm{ad}}), \omega_{\boldsymbol{\lambda}}(z_{\mathrm{ad}})\} + \{\omega_{\boldsymbol{\lambda}}(z_{\mathrm{ad}}), \boldsymbol{\xi}_{\boldsymbol{\lambda}}(z_{\mathrm{ad}})\}] \\ =& 0, \end{aligned} \tag{1.41}$$

and thus the time evolution z_{ad} generated by the classical generator $\boldsymbol{\xi}_{\boldsymbol{\lambda}}(z_{\mathrm{ad}})$ introduced by the classical analog of the quantum generator $\hat{\boldsymbol{\xi}}(\boldsymbol{\lambda};t)$ is actually adiabatic time evolution conserving the adiabatic invariant. In contrast to the quantal parallel transport, this is called the classical parallel transport.

1.3 Shortcuts to adiabaticity

In this section, we introduce two representative methods of shortcuts to adiabaticity [18], i.e., counter-diabatic driving [19–21] and Lewis-Riesenfeld invariant-based inverse engineering [34].

1.3.1 Counter-diabatic driving

In this section, we denote a generator of adiabatic time evolution as the total Hamiltonian

$$\hat{\mathcal{H}}^{\mathrm{tot}}(t) = \frac{d\boldsymbol{\lambda}}{dt} \cdot \hat{\boldsymbol{\xi}}(\boldsymbol{\lambda};t), \tag{1.42}$$

and then adiabatic time evolution is described as the solution of the Schrödinger equation

$$i\hbar \frac{\partial}{\partial t}|\psi_{\mathrm{ad}}(t)\rangle = \hat{\mathcal{H}}^{\mathrm{tot}}(t)|\psi_{\mathrm{ad}}(t)\rangle, \tag{1.43}$$

or equivalently

$$i\hbar \frac{\partial}{\partial t}\hat{U}_A(t) = \hat{\mathcal{H}}^{\mathrm{tot}}(t)\hat{U}_A(t), \tag{1.44}$$

by using the adiabatic transformation. The total Hamiltonian can be formally obtained by

$$\hat{\mathcal{H}}^{\mathrm{tot}}(t) = \left(i\hbar \frac{\partial}{\partial t}\hat{U}_A(t)\right)\hat{U}_A^{\dagger}(t). \tag{1.45}$$

Because the adiabatic transformation has phase degrees of freedom, there are a variety of the total Hamiltonians.

Berry's case
First we consider the adiabatic transformation that generates the adiabatic state discussed by Berry [21, 111]. In this case, the adiabatic transformation is given by

$$\hat{U}_A(t) = \sum_n \exp\left[-\frac{i}{\hbar}\int_0^t dt' E_n(\boldsymbol{\lambda};t') - \int_0^t dt' \frac{d\boldsymbol{\lambda}}{dt'} \cdot \langle n(\boldsymbol{\lambda};t')|\partial_{\boldsymbol{\lambda}} n(\boldsymbol{\lambda};t')\rangle\right] |n(\boldsymbol{\lambda};t)\rangle\langle n(\boldsymbol{\lambda};0)|, \tag{1.46}$$

and thus the total Hamiltonian is given by

$$\hat{\mathcal{H}}^{\mathrm{tot}}(t) = \hat{\mathcal{H}}(\boldsymbol{\lambda};t) + \hat{\mathcal{H}}^{\mathrm{cd}}(t), \tag{1.47}$$

9

where $\hat{\mathcal{H}}^{\mathrm{cd}}(t)$ is the counter-diabatic Hamiltonian

$$\hat{\mathcal{H}}^{\mathrm{cd}}(t) = i\hbar \frac{d\boldsymbol{\lambda}}{dt} \cdot \sum_n [1 - |n(\boldsymbol{\lambda};t)\rangle\langle n(\boldsymbol{\lambda};t)|] |\partial_{\boldsymbol{\lambda}} n(\boldsymbol{\lambda};t)\rangle\langle n(\boldsymbol{\lambda};t)|. \tag{1.48}$$

This counter-diabatic Hamiltonian can be rewritten as

$$\hat{\mathcal{H}}^{\mathrm{cd}}(t) = i\hbar \frac{d\boldsymbol{\lambda}}{dt} \cdot \sum_{\substack{n,m \\ (m \neq n)}} \frac{\langle m(\boldsymbol{\lambda};t)|(\partial_{\boldsymbol{\lambda}}\hat{\mathcal{H}}(\boldsymbol{\lambda};t))|n(\boldsymbol{\lambda};t)\rangle}{E_n(\boldsymbol{\lambda};t) - E_m(\boldsymbol{\lambda};t)} |m(\boldsymbol{\lambda};t)\rangle\langle n(\boldsymbol{\lambda};t)|, \tag{1.49}$$

which implies that the counter-diabatic Hamiltonian diverges when level crossing takes place, i.e., when adiabaticity is ill-defined [21].

General case
As discussed in Sec. 1.2.2, we have gauge degrees of freedom when a given path $\mathcal{C}$ in parameter space is not closed. Then the adiabatic transformation can take a general form

$$\hat{U}_A(t) = \sum_n e^{i\alpha_n(t)} |n(\boldsymbol{\lambda};t)\rangle\langle n(\boldsymbol{\lambda};0)|, \tag{1.50}$$

where $\alpha_n(t)$ is a real phase parameter. The total Hamiltonian becomes

$$\hat{\mathcal{H}}^{\mathrm{tot}}(t) = -\hbar \sum_n \frac{d\alpha_n}{dt} |n(\boldsymbol{\lambda};t)\rangle\langle n(\boldsymbol{\lambda};t)| + i\hbar \frac{d\boldsymbol{\lambda}}{dt} \cdot \sum_n |\partial_{\boldsymbol{\lambda}} n(\boldsymbol{\lambda};t)\rangle\langle n(\boldsymbol{\lambda};t)|, \tag{1.51}$$

and thus we can freely choose diagonal terms. These degrees of freedom enable us to, for example, minimize cost to implement counter-diabatic driving in experiments [114].

Non-Abelian case
When a Hamiltonian has degeneracies, the adiabatic transformation is given by

$$\hat{U}_A(t) = \sum_n \exp\left[-\frac{i}{\hbar} \int_0^t dt' E_n(\boldsymbol{\lambda};t')\right] \sum_{\mu,\nu} c_\mu^{(n)}(t) c_\nu^{(n)*}(0) |n,\mu(\boldsymbol{\lambda};t)\rangle\langle n,\nu(\boldsymbol{\lambda};0)|, \tag{1.52}$$

and then the total Hamiltonian is similar to Eq. (1.47), but the counter-diabatic Hamiltonian becomes [115]

$$\hat{\mathcal{H}}^{\mathrm{cd}}(t) = i\hbar \frac{d\boldsymbol{\lambda}}{dt} \cdot \sum_n \sum_\mu \left[1 - \sum_\nu |n,\nu(\boldsymbol{\lambda};t)\rangle\langle n,\nu(\boldsymbol{\lambda};t)|\right] |\partial_{\boldsymbol{\lambda}} n,\mu(\boldsymbol{\lambda};t)\rangle\langle n,\mu(\boldsymbol{\lambda};t)|, \tag{1.53}$$

(derivation is similar to the Berry's case and straightforward but a little bit complicated, see Appendix A.4 for details). In this thesis, we do not consider generalization of the non-Abelian case, but similar generalization to the Berry's case is possible.

Single spectrum case
The above counter-diabatic Hamiltonians can generate adiabatic time evolution of arbitrary states, i.e., including superposed states. This is why we need all energy eigenstates to construct the counter-diabatic Hamiltonian. However, for some applications, it is enough to generate adiabatic time evolution of an only single energy eigenstate. In such cases, we can simplify constructions of counter-diabatic terms.

For a given energy eigenstate $|n(\boldsymbol{\lambda};t)\rangle$, adiabatic time evolution of this energy eigenstate can be generated by the following reduced counter-diabatic Hamiltonian

$$\hat{\mathcal{H}}_n^{\mathrm{cd}}(t) = i\hbar \frac{d\boldsymbol{\lambda}}{dt} \cdot [1 - |n(\boldsymbol{\lambda};t)\rangle\langle n(\boldsymbol{\lambda};t)|] |\partial_{\boldsymbol{\lambda}} n(\boldsymbol{\lambda};t)\rangle\langle n(\boldsymbol{\lambda};t)| + \mathrm{H.c.}, \tag{1.54}$$

where H.c. represents the Hermitian conjugate [115]. This reduced counter-diabatic Hamiltonian can be rewritten as

$$\hat{\mathcal{H}}_n^{\mathrm{cd}}(t) = \hat{\mathcal{H}}^{\mathrm{cd}}(t) - \hat{\mathcal{H}}_n^{\mathrm{r}}(t), \tag{1.55}$$

where

$$\hat{\mathcal{H}}_n^{\mathrm{r}}(t) = i\hbar \frac{d\boldsymbol{\lambda}}{dt} \cdot \sum_{\substack{m,l \\ (m,l \neq n, m \neq l)}} |l(\boldsymbol{\lambda};t)\rangle\langle l(\boldsymbol{\lambda};t)|\partial_{\boldsymbol{\lambda}} m(\boldsymbol{\lambda};t)\rangle\langle m(\boldsymbol{\lambda};t)|. \tag{1.56}$$

These reduced terms do not act on $|n(\boldsymbol{\lambda};t)\rangle$, and thus the reduced counter-diabatic Hamiltonian can generate adiabatic time evolution of a given single energy eigenstate.

Variational approach
In the above formulas, we have to know energy eigenstates in order to construct the counter-diabatic Hamiltonian. Here, we introduce a variational approach, in which knowledge of energy eigenstates is not required [25].

We introduce the following operator

$$\hat{\boldsymbol{G}}(\boldsymbol{\lambda};t) = \frac{\partial}{\partial \boldsymbol{\lambda}}\hat{\mathcal{H}}(\boldsymbol{\lambda};t) + \frac{i}{\hbar}[\hat{\boldsymbol{\zeta}}(\boldsymbol{\lambda};t), \hat{\mathcal{H}}(\boldsymbol{\lambda};t)], \tag{1.57}$$

which is equal to $\hat{\boldsymbol{D}}(\boldsymbol{\lambda};t)$ if a trial operator $\hat{\boldsymbol{\zeta}}(\boldsymbol{\lambda};t)$ is equal to the generator of adiabatic time evolution $\hat{\boldsymbol{\xi}}(\boldsymbol{\lambda};t)$ from Eq. (1.27). Now we consider the Hilbert-Schmidt norm

$$||\hat{\boldsymbol{G}}(\boldsymbol{\lambda};t) - \hat{\boldsymbol{D}}(\boldsymbol{\lambda};t)||^2 = \mathrm{Tr}[(\hat{\boldsymbol{G}}(\boldsymbol{\lambda};t) - \hat{\boldsymbol{D}}(\boldsymbol{\lambda};t))^2] = \mathrm{Tr}[(\hat{\boldsymbol{G}}(\boldsymbol{\lambda};t))^2] - \mathrm{Tr}[(\hat{\boldsymbol{D}}(\boldsymbol{\lambda};t))^2], \tag{1.58}$$

which is non-negative from the definition and it becomes zero when $\hat{\boldsymbol{\zeta}}(\boldsymbol{\lambda};t)$ is $\hat{\boldsymbol{\xi}}(\boldsymbol{\lambda};t)$. Because the second term does not depend on $\hat{\boldsymbol{\zeta}}(\boldsymbol{\lambda};t)$, the problem to determine $\hat{\boldsymbol{\xi}}(\boldsymbol{\lambda};t)$ can be replaced with the problem to minimize the first term

$$\mathcal{S}[\hat{\boldsymbol{\zeta}}(\boldsymbol{\lambda};t)] = \mathrm{Tr}[(\hat{\boldsymbol{G}}(\boldsymbol{\lambda};t))^2], \tag{1.59}$$

with respect to a trial operator $\hat{\boldsymbol{\zeta}}(\boldsymbol{\lambda};t)$. This approach also enables us to construct approximate counter-diabatic Hamiltonians by supposing some limitations in a trial operator.

1.3.2 Lewis-Riesenfeld invariant-based inverse engineering

Next we introduce another representative method of shortcuts to adiabaticity called Lewis-Riesenfeld invariant-based inverse engineering [34].

In this method, the important concept is the Lewis-Riesenfeld invariants, which is also called the dynamical invariants [35]. For a given time-dependent Hamiltonian $\hat{\mathcal{H}}(t)$, the Lewis-Riesenfeld invariant $\hat{F}(t)$ satisfies

$$i\hbar \frac{\partial}{\partial t}\hat{F}(t) = [\hat{\mathcal{H}}(t), \hat{F}(t)]. \tag{1.60}$$

Obviously the density operator satisfies this equation, but $\hat{F}(t)$ is not limited to the density operator. From the Lewis-Riesenfeld theory, the solution of the Schrödinger equation

$$i\hbar \frac{\partial}{\partial t}|\Psi(t)\rangle = \hat{\mathcal{H}}(t)|\Psi(t)\rangle, \tag{1.61}$$

is expanded as

$$|\Psi(t)\rangle = \sum_n c_n |\psi_n(t)\rangle \tag{1.62}$$

where c_n is a time-independent coefficient and $|\psi_n(t)\rangle$ is the dynamical mode. We can show that the dynamical mode $|\psi_n(t)\rangle$ is given by

$$|\psi_n(t)\rangle = e^{i\alpha_n(t)}|\phi_n(t)\rangle, \tag{1.63}$$

11

where $|\phi_n(t)\rangle$ is the eigenvector of $\hat{F}(t)$. Here, $\alpha_n(t)$ is called the Lewis-Riesenfeld phase, which is given by

$$\alpha_n(t) = \frac{1}{\hbar} \int_0^t dt' \langle \phi_n(t')| \left(i\hbar \frac{\partial}{\partial t'} - \hat{\mathcal{H}}(t') \right) |\phi_n(t')\rangle, \tag{1.64}$$

(for details of the Lewis-Riesenfeld theory, see Appendix A.5).

In Lewis-Riesenfeld invariant-based inverse engineering, we first consider a given Lewis-Riesenfeld invariant

$$\hat{F}(t) = \sum_n \lambda_n |\phi_n(t)\rangle\langle\phi_n(t)|, \tag{1.65}$$

with certain time-dependent Hamiltonian $\mathcal{H}(t)$ satisfying Eq. (1.60). Then dynamics under the Hamiltonian $\mathcal{H}(t)$ is given by the following time evolution operator

$$\hat{U}_{\mathrm{LR}}(t) = \sum_n e^{i\alpha_n(t)} |\phi_n(t)\rangle\langle\phi_n(0)|, \tag{1.66}$$

i.e., the Schrödinger equation is given by

$$i\hbar \frac{\partial}{\partial t} \hat{U}_{\mathrm{LR}}(t) = \hat{\mathcal{H}}(t)\hat{U}_{\mathrm{LR}}(t). \tag{1.67}$$

By formally solving this equation, we find that the Hamiltonian is given by

$$\begin{aligned} \hat{\mathcal{H}}(t) &= \left(i\hbar \frac{\partial}{\partial t} \hat{U}_{\mathrm{LR}}(t) \right) \hat{U}_{\mathrm{LR}}^\dagger(t) \\ &= -\hbar \sum_n \dot{\alpha}_n(t) |\phi_n(t)\rangle\langle\phi_n(t)| + i\hbar \sum_n |\partial_t \phi_n(t)\rangle\langle\phi_n(t)|. \end{aligned} \tag{1.68}$$

This actually resembles the total Hamiltonian $\hat{\mathcal{H}}^{\mathrm{tot}}(t)$ in counter-diabatic driving, but it should be noted that $\{|\phi_n(t)\rangle\}$ are not the eigenstates of a reference Hamiltonian $\hat{\mathcal{H}}(t)$ in counter-diabatic driving, but the eigenvectors of the Lewis-Riesenfeld invariant $\hat{F}(t)$. The condition that the Hamiltonian (1.68) equals to the given Hamiltonian $\hat{\mathcal{H}}(t)$ determines time-dependence of the given Hamiltonian. In order to obtain a target state, the condition

$$[\hat{\mathcal{H}}(0), \hat{F}(0)] = 0, \quad [\hat{\mathcal{H}}(t_f), \hat{F}(t_f)] = 0, \tag{1.69}$$

must be satisfied for a given initial time $t = 0$ and a given final time $t = t_f$. Then the eigenstates of the Hamiltonian $\hat{\mathcal{H}}(t)$ and the eigenvectors of $\hat{F}(t)$ coincide, and thus the initial and the final populations of the eigenstates coincide. In this sense, we can speedup adiabatic time evolution, i.e., we can obtain the identical state to the state generated via adiabatic time evolution. However, it should be noted that a state differs from adiabatic time evolution in duration.

1.4 Examples of shortcuts to adiabaticity

In this section, we introduce examples of shortcuts to adiabaticity, which are relevant to the present thesis. Hereafter, we do not explicitly express parameter-dependence, but directly denote time-dependence.

1.4.1 Counter-diabatic driving in two-level systems

As the first example, we consider a two-level system

$$\hat{\mathcal{H}}(t) = -\boldsymbol{h}(t) \cdot \hat{\boldsymbol{\sigma}}, \tag{1.70}$$

where $\boldsymbol{h}(t)$ is a time-dependent magnetic field and $\hat{\boldsymbol{\sigma}} = (\hat{\sigma}_x, \hat{\sigma}_y, \hat{\sigma}_z)$ is the Pauli spin. Here, we put $\hbar = 1$. We derive the counter-diabatic term according to Berry [21]. From Eq. (1.49), the counter-diabatic Hamiltonian is given by

$$\hat{\mathcal{H}}^{\mathrm{cd}}(t) = i \sum_{\substack{n,m \\ (m \neq n)}} \frac{\hat{P}_m(\partial_t \hat{\mathcal{H}}(t))\hat{P}_n}{E_n(t) - E_m(t)} = -\frac{i\dot{\boldsymbol{h}}(t)}{2|\boldsymbol{h}(t)|} \cdot (\hat{P}_-(t)\hat{\boldsymbol{\sigma}}\hat{P}_+(t) - \hat{P}_+(t)\hat{\boldsymbol{\sigma}}\hat{P}_-(t)), \tag{1.71}$$

where $\hat{P}_\pm(t)$ is the projection operator associated with the ground state and the excited state

$$\hat{P}_\pm(t) = \frac{\boldsymbol{h}(t) \cdot \hat{\boldsymbol{\sigma}} \pm |\boldsymbol{h}(t)|}{2|\boldsymbol{h}(t)|}. \tag{1.72}$$

Then, by substituting Eq. (1.72) for Eq. (1.71), we obtain

$$\hat{\mathcal{H}}^{\mathrm{cd}}(t) = \boldsymbol{f}(t) \cdot \hat{\boldsymbol{\sigma}}, \tag{1.73}$$

where

$$\boldsymbol{f}(t) = \frac{\boldsymbol{h}(t) \times \dot{\boldsymbol{h}}(t)}{2|\boldsymbol{h}(t)|^2}. \tag{1.74}$$

Therefore, counter-diabatic driving requires an additional magnetic field along the direction perpendicular to the original magnetic field and its time derivative. Note that it is also possible to construct the same counter-diabatic terms by using the eigenstates of the reference Hamiltonian (1.70).

1.4.2 Lewis-Riesenfeld invariant-based inverse engineering in two-level systems

Next, we show Lewis-Riesenfeld invariant-based inverse engineering in two-level systems according to Chen *et al.* [36].

For the same two-level Hamiltonian (1.70), the eigenstates are given by

$$\begin{cases} |n_-(t)\rangle = \cos\dfrac{\theta}{2}e^{i\varphi}|\uparrow\rangle + \sin\dfrac{\theta}{2}|\downarrow\rangle, \\ |n_+(t)\rangle = \sin\dfrac{\theta}{2}|\uparrow\rangle - \cos\dfrac{\theta}{2}e^{-i\varphi}|\downarrow\rangle, \end{cases} \tag{1.75}$$

where time-dependent angles $\theta = \theta(t)$ and $\varphi = \varphi(t)$ satisfy

$$\cos\theta = -\frac{h^z(t)}{|\boldsymbol{h}(t)|}, \tag{1.76}$$

and

$$\tan\varphi = -\frac{h^y(t)}{h^x(t)}. \tag{1.77}$$

The eigenstates of any two-level Hamiltonian can be written in the form (1.75), and thus we assume that the eigenvectors of the Lewis-Riesenfeld invariant are given by

$$\begin{cases} |\phi_-(t)\rangle = \cos\dfrac{\gamma}{2}e^{i\beta}|\uparrow\rangle + \sin\dfrac{\gamma}{2}|\downarrow\rangle, \\ |\phi_+(t)\rangle = \sin\dfrac{\gamma}{2}|\uparrow\rangle - \cos\dfrac{\gamma}{2}e^{-i\beta}|\downarrow\rangle, \end{cases} \tag{1.78}$$

where $\gamma = \gamma(t)$ and $\beta = \beta(t)$ are certain time-dependent angles, and also assume that the eigenvalues of the Lewis-Riesenfeld invariant is given by $\lambda_\pm = \pm h_0$. Then the Lewis-Riesenfeld invariant is given by

$$\hat{F}(t) = \sum_\pm \lambda_\pm |\phi_\pm(t)\rangle\langle\phi_\pm(t)| = h_0 \begin{pmatrix} -\cos\gamma & -\sin\gamma e^{i\beta} \\ -\sin\gamma e^{-i\beta} & \cos\gamma \end{pmatrix}. \tag{1.79}$$

Then the Lewis-Riesenfeld phase is calculated as

$$\alpha_\pm(t) = \pm \int_0^t dt' \left[\dot{\beta} \cos^2 \frac{\gamma}{2} - h^z \cos \gamma - \sqrt{(h^x)^2 + (h^y)^2} \sin \gamma \cos(\beta - \varphi) \right], \tag{1.80}$$

and thus, by inversely engineering the total Hamiltonian, we obtain

$$\hat{\mathcal{H}}^{\text{tot}}(t) = \begin{pmatrix} M & N e^{i\beta} \\ N^* e^{-i\beta} & -M \end{pmatrix}, \tag{1.81}$$

where

$$\begin{cases} M = -h^z \cos^2 \gamma - \sqrt{(h^x)^2 + (h^y)^2} \sin \gamma \cos \gamma \cos(\beta - \varphi) - \dfrac{1}{2} \dot{\beta} \sin^2 \gamma, \\ N = [-h^z \cos \gamma - \sqrt{(h^x)^2 + (h^y)^2} \sin \gamma \cos(\beta - \varphi) + \dfrac{1}{2} \dot{\beta} \cos \gamma] \sin \gamma - \dfrac{i}{2} \dot{\gamma}. \end{cases} \tag{1.82}$$

This Hamiltonian should be identical to the two-level Hamiltonian (1.70), and thus we obtain the auxiliary equations

$$\begin{cases} \dot{\gamma} = -2\sqrt{(h^x)^2 + (h^y)^2} \sin(\beta - \varphi), \\ (2h^z - \dot{\beta}) \sin \gamma = 2\sqrt{(h^x)^2 + (h^y)^2} \cos \gamma \cos(\beta - \varphi). \end{cases} \tag{1.83}$$

In order to obtain a target state, it should satisfy the commutation relations at time $t = 0$ and t_f, and thus we obtain the conditions

$$\begin{cases} \sqrt{(h^x)^2 + (h^y)^2} \sin \gamma \sin(\beta - \varphi) = 0, \\ h^z \sin \gamma e^{\pm i\beta} - \sqrt{(h^x)^2 + (h^y)^2} \cos \gamma e^{\pm i\varphi} = 0, \end{cases} \tag{1.84}$$

for time $t = 0$ and t_f. In contrast to counter-diabatic driving, in Lewis-Riesenfeld invariant-based inverse engineering, we design the time-dependent parameters $\gamma(t)$ and $\beta(t)$ to obtain the desired state. Then, Eq. (1.84) should be satisfied at time $t = 0$ and t_f to avoid final excitations. We can find time-dependence of the magnetic field in the Hamiltonian from Eq. (1.83).

1.4.3 Counter-diabatic driving in harmonic oscillators

As the second example, we consider a harmonic oscillator

$$\hat{\mathcal{H}}(t) = \hbar\omega(t) \left(\hat{a}^\dagger \hat{a} + \frac{1}{2} \right), \tag{1.85}$$

where $\omega(t)$ is a time-dependent frequency and $\hat{a}$ ($\hat{a}^\dagger$) is the annihilation (creation) operator. It should be noted that the annihilation and creation operators depend on time as

$$\begin{cases} \hat{a} = \sqrt{\dfrac{m\omega(t)}{2\hbar}} \left(\hat{x} + \dfrac{i}{m\omega(t)} \hat{p} \right), \\ \hat{a}^\dagger = \sqrt{\dfrac{m\omega(t)}{2\hbar}} \left(\hat{x} - \dfrac{i}{m\omega(t)} \hat{p} \right), \end{cases} \tag{1.86}$$

where mass m and the position and momentum operators $\hat{x}$ and $\hat{p}$ come from another representation of the Hamiltonian

$$\hat{\mathcal{H}}(t) = \frac{\hat{p}^2}{2m} + \frac{1}{2} m(\omega(t))^2 \hat{x}^2. \tag{1.87}$$

This time (frequency) dependence of the annihilation and creation operators, i.e., that of the Fock state $|n\rangle$, is often neglected, but in order to neglect this time dependence, the adiabatic limit $|\dot{\omega}(t)/\omega(t)| \ll 1$ should be satisfied.

We will show the derivation according to Muga *et al.* [23]. The Fock state $|n\rangle$ in the coordinate representation is given by

$$\langle x|n\rangle = \frac{1}{\sqrt{2^n n!}} \left(\frac{m\omega(t)}{\pi\hbar}\right)^{1/4} \exp\left[-\frac{m\omega(t)}{2\hbar}x^2\right] H_n\left(\sqrt{\frac{m\omega(t)}{\hbar}}x\right), \tag{1.88}$$

where $H_n(\cdot)$ is the Hermite polynomial. By differentiating with respect to time, we obtain

$$\langle x|\partial_t n\rangle = \left(\frac{1}{4} - \frac{m\omega(t)}{2\hbar}x^2\right)\frac{\dot{\omega}(t)}{\omega(t)}\langle x|n\rangle + \sqrt{\frac{m\omega(t)}{2\hbar}}x\frac{\dot{\omega}(t)}{\omega(t)}\sqrt{n}\langle x|n-1\rangle, \tag{1.89}$$

i.e.,

$$|\partial_t n\rangle = \left(\frac{1}{4} - \frac{m\omega(t)}{2\hbar}\hat{x}^2\right)\frac{\dot{\omega}(t)}{\omega(t)}|n\rangle + \sqrt{\frac{m\omega(t)}{2\hbar}}\hat{x}\frac{\dot{\omega}(t)}{\omega(t)}\sqrt{n}|n-1\rangle. \tag{1.90}$$

Here, we use $H'_n(\cdot) = 2nH_{n-1}(\cdot)$. Because the position operator is given by

$$\hat{x} = \sqrt{\frac{\hbar}{2m\omega(t)}}(\hat{a}^\dagger + \hat{a}), \tag{1.91}$$

Eq. (1.90) becomes

$$|\partial_t n\rangle = \frac{\dot{\omega}(t)}{4\omega(t)}(\hat{a}^2 - \hat{a}^{\dagger 2})|n\rangle, \tag{1.92}$$

and thus the counter-diabatic Hamiltonian is given by

$$\hat{\mathcal{H}}^{\mathrm{cd}}(t) = i\hbar\frac{\dot{\omega}(t)}{4\omega(t)}(\hat{a}^2 - \hat{a}^{\dagger 2}). \tag{1.93}$$

Chapter 2

Quantum annealing

In this chapter, we introduce quantum annealing. First, we briefly review the context of quantum annealing in Sec. 2.1. The theory of quantum annealing is summarized in Sec. 2.2. We show some classical algorithms, which simulate quantum annealing in some sense, in Sec. 2.3. In Sec. 2.4, we introduce shortcuts to adiabaticity for quantum annealing.

2.1 Overview

Historically, quantum annealing was first introduced as a method to obtain the ground state of a system with multi-well potential energy [116–119]. There, mass of a particle is first set to be small in order to allow quantum tunneling. Then, it is changed to be large in order to make a state localized at the minimum of potential energy. In other words, kinetic terms are first set to be large and later potential terms are enlarged. Their motivation was to solve combinatorial optimization problems [116] and to obtain the ground state for molecules from the viewpoint of chemistry [117–119].

Later, this method was translated into spin systems in order to obtain the ground state of spin glasses, where a transverse field was utilized as a source of quantum fluctuations instead of mass of a particle [5]. There, a transverse field is first set to be large, and then it is turned off. It was soon implemented in experiments by using disordered magnets [120,121]. It was also pointed out that the idea of quantum annealing can be applied to solve some kind of computational problems [122,123], which is called adiabatic quantum computation. If we can use arbitrary Hamiltonians, adiabatic quantum computation is known to be universal [124]. In contrast to adiabatic quantum computation, in quantum annealing, the target Hamiltonian is usually restricted to the Ising-type Hamiltonian and quantum fluctuations are usually induced by a transverse field. Furthermore, coupling to thermal environment is usually assumed in the recent context, nevertheless it was not assumed in the beginning.

Both quantum annealing and adiabatic quantum computation rely on real-time quantum dynamics, and thus we need quantum devices in order to implement them. Recently, some companies and universities have been chasing such quantum devices. For quantum annealing, D-Wave Systems pronounced that they developed such a quantum device implementing quantum annealing [3]. Some evidence of quantumness, i.e., evidence that their machines actually implement quantum annealing, has been reported [4,125,126], while it is still under discussion if their machines really implement quantum annealing and if entanglement really help to solve problems [4,127–130]. Even so, their quantum annealers have already been utilized to solve some social problems [6–8].

However, in quantum annealing, entanglement is not always necessary or small entanglement is sometimes enough to obtain the solution, and thus semi-classical or classical algorithms works well in some cases. Therefore, the path-integral Monte Carlo method has been often used in order to investigate the performance of quantum annealing in large systems [131,132], which is recently called simulated quantum annealing. Classical spin models of quantum annealing has been also considered [127,129]. Both similarities and differences between these classical algorithms and D-Wave machines have been reported [4,127–130].

It is also of great interest to seek for improvements in performance of quantum annealing. There,

we intend to speedup quantum annealing processes and to increase possibility obtaining good solutions. For these purpose, we could utilize different paths during quantum annealing processes [133]. To utilize non-stoquastic Hamiltonians is one of the methods choosing different paths and it is expected to improve quantum annealing [134–139]. Here, stoquastic Hamiltonians are quantum Hamiltonians that can be classically simulated by using the Monte Carlo simulation without the negative sign problem [140], and non-stoquastic Hamiltonians are those that cannot be classically simulated. It is expected that non-stoquastic Hamiltonians show strong quantum fluctuations, and thus we have much chance to perform quantum annealing efficiently. However, it should be noted that there is no evidence that all non-stoquastic Hamiltonians show strong quantumness and it is still under discussion which forms of non-stoquastic Hamiltonians can improve quantum annealing. Another method is inhomogeneous driving, in which we induce spacial inhomogeneity in quantum fluctuations [141–151]. This method has recently been paid attention because it can be implemented by using current machines. Indeed, both theoretically and experimentally improvements have been reported.

2.2 Method

In quantum annealing [5], or in some of adiabatic quantum computation [122, 123], a solution of a given problem is encoded onto the ground state of a problem Hamiltonian $\hat{\mathcal{H}}_P$. In order to obtain this ground state of the problem Hamiltonian, we start with the ground state of a driver Hamiltonian $\hat{\mathcal{H}}_V$, of which the ground state is trivial. For example, the transverse field Hamiltonian

$$\hat{\mathcal{H}}_V = -\sum_{i=1}^{N} h_i^x \hat{\sigma}_i^x, \tag{2.1}$$

where we assume $h_i^x > 0$, is one of the simplest candidates for a driver Hamiltonian. The ground state of the transverse field Hamiltonian (2.1) is the quantum paramagnetic state,

$$|+\rangle^{\otimes N} = \bigotimes_{i=1}^{N} |+\rangle_i = \bigotimes_{i=1}^{N} \frac{1}{\sqrt{2}} (|\uparrow\rangle_i + |\downarrow\rangle_i), \tag{2.2}$$

where all the states in the computational basis are superposed with equal weight $2^{-N/2}$. Now, we consider the following quantum annealing Hamiltonian

$$\hat{\mathcal{H}}(t) = g(t/t_f)\hat{\mathcal{H}}_P + [1 - g(t/t_f)]\hat{\mathcal{H}}_V, \tag{2.3}$$

where $g(\cdot)$ is a differentiable function satisfying $g(0) = 0$ and $g(1) = 1$, and t_f is the annealing time. Then, the adiabatic theorem (see, Sec. 1.2.1) ensures that a state reaches the ground state of the problem Hamiltonian, i.e., we can obtain the solution of the given problem, if the annealing process is slow enough in time. It should be noted that a choice of a driver Hamiltonian is arbitrary, but it must not commute with the problem Hamiltonian

$$[\hat{\mathcal{H}}_P, \hat{\mathcal{H}}_V] \neq 0. \tag{2.4}$$

Otherwise, gap closing takes place and we fail to obtain the ground state.

In quantum annealing [5], a problem Hamiltonian is usually given by the form of the Ising-type Hamiltonians

$$\begin{aligned}
\hat{\mathcal{H}}_P &= -\frac{1}{2} \sum_{i,j=1}^{N} J_{ij} \hat{\sigma}_i^z \hat{\sigma}_j^z - \sum_{i=1}^{N} h_i^z \hat{\sigma}_i^z \\
&= -\sum_{\substack{i,j=1 \\ (i<j)}}^{N} J_{ij} \hat{\sigma}_i^z \hat{\sigma}_j^z - \sum_{i=1}^{N} h_i^z \hat{\sigma}_i^z.
\end{aligned} \tag{2.5}$$

For some problems, more than three-body interactions can appear, but it can be decomposed into two-body interactions [152].

2.3 Classical algorithms

We cannot apply quantum annealing to systems with large number of qubits by using classical computers because quantum annealing is based on real-time quantum dynamics. Therefore, we need quantum annealers or classical algorithms in order to implement quantum annealing. In this section, we introduce some examples of classical algorithms.

2.3.1 Path integral Monte Carlo method

For a given quantum annealing Hamiltonian (2.3) at time t, we consider the partition function describing a thermal equilibrium state

$$Z_\beta(t) = \text{Tr} e^{-\beta \hat{\mathcal{H}}(t)}, \tag{2.6}$$

at an inverse temperature β. By using Suzuki-Trotter decomposition, we obtain

$$Z_\beta(t) = \lim_{M \to \infty} \text{Tr}\{e^{-\beta[1-g(t/t_f)]\hat{\mathcal{H}}_V/M} e^{-\beta g(t/t_f)\hat{\mathcal{H}}_P/M}\}^M. \tag{2.7}$$

We introduce classical Ising spins and the computational basis

$$|\boldsymbol{s}_k\rangle = |\sigma_{1,k}\sigma_{2,k}\cdots\sigma_{N,k}\rangle, \tag{2.8}$$

where the following relations

$$\hat{\sigma}_i^z|\boldsymbol{s}_k\rangle = \sigma_{i,k}|\boldsymbol{s}_k\rangle, \tag{2.9}$$

and

$$\hat{\sigma}_i^x|\boldsymbol{s}_k\rangle = \hat{\sigma}_i^x|\sigma_{1,k}\sigma_{2,k}\cdots\sigma_{i,k}\cdots\sigma_{N,k}\rangle = |\sigma_{1,k}\sigma_{2,k}\cdots(-\sigma_{i,k})\cdots\sigma_{N,k}\rangle \tag{2.10}$$

hold. We also introduce the identity operator

$$\hat{1} = \sum_{\boldsymbol{s}} |\boldsymbol{s}\rangle\langle\boldsymbol{s}|, \tag{2.11}$$

and then the partition function is rewritten as

$$\begin{aligned}
Z_\beta(t) &= \lim_{M \to \infty} \sum_{\boldsymbol{s}_1} \langle\boldsymbol{s}_1|\{e^{-\beta[1-g(t/t_f)]\hat{\mathcal{H}}_V/M} e^{-\beta g(t/t_f)\hat{\mathcal{H}}_P/M}\}^M|\boldsymbol{s}_1\rangle \\
&= \lim_{M \to \infty} \sum_{\boldsymbol{s}_1,\cdots,\boldsymbol{s}_M} \langle\boldsymbol{s}_1|e^{-\beta[1-g(t/t_f)]\hat{\mathcal{H}}_V/M} e^{-\beta g(t/t_f)\hat{\mathcal{H}}_P/M}|\boldsymbol{s}_M\rangle \\
&\quad \times \langle\boldsymbol{s}_M|e^{-\beta[1-g(t/t_f)]\hat{\mathcal{H}}_V/M} e^{-\beta g(t/t_f)\hat{\mathcal{H}}_P/M}|\boldsymbol{s}_{M-1}\rangle \\
&\quad \cdots \\
&\quad \times \langle\boldsymbol{s}_2|e^{-\beta[1-g(t/t_f)]\hat{\mathcal{H}}_V/M} e^{-\beta g(t/t_f)\hat{\mathcal{H}}_P/M}|\boldsymbol{s}_1\rangle.
\end{aligned} \tag{2.12}$$

From Eq. (2.9), the problem Hamiltonian $\hat{\mathcal{H}}_P$ in Eq. (2.12) becomes a classical Hamiltonian with classical Ising spins $\{\sigma_{i,k}\}$. Then the problem is how to calculate

$$\langle\boldsymbol{s}_k|e^{-\beta[1-g(t/t_f)]\hat{\mathcal{H}}_V/M}|\boldsymbol{s}_{k-1}\rangle, \tag{2.13}$$

and how to transform the partition function (2.12) into the form of the partition function of a classical spin model. For the transverse field Hamiltonian (2.1), this quantity becomes

$$
\begin{aligned}
\langle \boldsymbol{s}_k | e^{-\beta[1-g(t/t_f)]\hat{\mathcal{H}}_V/M} | \boldsymbol{s}_{k-1}\rangle =& \langle \boldsymbol{s}_k | \prod_{i=1}^{N} e^{\beta[1-g(t/t_f)]h_i^x \hat{\sigma}_i^x/M} | \boldsymbol{s}_{k-1}\rangle \\
=& \langle \boldsymbol{s}_k | \prod_{i=1}^{N} \left\{ \cosh \frac{\beta[1-g(t/t_f)]h_i^x}{M} + \hat{\sigma}_i^x \sinh \frac{\beta[1-g(t/t_f)]h_i^x}{M} \right\} | \boldsymbol{s}_{k-1}\rangle \\
=& \prod_{i=1}^{N} \left\{ \delta_{\sigma_{i,k},\sigma_{i,k-1}} \cosh \frac{\beta[1-g(t/t_f)]h_i^x}{M} + \delta_{\sigma_{i,k},(-\sigma_{i,k-1})} \sinh \frac{\beta[1-g(t/t_f)]h_i^x}{M} \right\} \\
=& \prod_{i=1}^{N} \sqrt{ \sinh \frac{\beta[1-g(t/t_f)]h_i^x}{M} \cosh \frac{\beta[1-g(t/t_f)]h_i^x}{M} } \\
& \times \left\{ \tanh \frac{\beta[1-g(t/t_f)]h_i^x}{M} \right\}^{-\frac{1}{2}\sigma_{i,k}\sigma_{i,k-1}} \\
=& \left\{ \frac{1}{2} \sinh \frac{2\beta[1-g(t/t_f)]h_i^x}{M} \right\}^{N/2} \\
& \times \prod_{i=1}^{N} \exp \left[-\frac{1}{2} \log \left\{ \tanh \frac{\beta[1-g(t/t_f)]h_i^x}{M} \right\} \sigma_{i,k}\sigma_{i,k-1} \right] \\
=& \left\{ \frac{1}{2} \sinh \frac{2\beta[1-g(t/t_f)]h_i^x}{M} \right\}^{N/2} \\
& \times \exp \left[-\frac{1}{2} \sum_{i=1}^{N} \log \left\{ \tanh \frac{\beta[1-g(t/t_f)]h_i^x}{M} \right\} \sigma_{i,k}\sigma_{i,k-1} \right].
\end{aligned}
\tag{2.14}
$$

From the problem Hamiltonian (2.5) and this result, we can replace the partition function for the quantum annealing Hamiltonian with the partition function for a classical Hamiltonian $\mathcal{H}_C$ as

$$
Z_\beta(t) = \lim_{M \to \infty} A^{MN} \sum_{\{\boldsymbol{s}_k\}} e^{-\beta \mathcal{H}_C},
\tag{2.15}
$$

where

$$
A = \sqrt{ \frac{1}{2} \sinh \frac{2\beta[1-g(t/t_f)]h_i^x}{M} },
\tag{2.16}
$$

and

$$
\begin{aligned}
\mathcal{H}_C =& \sum_{k=1}^{M} \frac{g(t/t_f)}{M} \left(-\frac{1}{2} \sum_{i,j=1}^{N} J_{ij}\sigma_{i,k}\sigma_{j,k} - \sum_{i=1}^{N} h_i^z \sigma_{i,k} \right) \\
& + \sum_{k=1}^{M} \frac{1}{2\beta} \sum_{i=1}^{N} \log \left\{ \tanh \frac{\beta[1-g(t/t_f)]h_i^x}{M} \right\} \sigma_{i,k}\sigma_{i,k+1},
\end{aligned}
\tag{2.17}
$$

with $\sigma_{i,M+1} = \sigma_{i,1}$. This Hamiltonian is nothing but the classical Ising Hamiltonian with an additional dimension. The path integral Monte Carlo method is a method to simulate this classical Ising Hamiltonian by using the Markov chain Monte Carlo method (see Appendix B.1, for details). In particular, we call this method simulated quantum annealing when we consider a quantum annealing process during path integral Monte Carlo simulation. This method has been utilized in order to simulate quantum annealing in large systems [131, 132]. However, it is still unclear if this method can appropriately describe quantum annealing or not.

2.3.2 Classical models

Shin-Smith-Smolin-Vazirani model
The Shin-Smith-Smolin-Vazirani model [127,129] is the planar rotor model, where we replace the Pauli matrices with planar rotors as

$$\begin{cases} \hat{\sigma}_i^x \to \sin\theta_i, \\ \hat{\sigma}_i^z \to \cos\theta_i. \end{cases} \tag{2.18}$$

Therefore the classical Hamiltonian of the Shin-Smith-Smolin-Vazirani model is given by

$$\mathcal{H}_t = g(t/t_f)\mathcal{H}_P + [1 - g(t/t_f)]\mathcal{H}_V, \tag{2.19}$$

where the problem Hamiltonian and the driver Hamiltonian are described by planar rotors as

$$\mathcal{H}_P = -\sum_{\substack{i,j=1 \\ (i<j)}}^{N} J_{ij}\cos\theta_i\cos\theta_j - \sum_{i=1}^{N} h_i^z\cos\theta_i, \tag{2.20}$$

and

$$\mathcal{H}_V = -\sum_{i=1}^{N} h_i^x\sin\theta_i. \tag{2.21}$$

Here, its dynamics is governed by effective fields [127].

In order to reproduce the results of the D-Wave machines, Shin *et al.* considered a realistic update process, i.e., a Metropolis-type update [129]. There, at each time step, we consider a random update of an angle θ_i in accordance with the Metropolis method. That is, for a given angle θ_i, we replace it with a randomly picked angle $\bar{\theta}_i$ with probability

$$w(\bar{\theta}_i|\theta_i) = \max\{1, e^{-\beta\Delta\mathcal{H}_t}\}, \tag{2.22}$$

where $\Delta\mathcal{H}_t$ is the energy difference associated with the transition $\theta_i \to \bar{\theta}_i$. For fine tuned parameters, strong correlations between the results of the D-Wave machines and those of this model were reported [129,130].

Classical spin dynamics model
The replacement of quantum spins with three-dimensional classical spins was also considered [4]. The Pauli matrices are replaced with the three-dimensional unit vectors

$$\hat{\boldsymbol{\sigma}}_i \to \boldsymbol{m}_i, \tag{2.23}$$

where $\boldsymbol{m}_i$ satisfies $|\boldsymbol{m}_i| = 1$. Then the classical spin Hamiltonian is given by

$$\mathcal{H}_t = g(t/t_f)\mathcal{H}_P + [1 - g(t/t_f)]\mathcal{H}_V, \tag{2.24}$$

where the problem Hamiltonian and the driver Hamiltonian are described by classical spin Hamiltonians

$$\mathcal{H}_P = -\sum_{\substack{i,j=1 \\ (i<j)}}^{N} J_{ij}m_i^z m_j^z - \sum_{i=1}^{N} h_i^z m_i^z, \tag{2.25}$$

and

$$\mathcal{H}_V = -\sum_{i=1}^{N} h_i^x m_i^x. \tag{2.26}$$

Then, classical spin dynamics is given by the torque equation

$$\dot{\boldsymbol{m}}_i(t) = \boldsymbol{h}_i^{\mathrm{eff}}(t) \times \boldsymbol{m}_i(t), \tag{2.27}$$

where $\boldsymbol{h}_i^{\mathrm{eff}}(t)$ is an effective magnetic field given by

$$\boldsymbol{h}_i^{\mathrm{eff}}(t) = -\frac{\partial \mathcal{H}_t}{\partial \boldsymbol{m}_i}. \tag{2.28}$$

This equation of motion shows deterministic classical dynamics. In order to induce randomness, Boixo *et al.* [4] introduced randomness by perturbing the initial state as

$$\boldsymbol{m}_i(0) = \begin{pmatrix} \sqrt{1 - \delta_i^2 - \eta_i^2} \\ \delta_i \\ \eta_i \end{pmatrix}, \tag{2.29}$$

with small random perturbations δ_i and η_i. As the result, it was found that this model shows poor correlations with the D-Wave machines [4]. However, it might be still possible to reproduce similar results by tuning appropriate randomness or updates.

2.4 Application of shortcuts to adiabaticity

In this section, we introduce shortcuts to adiabaticity for quantum annealing according to Takahashi [89], where the mean-field approximation is applied to Lewis-Riesenfeld invariant-based inverse engineering.

First we introduce another derivation of Lewis-Riesenfeld invariant-based inverse engineering in two-level systems. For a two-level Hamiltonian

$$\hat{\mathcal{H}}(t) = -\boldsymbol{h}(t) \cdot \hat{\boldsymbol{\sigma}}, \tag{2.30}$$

we assume the following Lewis-Riesenfeld invariant

$$\hat{F}(t) = -\boldsymbol{n}(t) \cdot \hat{\boldsymbol{\sigma}}, \tag{2.31}$$

where $\boldsymbol{n}(t)$ is an three dimensional unit vector. This invariant should satisfy Eq. (1.60), and thus we obtain

$$\dot{\boldsymbol{n}}(t) = 2\boldsymbol{n}(t) \times \boldsymbol{h}(t). \tag{2.32}$$

For conventional quantum annealing, we do not use a magnetic field along y-axis, and thus we assume $h^y = 0$. Then, by using the following expression

$$\boldsymbol{n}(t) = \begin{pmatrix} \sin\gamma \cos\beta \\ -\sin\gamma \sin\beta \\ \cos\gamma \end{pmatrix}, \tag{2.33}$$

we obtain

$$\begin{cases} \dot{\gamma} = -2h^x \sin\beta, \\ (2h^z - \dot{\beta}) \sin\gamma = 2h^x \cos\gamma \cos\beta. \end{cases} \tag{2.34}$$

This is actually identical to Eq. (1.83) with $h^y = 0$ and $\varphi = 0$.

Next, we consider the following Hamiltonian

$$\hat{\mathcal{H}}(t) = f(t) \left(-\frac{J}{2N} \sum_{i,j=1}^{N} \hat{\sigma}_i^z \hat{\sigma}_j^z - h^z \sum_{i=1}^{N} \hat{\sigma}_i^z \right) - h^x(t) \sum_{i=1}^{N} \hat{\sigma}_i^x, \tag{2.35}$$

and we consider Lewis-Riesenfeld invariant-based inverse engineering for this model according to Takahashi [89]. In a similar way to the two-level case, we assume the following Lewis-Riesenfeld invariant

$$\hat{F}(t) = -\boldsymbol{n}(t) \cdot \sum_{i=1}^{N} \hat{\boldsymbol{\sigma}}_i. \tag{2.36}$$

Then, the commutation relation between the Hamiltonian (2.35) and the invariant (2.36) is given by

$$[\hat{\mathcal{H}}(t), \hat{F}(t)] = -2i \left\{ -\frac{f(t)J}{2N} \sum_{i,j=1}^{N} [(n^x \hat{\sigma}_i^y - n^y \hat{\sigma}_i^x) \hat{\sigma}_j^z + \hat{\sigma}_i^z (n^x \hat{\sigma}_j^y - n^y \hat{\sigma}_j^x)] \right. \tag{2.37}$$
$$\left. -f(t)h^z \sum_{i=1}^{N} (n^x \hat{\sigma}_i^y - n^y \hat{\sigma}_i^x) - h^x(t) \sum_{i=1}^{N} (n^y \hat{\sigma}_i^z - n^z \hat{\sigma}_i^y) \right\}.$$

Here we utilize the mean-field approximation

$$(n^x \hat{\sigma}_i^y - n^y \hat{\sigma}_i^x) \hat{\sigma}_j^z + \hat{\sigma}_i^z (n^x \hat{\sigma}_j^y - n^y \hat{\sigma}_j^x) \approx (n^x \langle \hat{\sigma}_i^y \rangle - n^y \langle \hat{\sigma}_i^x \rangle) \hat{\sigma}_j^z + (n^x \hat{\sigma}_i^y - n^y \hat{\sigma}_i^x) \langle \hat{\sigma}_j^z \rangle$$
$$+ \langle \hat{\sigma}_i^z \rangle (n^x \hat{\sigma}_j^y - n^y \hat{\sigma}_j^x) + \hat{\sigma}_i^z (n^x \langle \hat{\sigma}_j^y \rangle - n^y \langle \hat{\sigma}_j^x \rangle), \tag{2.38}$$

and introduce the mean-field ansatz

$$\langle \hat{\boldsymbol{\sigma}}_i \rangle \approx \boldsymbol{n}. \tag{2.39}$$

Then the commutation relation becomes

$$[\hat{\mathcal{H}}(t), \hat{F}(t)] = -2i \left\{ f(t)(Jn^z + h^z)n^y \sum_{i=1}^{N} \hat{\sigma}_i^x + [-f(t)(Jn^z + h^z)n^x + h^x(t)n^z] \sum_{i=1}^{N} \hat{\sigma}_i^y - h^x(t)n^y \sum_{i=1}^{N} \hat{\sigma}_i^z \right\}. \tag{2.40}$$

Therefore, Eqs. (1.60) and (2.33) lead to the auxiliary equations

$$\begin{cases} \dot{\gamma} = -2h^x(t)\sin\beta, \\ [2f(t)(J\cos\gamma + h^z) - \dot{\beta}]\sin\gamma = 2h^x(t)\cos\gamma\cos\beta. \end{cases} \tag{2.41}$$

Then, we design β and γ to obtain a target state and determine time-dependence of $h^x(t)$ and $f(t)$ from these auxiliary equations. Although this method shows high fidelity to the result of adiabatic time evolution, it cannot be applied to generic systems. Here we will see a generic Hamiltonian

$$\hat{\mathcal{H}}(t) = f(t) \left(-\frac{1}{2} \sum_{i,j=1}^{N} J_{ij} \hat{\sigma}_i^z \hat{\sigma}_j^z - \sum_{i=1}^{N} h_i^z \hat{\sigma}_i^z \right) - h^x(t) \sum_{i=1}^{N} \hat{\sigma}_i^x, \tag{2.42}$$

where J_{ij} and h_i^z are site-dependent random numbers, and J_{ij} satisfies $J_{ij} = J_{ji}$ and $J_{ii} = 0$. Similarly to the case of the Hamiltonian (2.35), we assume the following Lewis-Riesenfeld invariant

$$\hat{F}(t) = -\sum_{i=1}^{N} \boldsymbol{n}_i(t) \cdot \hat{\boldsymbol{\sigma}}_i, \tag{2.43}$$

where $\boldsymbol{n}_i(t)$ also becomes site-dependent. We again utilize the mean-field approximation and the site-dependent version of the mean-field ansatz

$$\langle \hat{\boldsymbol{\sigma}}_i \rangle \approx \boldsymbol{n}_i(t), \tag{2.44}$$

we obtain

$$[\hat{\mathcal{H}}(t), \hat{F}(t)] = -2i \sum_{i=1}^{N} \left\{ f(t) \left(\sum_{j=1}^{N} J_{ij} n_j^z + h_i^z \right) n_i^y \hat{\sigma}_i^x \right. $$
$$\left. - \left[f(t) \left(\sum_{j=1}^{N} J_{ij} n_j^z + h_i^z \right) n_i^x - h^x(t) n_i^z \right] \hat{\sigma}_i^y - h^x(t) n_i^y \hat{\sigma}_i^z \right\}. \tag{2.45}$$

By putting

$$\boldsymbol{n}_i(t) = \begin{pmatrix} \sin\gamma_i \cos\beta_i \\ -\sin\gamma_i \sin\beta_i \\ \cos\gamma_i \end{pmatrix}, \tag{2.46}$$

we obtain the auxiliary equations

$$\begin{cases} \dot{\gamma}_i = -2h^x(t) \sin\beta_i, \\ \left[2f(t) \left(\sum_{j=1}^{N} J_{ij} \cos\gamma_j + h_i^z \right) - \dot{\beta}_i \right] \sin\gamma_i = 2h^x(t) \cos\gamma_i \cos\beta_i. \end{cases} \tag{2.47}$$

However, for generic J_{ij} and h_i^z, to find parameters satisfying these auxiliary equations is hardly possible, i.e., it is difficult to apply the present method to generic problems of quantum annealing.

In the next chapter, we show a possible method of shortcuts to adiabaticity for quantum annealing, which is based on a classical model of quantum annealing and shortcuts to adiabaticity in classical spin systems.

Chapter 3

Shortcuts to adiabaticity for classical spin systems

In this chapter, we discuss shortcuts to adiabaticity for classical spin systems. In Sec. 3.1, we review classical spin dynamics and introduce the concept of stationary states and criticality. In Sec. 3.2, we discuss counter-diabatic terms for classical spin systems. Through a simple model, we demonstrate properties of our method in Sec. 3.3. We apply our method to a classical model of quantum annealing in Sec. 3.4. We summarize our method and results in Sec. 3.5. Note that this chapter is based on a series of the articles by the present author [30, 109].

3.1 Classical spin dynamics

First, we introduce canonical dynamics of classical spin systems. In this thesis, we define a classical spin as a three-dimensional unit vector

$$\boldsymbol{m}_i = (m_i^x, m_i^y, m_i^z), \quad |\boldsymbol{m}_i| = 1, \tag{3.1}$$

and consider classical spin systems consisting of N spins. Now, we consider a classical spin system described by a time-dependent Hamiltonian $\mathcal{H}_t(\{\boldsymbol{m}_i\})$. Dynamics of this system is governed by the torque equation

$$\dot{\boldsymbol{m}}_i(t) = 2\boldsymbol{m}_i(t) \times \boldsymbol{h}_i^{\text{eff}}(t), \tag{3.2}$$

where a dot represents the time derivative and $\boldsymbol{h}_i^{\text{eff}}(t)$ is an effective field applied to the ith spin, which is given by

$$\boldsymbol{h}_i^{\text{eff}}(t) = -\frac{\partial \mathcal{H}_t}{\partial \boldsymbol{m}_i}. \tag{3.3}$$

We can view this torque equation as the classical limit of the Heisenberg equation

$$i\frac{\partial}{\partial t}\langle \hat{\boldsymbol{\sigma}}_i(t) \rangle = \langle [\hat{\boldsymbol{\sigma}}_i(t), \hat{\mathcal{H}}(t)] \rangle, \tag{3.4}$$

where $\hat{\mathcal{H}}(t)$ is the quantum counterpart of the classical spin Hamiltonian $\mathcal{H}_t(\{\boldsymbol{m}_i\})$, which is given by

$$\hat{\mathcal{H}}(t) = \mathcal{H}_t(\{\hat{\boldsymbol{\sigma}}_i\}), \tag{3.5}$$

and $\hat{\boldsymbol{\sigma}}_i(t)$ is the Pauli matrices in the Heisenberg picture

$$\hat{\boldsymbol{\sigma}}_i(t) = \bar{\mathcal{T}} \exp\left[i \int_0^t dt' \hat{\mathcal{H}}(t')\right] \hat{\boldsymbol{\sigma}}_i \mathcal{T} \exp\left[-i \int_0^t dt' \hat{\mathcal{H}}(t')\right], \quad \hat{\boldsymbol{\sigma}}_i = (\hat{\sigma}_i^x, \hat{\sigma}_i^y, \hat{\sigma}_i^z). \tag{3.6}$$

Here, $\mathcal{T}$ is the time ordering operator and $\bar{\mathcal{T}}$ is the time anti-ordering operator.

We show the correspondence between the classical equations of motion (3.2) and the quantum equations of motion (3.4) by using an example. As an example, we consider the following time-dependent classical Ising Hamiltonian

$$\mathcal{H}_t(\{\boldsymbol{m}_i\}) = -\frac{1}{2} \sum_{i,j=1}^{N} J_{ij}(t) m_i^z m_j^z - \sum_{i=1}^{N} \boldsymbol{h}_i(t) \cdot \boldsymbol{m}_i, \tag{3.7}$$

where, $J_{ij}(t)$ is the strength of the Ising interaction and $\boldsymbol{h}_i = (h_i^x, h_i^y, h_i^z)$ is a local magnetic field. Here, we assume $J_{ij} = J_{ji}$ and $J_{ii} = 0$. Under this Hamiltonian, an effective field applied to the ith spin is given by

$$\begin{cases} h_i^{\mathrm{eff},x}(t) = h_i^x(t), \\ h_i^{\mathrm{eff},y}(t) = h_i^y(t), \\ h_i^{\mathrm{eff},z}(t) = \sum_{j=1}^{N} J_{ij}(t) m_j^z(t) + h_i^z(t), \end{cases} \tag{3.8}$$

and thus the classical equations of motion are given by

$$\begin{cases} \dot{m}_i^x(t) = 2 \left[\left(\sum_{j=1}^{N} J_{ij}(t) m_j^z(t) + h_i^z(t) \right) m_i^y(t) - h_i^y(t) m_i^z(t) \right], \\ \dot{m}_i^y(t) = 2 \left[h_i^x(t) m_i^z(t) - \left(\sum_{j=1}^{N} J_{ij}(t) m_j^z(t) + h_i^z(t) \right) m_i^x(t) \right], \\ \dot{m}_i^z(t) = 2[h_i^y(t) m_i^x(t) - h_i^x(t) m_i^y(t)]. \end{cases} \tag{3.9}$$

In contrast, by using Eq. (3.5), the quantum counterpart of the classical Hamiltonian (3.7) is given by

$$\hat{\mathcal{H}}(t) = -\frac{1}{2} \sum_{i,j=1}^{N} J_{ij}(t) \hat{\sigma}_i^z \hat{\sigma}_j^z - \sum_{i=1}^{N} \boldsymbol{h}_i(t) \cdot \hat{\boldsymbol{\sigma}}_i, \tag{3.10}$$

and then, the quantum equations of motion are given by

$$\begin{cases} \frac{\partial}{\partial t} \langle \hat{\sigma}_i^x(t) \rangle = 2 \left[\left\langle \left(\sum_{j=1}^{N} J_{ij}(t) \hat{\sigma}_j^z(t) + h_i^z(t) \right) \hat{\sigma}_i^y(t) \right\rangle - h_i^y(t) \langle \hat{\sigma}_i^z(t) \rangle \right], \\ \frac{\partial}{\partial t} \langle \hat{\sigma}_i^y(t) \rangle = 2 \left[h_i^x(t) \langle \hat{\sigma}_i^z(t) \rangle - \left\langle \left(\sum_{j=1}^{N} J_{ij}(t) \hat{\sigma}_j^z(t) + h_i^z(t) \right) \hat{\sigma}_i^x(t) \right\rangle \right], \\ \frac{\partial}{\partial t} \langle \hat{\sigma}_i^z(t) \rangle = 2[h_i^y(t) \langle \hat{\sigma}_i^x(t) \rangle - h_i^x(t) \langle \hat{\sigma}_i^y(t) \rangle]. \end{cases} \tag{3.11}$$

These equations of motion give quantum dynamics under the Hamiltonian (3.10). In this case, we have correlation terms, for example, $\langle \hat{\sigma}_i^z(t) \hat{\sigma}_j^x(t) \rangle$, and those lead to the Bogoliubov-Born-Green-Kirkwood-Yvon hierarchy of spin operators. However, this hierarchy is resolved when we take the classical limit, i.e., correlation terms are decomposed as $\langle \hat{\sigma}_i^z(t) \hat{\sigma}_j^x(t) \rangle \approx \langle \hat{\sigma}_i^z(t) \rangle \langle \hat{\sigma}_j^x(t) \rangle$ in the classical limit. Then, the classical equations of motion (3.9) and the quantum equations of motion (3.11) become identical. This correspondence holds even if we consider other classical spin Hamiltonians and their quantum counterparts.

Next, we will also view the classical equations of motion (3.2) as the canonical equations of motion. In order to show this viewpoint, we introduce canonical variables $\{q_i, p_i\}_{i=1}^N$ satisfying

$$\begin{cases} m_i^x = \sqrt{1-(2q_i)^2}\cos p_i, \\ m_i^y = -\sqrt{1-(2q_i)^2}\sin p_i, \\ m_i^z = 2q_i, \end{cases} \tag{3.12}$$

and then the canonical equations of motion are given by a set of the Hamilton equations

$$\dot{q}_i = \frac{\partial \mathcal{H}_t}{\partial p_i}, \quad \dot{p}_i = -\frac{\partial \mathcal{H}_t}{\partial q_i}. \tag{3.13}$$

Here, from Eq. (3.12), the following equations

$$\begin{cases} \dfrac{\partial \mathcal{H}_t}{\partial p_i} = \dfrac{\partial m_i^x}{\partial p_i}\dfrac{\partial \mathcal{H}_t}{\partial m_i^x} + \dfrac{\partial m_i^y}{\partial p_i}\dfrac{\partial \mathcal{H}_t}{\partial m_i^y} \\ \qquad = m_i^y \dfrac{\partial \mathcal{H}_t}{\partial m_i^x} - m_i^x \dfrac{\partial \mathcal{H}_t}{\partial m_i^y}, \\ \dfrac{\partial \mathcal{H}_t}{\partial q_i} = \dfrac{\partial m_i^x}{\partial q_i}\dfrac{\partial \mathcal{H}_t}{\partial m_i^x} + \dfrac{\partial m_i^y}{\partial q_i}\dfrac{\partial \mathcal{H}_t}{\partial m_i^y} + \dfrac{\partial m_i^z}{\partial q_i}\dfrac{\partial \mathcal{H}_t}{\partial m_i^z} \\ \qquad = \dfrac{-2m_i^z m_i^x}{m_i^{x2}+m_i^{y2}}\dfrac{\partial \mathcal{H}_t}{\partial m_i^x} + \dfrac{-2m_i^z m_i^y}{m_i^{x2}+m_i^{y2}}\dfrac{\partial \mathcal{H}_t}{\partial m_i^y} + 2\dfrac{\partial \mathcal{H}_t}{\partial m_i^z}, \end{cases} \tag{3.14}$$

and

$$\begin{cases} \dot{m}_i^x = \dfrac{\partial m_i^x}{\partial q_i}\dot{q}_i + \dfrac{\partial m_i^x}{\partial p_i}\dot{p}_i \\ \qquad = \dfrac{-2m_i^z m_i^x}{m_i^{x2}+m_i^{y2}}\dot{q}_i + m_i^y \dot{p}_i, \\ \dot{m}_i^y = \dfrac{\partial m_i^y}{\partial q_i}\dot{q}_i + \dfrac{\partial m_i^y}{\partial p_i}\dot{p}_i \\ \qquad = \dfrac{-2m_i^z m_i^y}{m_i^{x2}+m_i^{y2}}\dot{q}_i - m_i^x \dot{p}_i, \\ \dot{m}_i^z = \dfrac{\partial m_i^z}{\partial q_i}\dot{q}_i \\ \qquad = 2\dot{q}_i, \end{cases} \tag{3.15}$$

hold. By using Eqs. (3.13) and (3.14), Eq. (3.15) becomes the classical equations of motion (3.2), and thus we can view the classical equations of motion (3.2) as the canonical equations of motion.

Now, we introduce the concept of instantaneous stationary states and their criticality. An instantaneous stationary state $\{\boldsymbol{m}_i\}$ is specified by a minimum of the Hamiltonian $\mathcal{H}_t(\{\boldsymbol{m}_i\})$ as a function of canonical variables

$$\boldsymbol{z} = \{q_1, q_2, \cdots, q_N; p_1, p_2, \cdots, p_N\}, \tag{3.16}$$

i.e., defined by $\{\boldsymbol{m}_i\}$ satisfying

$$\frac{\partial \mathcal{H}_t}{\partial \boldsymbol{z}} = 0. \tag{3.17}$$

From Eq. (3.13), this condition is identical to

$$\dot{\boldsymbol{z}} = \{\dot{q}_1, \dot{q}_2, \cdots, \dot{q}_N; \dot{p}_1, \dot{p}_2, \cdots, \dot{p}_N\} = 0, \tag{3.18}$$

i.e., instantaneous stationary states are nothing but states at classical fixed points. In particular, the instantaneous stationary state corresponding to the global minimum of the Hamiltonian $\mathcal{H}_t(\{\boldsymbol{m}_i\})$ is

called the instantaneous ground state. An instantaneous stationary state is called critical when the determinant of the Hessian matrix is also zero

$$\det\left[\frac{\partial^2 \mathcal{H}_t}{\partial z_i \partial z_j}\right] = 0. \tag{3.19}$$

From Eq. (3.13), this condition is identical to

$$\det\left[\frac{\partial \dot{z}_j}{\partial z_i}\right] = 0, \tag{3.20}$$

i.e., the determinant of the Jacobian matrix of $\dot{z}$ as a function of z is zero. It implies that mapping between z and $\dot{z}$ is not bijection or that the inverse of $\dot{z}$ as a function of z is not differentiable.

3.2 Classical counter-diabatic driving

In this section, we introduce exact counter-diabatic driving for classical spin systems. The main point is that any state of classical spin systems can be described by using product states of two-level quantum systems, and thus counter-diabatic Hamiltonians for classical spin systems should be constructed by using the counter-diabatic Hamiltonian for a two-level system (1.73).

From Eq. (3.2), we can view a classical spin in a classical spin system as a two-level system under a magnetic field (3.3), and thus the counter-diabatic term for this classical spin should be given by the counter-diabatic Hamiltonian (1.73) with the counter-diabatic field (1.74) under a magnetic field (3.3). Therefore, for a given classical spin system described by a Hamiltonian $\mathcal{H}_t(\{\boldsymbol{m}_i\})$, the counter-diabatic Hamiltonian should be given by

$$\mathcal{H}_t^{\mathrm{cd}}(\{\boldsymbol{m}_i\}) = \sum_{i=1}^{N} \boldsymbol{f}_i(t) \cdot \boldsymbol{m}_i, \tag{3.21}$$

where $\boldsymbol{f}_i(t)$ is the counter-diabatic field

$$\boldsymbol{f}_i(t) = \frac{\boldsymbol{h}_i^{\mathrm{eff}}(t) \times \dot{\boldsymbol{h}}_i^{\mathrm{eff}}(t)}{2|\boldsymbol{h}_i^{\mathrm{eff}}(t)|^2}. \tag{3.22}$$

Then classical equations of motion under the total Hamiltonian

$$\mathcal{H}_t^{\mathrm{tot}}(\{\boldsymbol{m}_i\}) = \mathcal{H}_t(\{\boldsymbol{m}_i\}) + \mathcal{H}_t^{\mathrm{cd}}(\{\boldsymbol{m}_i\}), \tag{3.23}$$

are given by

$$\dot{\boldsymbol{m}}_i(t) = 2\boldsymbol{m}_i(t) \times [\boldsymbol{h}_i^{\mathrm{eff}}(t) - \boldsymbol{f}_i(t)]. \tag{3.24}$$

This counter-diabatic Hamiltonian (3.21) is actually the exact counter-diabatic Hamiltonian for classical spin systems and the solution of Eq. (3.24) is an instantaneous stationary state if the initial state is an instantaneous stationary state. Indeed, the angle $\theta_i(t)$ between a classical spin $\boldsymbol{m}_i(t)$ and a corresponding effective field $\boldsymbol{f}_i(t)$ is always conserved. By differentiating the following quantity

$$\cos\theta_i(t) = \boldsymbol{m}_i(t) \cdot \frac{\boldsymbol{h}_i^{\mathrm{eff}}(t)}{|\boldsymbol{h}_i^{\mathrm{eff}}(t)|}, \tag{3.25}$$

with respect to time t, we obtain

$$\begin{aligned}
\frac{d}{dt}\cos\theta_i(t) &= \dot{\boldsymbol{m}}_i(t) \cdot \frac{\boldsymbol{h}_i^{\mathrm{eff}}(t)}{|\boldsymbol{h}_i^{\mathrm{eff}}(t)|} + \boldsymbol{m}_i(t) \cdot \frac{d}{dt}\frac{\boldsymbol{h}_i^{\mathrm{eff}}(t)}{|\boldsymbol{h}_i^{\mathrm{eff}}(t)|} \\
&= 2\{\boldsymbol{m}_i(t) \times [\boldsymbol{h}_i^{\mathrm{eff}}(t) - \boldsymbol{f}_i(t)]\} \cdot \frac{\boldsymbol{h}_i^{\mathrm{eff}}(t)}{|\boldsymbol{h}_i^{\mathrm{eff}}(t)|} + \boldsymbol{m}_i(t) \cdot \frac{d}{dt}\frac{\boldsymbol{h}_i^{\mathrm{eff}}(t)}{|\boldsymbol{h}_i^{\mathrm{eff}}(t)|} \\
&= -2[\boldsymbol{m}_i(t) \times \boldsymbol{f}_i(t)] \cdot \frac{\boldsymbol{h}_i^{\mathrm{eff}}(t)}{|\boldsymbol{h}_i^{\mathrm{eff}}(t)|} + \boldsymbol{m}_i(t) \cdot \frac{d}{dt}\frac{\boldsymbol{h}_i^{\mathrm{eff}}(t)}{|\boldsymbol{h}_i^{\mathrm{eff}}(t)|}.
\end{aligned} \tag{3.26}$$

Here, we have

$$2\boldsymbol{m}_i(t) \times \boldsymbol{f}_i(t) = \frac{\boldsymbol{m}_i(t) \times (\boldsymbol{h}_i^{\mathrm{eff}}(t) \times \dot{\boldsymbol{h}}_i^{\mathrm{eff}}(t))}{|\boldsymbol{h}_i^{\mathrm{eff}}(t)|^2}$$

$$= \frac{(\boldsymbol{m}_i(t) \cdot \dot{\boldsymbol{h}}_i^{\mathrm{eff}}(t))\boldsymbol{h}_i^{\mathrm{eff}}(t) - (\boldsymbol{m}_i(t) \cdot \boldsymbol{h}_i^{\mathrm{eff}}(t))\dot{\boldsymbol{h}}_i^{\mathrm{eff}}(t)}{|\boldsymbol{h}_i^{\mathrm{eff}}(t)|^2}, \tag{3.27}$$

and

$$\frac{d}{dt}\frac{\boldsymbol{h}_i^{\mathrm{eff}}(t)}{|\boldsymbol{h}_i^{\mathrm{eff}}(t)|} = \frac{\boldsymbol{h}_i^{\mathrm{eff}}(t)}{|\boldsymbol{h}_i^{\mathrm{eff}}|} - \frac{\boldsymbol{h}_i^{\mathrm{eff}}(t) \cdot \dot{\boldsymbol{h}}_i^{\mathrm{eff}}(t)}{|\boldsymbol{h}_i^{\mathrm{eff}}(t)|^3}, \tag{3.28}$$

and thus

$$\frac{d}{dt}\cos\theta_i(t) = 0. \tag{3.29}$$

Starting from the ground state, stationary state tracking remains in the ground state if neither first order transitions nor criticality take place. It should be noted that stationary state tracking results in one of the metastable states if a first order transition takes place, or in even divergence if criticality happens. It should be also noted that we do not need to know tracked instantaneous stationary states but just solve Eq. (3.24), then we can track instantaneous stationary states.

Note that the counter-diabatic Hamiltonian (3.21) can be obtained by using the mean-field approximation in the corresponding quantum spin Hamiltonian. For a quantum spin Hamiltonian $\hat{\mathcal{H}}(t) = \mathcal{H}_t(\{\boldsymbol{\sigma}_i\})$, the mean-field approximation leads to

$$\hat{\mathcal{H}}_{\mathrm{MF}}(t) = -\sum_{i=1}^{N} \boldsymbol{h}_i^{\mathrm{eff}}(t) \cdot \hat{\boldsymbol{\sigma}}_i, \tag{3.30}$$

which is an ensemble of N two-level systems. The counter-diabatic Hamiltonian for this Hamiltonian is given by

$$\hat{\mathcal{H}}_{\mathrm{MF}}^{\mathrm{cd}}(t) = \sum_{i=1}^{N} \boldsymbol{f}_i(t) \cdot \hat{\boldsymbol{\sigma}}_i. \tag{3.31}$$

This can be also used as the classical-approximate counter-diabatic Hamiltonian for the original quantum spin Hamiltonian $\hat{\mathcal{H}}(t)$. In this case, we first solve Eq. (3.24) to obtain classical stationary dynamics and then construct counter-diabatic fields (3.22).

3.3 Demonstration in a simple model

In this section, we show basic properties of our method. Here, we introduce the following paradigmatic model

$$\mathcal{H}_t(\{\boldsymbol{m}_i\}) = -\frac{J}{2N}\sum_{i,j=1}^{N} m_i^z m_j^z - h^z(t)\sum_{i=1}^{N} m_i^z - h^x(t)\sum_{i=1}^{N} m_i^x, \tag{3.32}$$

where the coupling strength J is a positive constant. By introducing the quantity

$$m_\alpha(t) = \frac{1}{N}\sum_{i=1}^{N} m_i^\alpha(t), \quad \alpha = x, y, z, \tag{3.33}$$

the Hamiltonian (3.32) is rewritten as

$$\mathcal{H}_t(\{\boldsymbol{m}\}) = N\left(-\frac{J}{2}m_z^2 - h^z(t)m_z - h^x(t)m_x\right). \tag{3.34}$$

This model has been widely investigated in various context. Without a transverse field this model is known as the Husimi-Temperley model [153, 154] and also the Curie-Weiss model [155], and with a

transverse field as the Stoner-Wohlfarth model [156]. From the Hamiltonian (3.34), stationary states should be states on the x-z plane. Therefore, in order to find stationary states, we set

$$\begin{cases} m_x = \sin\theta, \\ m_z = \cos\theta, \end{cases} \tag{3.35}$$

and thus energy of stationary states is given by

$$E = N\left(-\frac{J}{2}\cos^2\theta - h^z\cos\theta - h^x\sin\theta\right), \tag{3.36}$$

where θ satisfies

$$\frac{\partial E}{\partial\theta} = N(J\sin\theta\cos\theta + h^z\sin\theta - h^x\cos\theta) = 0. \tag{3.37}$$

The spinodal line, where a metastable state becomes unstable, is specified by Eq. (3.37) and

$$\frac{\partial^2 E}{\partial\theta^2} = N[J(\cos^2\theta - \sin^2\theta) + h^z\cos\theta + h^x\sin\theta] = 0. \tag{3.38}$$

Equations (3.37) and (3.38) lead to

$$\begin{cases} h^x - J\sin^3\theta = 0, \\ h^z + J\cos^3\theta = 0, \end{cases} \tag{3.39}$$

and thus

$$\frac{h^x}{h^z} = -\tan^3\theta, \tag{3.40}$$

holds. By using this equation, the condition (3.37) becomes

$$J^{2/3} = (h^x)^{2/3} + (h^z)^{2/3}. \tag{3.41}$$

This condition gives the spinodal line, which is also called the Stoner-Wohlfarth astroid [156, 157]. Note that this condition is identical to the condition of criticality (3.19) in this model. We depict the phase diagram of this model in Fig. 3.1.

Here we demonstrate the following three cases: (i) no transition takes place, (ii) a first order transition takes place, and (iii) the system undergoes criticality after a first order transition. These cases can be realized by assuming the magnetic fields as

$$\begin{cases} h^x(t) = h_0\sin\dfrac{\pi t}{\tau}, \\ h^z(t) = \dfrac{J}{2}\cos\dfrac{\pi t}{\tau}, \end{cases} \tag{3.42}$$

and by tuning a parameter h_0. Here τ is the operation time. With these magnetic fields, we can test above three cases, i.e., with a parameter h_0 satisfying (i) $h_0/J > 1$, (ii) $0 < h_0/J < 1/2$, and (iii) $1/2 \leq h_0/J \leq 1$, with the same initial and final parameters, i.e.,

$$\begin{cases} h^x(0) = 0, \quad h^z(0) = \dfrac{J}{2}, \\ h^x(\tau) = 0, \quad h^z(\tau) = -\dfrac{J}{2}. \end{cases} \tag{3.43}$$

The ground state with these initial parameters becomes the spin up state, and the ground (metastable) state with these final parameters becomes the spin down (up) state. We perform numerical simulations with the parameters (i) $h_0/J = 5/4$ (purple curves), (ii) $h_0/J = 1/4$ (green curves), and (iii) $h_0/J = 3/4$ (cyan curves), and depict the results in Fig. 3.2. The result of numerical simulations clearly shows the expected properties of our method.
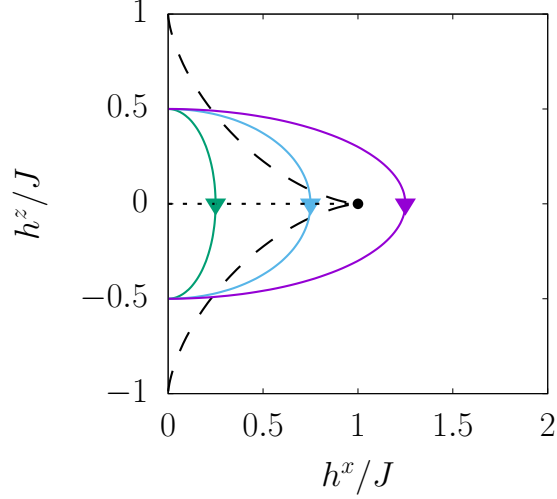
Figure3.1   Phase diagram of the classical Hamiltonian (3.32). The horizontal axis is the transverse magnetic field and the vertical axis is the longitudinal magnetic field. Both axes are scaled by the strength of interaction. The dotted line represents the points showing first order transitions, i.e., the ground state shows a first order transition there. The dashed curve and the black dot represent the points showing criticality. A metastable state shows criticality at the dashed line and the ground state shows criticality at the black dot. Three arrows represent schemes that we will consider. This figure is the reuse of the published article [30].
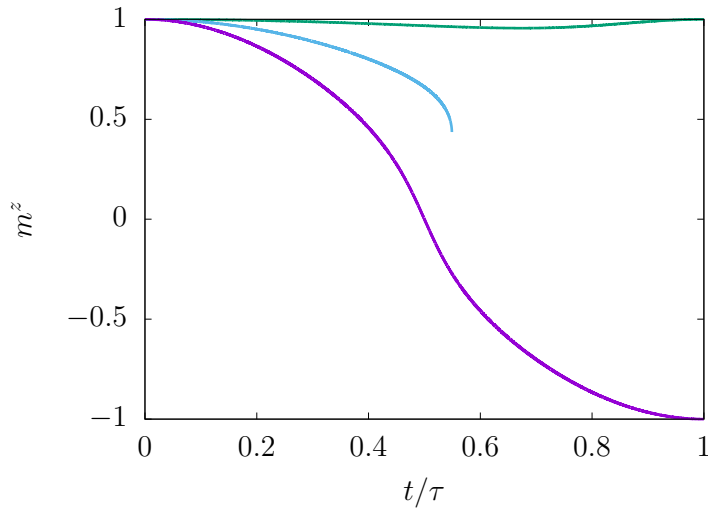
Figure3.2   Instantaneous stationary magnetization dynamics tracked by our method. The horizontal axis is time scaled by the operation time. The vertical axis is magnetization. Our method results in (i; purple) the exact ground state, (ii; green) the metastable state due to a first order transition, and (iii; cyan) divergence due to criticality. These three curves are associated with three arrows in Fig. 3.1. This figure is the reuse of the published article [30].

30

3.4 Mimicking the procedure of quantum annealing

In this section we attempt applying our method to the procedure of quantum annealing by considering a classical model of quantum annealing and its classical spin dynamics.

As explained in Sec. 2.3.2, we replace the Pauli matrices with classical spins expressed by three-dimensional unit vectors as

$$\hat{\boldsymbol{\sigma}}_i \to \boldsymbol{m}_i, \tag{3.44}$$

where $\boldsymbol{m}_i$ satisfies $|\boldsymbol{m}_i| = 1$. Then, the Hamiltonian of a classical model of quantum annealing is given by

$$\mathcal{H}_t = g(t/\tau)\mathcal{H}_P + [1 - g(t/\tau)]\mathcal{H}_V, \tag{3.45}$$

where the classical problem Hamiltonian and the classical driver Hamiltonian are given by

$$\mathcal{H}_P = -\frac{1}{2}\sum_{i,j=1}^{N} J_{ij} m_i^z m_j^z - \sum_{i=1}^{N} h_i^z m_i^z, \tag{3.46}$$

and

$$\mathcal{H}_V = -\sum_{i=1}^{N} h_i^x m_i^x. \tag{3.47}$$

Here, $g(t/\tau)$ is a differentiable function of time satisfying $g(0) = 0$ and $g(1) = 1$. We assume

$$g(t/\tau) = \frac{1}{2}\left[1 - \cos\frac{\pi t}{\tau}\right], \tag{3.48}$$

with which the counter-diabatic terms for the Hamiltonian (3.45) disappear at the initial and final time. It should be noted that the ground state of the classical problem Hamiltonian (3.46) and that of the quantum problem Hamiltonian

$$\hat{\mathcal{H}}_P = -\frac{1}{2}\sum_{i,j=1}^{N} J_{ij} \hat{\sigma}_i^z \hat{\sigma}_j^z - \sum_{i=1}^{N} h_i^z \hat{\sigma}_i^z, \tag{3.49}$$

are identical. Therefore, the problem to obtain the ground state of the quantum problem Hamiltonian (3.49), which is the goal of quantum annealing, i.e., combinatorial problems, is equivalent to the problem to obtain the ground state of the classical problem Hamiltonian (3.46). Now, starting from the ground state of the initial Hamiltonian $\mathcal{H}_0 = \mathcal{H}_V$, we expect to reach the ground state of the final Hamiltonian $\mathcal{H}_\tau = \mathcal{H}_P$ by using our method. However, as demonstrated in the previous section, this does not always happen. When a first order transition takes place, the ground state becomes a metastable state. In addition to that, numerical simulations show even divergence if the criticality happens.

Hereafter, we consider the random field Ising model on the $L \times L$ square lattice, which can be exactly solved by using the maximum flow and minimum cut algorithm (see Appendix B.2 for details), and thus we can compare our method with the exact results. Here, the number of spins is given by $N = L^2$. For a fixed uniform interaction $J_{ij} = J$ and random longitudinal magnetic fields $\{h_i^z\}$, we repeat M simulations with different realization of random transverse magnetic fields $\{h_i^x\}$. We further repeat this process K times with different realization of random longitudinal magnetic fields $\{h_i^z\}$. Note that our method is free from the annealing time τ, and here we assume $\tau = 1$.

First we study a single shot. Here we assume that $M = 1$ and uniform transverse magnetic fields $h_i^x = h^x$. For other parameters, we set $J = 1$, $h_i^z = \pm 0.3$, $h^x = 1$, and $K = 3456$. We test with various system sizes and plot the failure probability obtaining the ground state in Fig. 3.3. For small system sizes $L \leq 8$ ($N \leq 64$), the failure probability is less than 1%, i.e., we can obtain the ground state with probability more than 99%. For system sizes around $L \sim 10$ ($N \sim 100$), the failure (success)
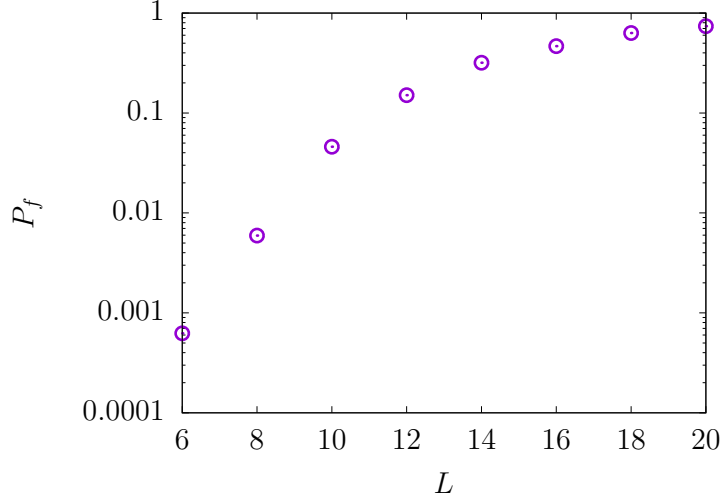
Figure3.3 Failure probability with respect to the system size. The horizontal axis represents system size and the vertical axis represents the failure probability due to first order transitions or criticality. The number of spins is given by $N = L^2$. This figure is the reuse of the published article [30].

probability is still around $\sim 10\%$ ($\sim 90\%$). However, the failure probability rapidly becomes worse and worse along with the system size. The failure happens due to the occurrence of first order transitions or criticality, and thus this result shows that the probability of these transitions and criticality grows rapidly along with increase of the system size. This could be associated with that number of possible states exponentially increases with the system size.

Next, we try inhomogeneous driving [133, 141–151]. Here we consider various M repetitions with different realization of random transverse magnetic fields $\{h_i^x\}$. We assume that random transverse magnetic fields are given by uniform random numbers $h_i^x \in [1, 2]$ and the other parameters are similar to the above case. Here we show that the failure probabilities decrease with increasing repetition M in Fig. 3.4. The way of decrease for fixed N would be given by

$$P_f \sim M^{-\gamma} \tag{3.50}$$

with an exponent γ. Therefore, with respect to the repetition of inhomogeneous driving M, the failure (success) probability decreases (increases) in a polynomial way. However, rate of decreasing γ becomes smaller and smaller along with system sizes. Indeed, as plotted in Fig. 3.5, the exponent γ seems to decrease in an exponential way

$$\gamma \sim e^{-\mathcal{O}(N)}. \tag{3.51}$$

This result implies that resolution of failures in our method would be exponentially hard along with system sizes. Therefore, unfortunately our method is not efficient to solve combinatorial optimization problems. This difficulty would also happen in genuine quantum annealing if quantumness is weak.

3.5 Summary

In this chapter, we discussed shortcuts to adiabaticity for classical spin systems. For the derivation of the counter-diabatic terms for a classical spin system, we utilized the analogy to a two-level systems because any state of a classical spin system can be described by using a product state of two-level systems. We also mentioned that the same counter-diabatic terms can be obtained by using the mean-field approximation in the corresponding quantum spin systems. We showed that our method can conserve angles between
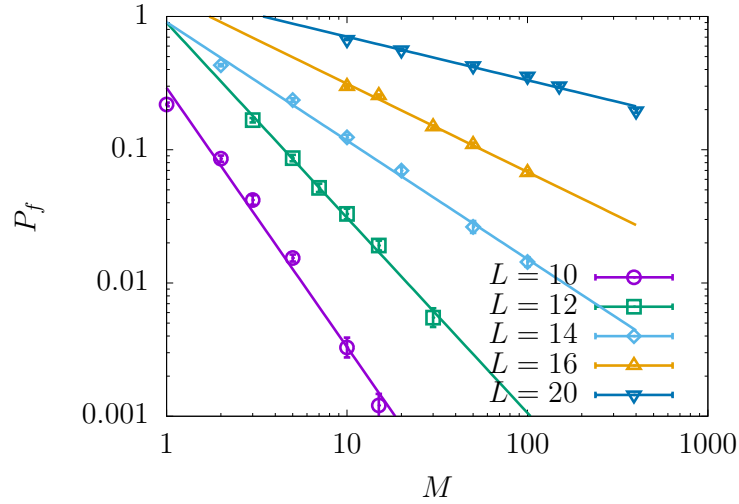
Figure3.4 Failure probability with respect to the repetition of inhomogeneous driving. The horizontal axis represents number of repetitions and the vertical axis is the failure probability. The system size is depicted from $L = 10$ to $L = 20$ (from $N = 100$ to $N = 400$). The error bars represent the standard errors of the binomial distribution. This figure is the reuse of the published article [30].
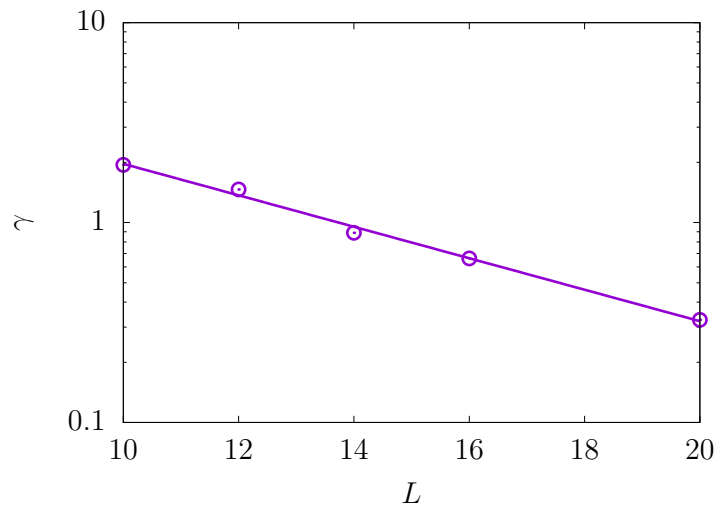
Figure3.5 Decreasing rate of the failure probability with respect to the system size. The horizontal axis represents system size and the vertical axis represents the exponent of decreasing. This figure is the reuse of the published article [30].

each classical spin and an effective field applied to it during time evolution. It means that if the initial state is given by a stationary state, then the system always tracks an instantaneous stationary state that originates in the initial stationary state. It should be stressed that our method can be implemented without knowing tracked instantaneous stationary states.

We demonstrated the basic properties of our method by using the simple model. Starting from the ground state, it was shown that stationary state tracking results in a metastable state when a first order transition takes place and in divergence when the criticality happens. We can obtain the exact ground state if neither first order transitions nor criticality take place.

We also applied our method to a classical model of quantum annealing. In this case, we can exactly solve problems that do not show first order transitions and criticality. However, we deterministically fail in obtaining the exact solution when a first order transition takes place and even in obtaining an approximate solution when criticality happens. We utilized the random-field Ising model on the $L \times L$ square lattice, which can be exactly solved by using the maximum flow and minimum cut algorithm. We found that a number of such failure in obtaining the exact ground state rapidly increases along with the system size. We attempted resolving this difficulty by making use of inhomogeneous driving. We found that first order transitions and criticality can be actually removed when we apply inhomogeneous driving. However, it was also found that to find such inhomogeneity is exponentially hard with respect to the system size. Our results would give insight into genuine quantum annealing.

Chapter 4

Macroscopic entanglement generation in bosonic Josephson junctions

In this chapter, we introduce the concept of macroscopically entangled states and bosonic Josephson junctions. After an overview in Sec. 4.1, we introduce the quantum Fisher information through the framework of quantum metrology and characterize macroscopic entanglement in Sec. 4.2. We review collective spin systems and consider their entangled states in Sec. 4.3. In Sec. 4.4, We introduce bosonic Josephson junctions, which can be described as collective spin systems. We consider shortcuts to adiabaticity for bosonic Josephson junctions in Sec. 4.5.

4.1   Overview

Entanglement is a resource of weird phenomena in quantum mechanics and also a resource of quantum science and technologies. It actually leads to counter-intuitive phenomena, for example, non-locality of quantum mechanics [158]. However, this example does not imply incompleteness of quantum mechanics. Indeed, we can observe non-locality of quantum mechanics in experiments [159]. Moreover, this weird phenomenon can actually be utilized as a resource of quantum science and technologies. For instance, quantum teleportation enables us to transfer an unknown quantum state to a distant place [160]. This technique can be applied to quantum communication [161] and quantum computation [162]. In this manner, now is the time to exploit weirdness of quantum mechanics as a resource of new technologies.

The Schrödinger's cat is also such an illustrative example of weired quantum phenomena [163–165], which has caused a fundamental question of macroscopic realism [166–168]. Not only the fundamental interest, but also cat states, which are superpositions of macroscopically distinct states, can bring a lot of benefit in practical use. One of such application is quantum metrology [11–13]. In quantum metrology, macroscopically entangled states enable us to estimate unknown parameters with high precision beyond the classical limitation [14–16]. Cat states have been realized in various systems, for example, an atom with classically distinct properties [169, 170], counter-propagating current states in a superconducting quantum interference device [171], coherent states of photons [172–174], qubits consisting of photons [175], a single-molecular magnet [176, 177], and trapped atoms [178–180]. We can implement quantum metrology with these cat states by using similar interferometric protocols nevertheless these cat states consist of quite different physical systems. This is because interferometric protocols can be viewed as mathematically equivalent processes known as the quantum Rosetta stone for interferometry, which showed that three interferometric protocols, i.e., the Mach-Zehnder interferometer, the Ramsey spectroscopy, and the quantum logic circuit, are equivalent [181]. However, it should be noted that unknown parameters, which we can estimate, differ depending on physical systems. Therefore, it is important to create cat states in various physical systems. However, concerning atomic systems, number of atoms forming cat states is still limited up to a dozen of atoms [178–180]. It has been expected to create cat states in large atomic systems beyond systems consisting of a dozen of trapped ions.

Bose-Einstein condensates can be candidates for such atomic systems because of their controlability and

isolatedness. Indeed, it is known that the ground state of a bosonic Josephson junction, which consists of two coupled Bose-Einstein condensates, can be a cat state [182, 183]. However, there is no experiments realizing cat states in bosonic Josephson junctions. This is because decoherence easily destroys cat states. In particular, it is known that particle losses, which are inevitable in Bose-Einstein condensation experiments, disturb formation of cat states in bosonic Josephson junctions [184]. Speedup of generation schemes could be one of the resolution of minimizing bad influence of particle losses. Therefore, we are interested in shortcuts to adiabaticity in bosonic Josephson junctions.

4.2 Macroscopic entanglement

First we introduce the concept of the quantum Fisher information through the idea of quantum metrology and after that we define macroscopic entanglement by using the quantum Fisher information. In quantum metrology [11–13], we estimate an unknown parameter θ from an outcome of measurement μ. For simplicity, we assume that the parameter θ and the outcome μ are one-dimensional parameters. Here, we denote the probability distribution of the outcome μ when the unknown parameter is θ by $P(\mu|\theta)$. We introduce an estimator $\Theta(\mu)$, which outputs an estimated value of θ from the outcome of measurement μ. The mean value of estimation and its variance are given by

$$\bar{\Theta} = \sum_\mu P(\mu|\theta)\Theta(\mu), \tag{4.1}$$

and

$$(\Delta\Theta)^2 = \sum_\mu P(\mu|\theta)[\Theta(\mu) - \bar{\Theta}]^2. \tag{4.2}$$

This estimator is called a locally unbiased estimator when $\bar{\Theta} = \theta$. For such a locally unbiased estimator, the variance (4.2) is bounded as

$$(\Delta\Theta)^2 \geq (\Delta\theta_{\mathrm{CR}})^2 = \frac{1}{F(\theta)}, \tag{4.3}$$

where $F(\theta)$ is the Fisher information [185, 186]

$$F(\theta) = \sum_\mu \frac{1}{P(\mu|\theta)} \left(\frac{\partial P(\mu|\theta)}{\partial\theta} \right)^2. \tag{4.4}$$

Here, $\Delta\theta_{\mathrm{CR}}$ is called the Cramér-Rao bound [187–189]. The equality holds when

$$\frac{\partial}{\partial\theta} \log P(\mu|\theta) = \lambda[\Theta(\mu) - \bar{\Theta}], \tag{4.5}$$

where λ is a real number (see Appendix A.6, for a proof of the Cramér-Rao bound). The Cramér-Rao bound implies that a given probe state, which gives the probability distribution, is potentially useful to estimate an unknown parameter when it gives large Fisher information. Note that when independent and identically distributed measurement is performed ν times, the Cramér-Rao bound is improved as $F(\theta) \to \nu F(\theta)$, which is a consequence of the additivity of the Fisher information. More generally, the Fisher information $F(\theta) = F[P(\mu|\theta)]$ satisfies the convexity [190]

$$F[pP(\mu|\theta) + (1-p)\bar{P}(\mu|\theta)] \leq pF[P(\mu|\theta)] + (1-p)F[\bar{P}(\mu|\theta)], \tag{4.6}$$

and, by assuming $P(\mu|\theta) = \prod_{i=1}^\nu P^{(i)}(\mu_i|\theta)$ and $\mu = \{\mu_1, \mu_2, \cdots, \mu_\nu\}$, the additivity [191]

$$F[P(\mu|\theta)] = \sum_{i=1}^\nu F[P^{(i)}(\mu_i|\theta)], \tag{4.7}$$

(see Appendix. A.7, for derivation of these properties).

In quantum mechanics, the probability distribution is given by

$$P(\mu|\theta) = \text{Tr}[\hat{\rho}_\theta \hat{E}_\mu], \tag{4.8}$$

where $\hat{\rho}_\theta$ is the density operator and $\hat{E}_\mu$ is positive operator-valued measurement, i.e., it satisfies

$$\hat{E}_\mu \geq 0, \quad \sum_\mu \hat{E}_\mu = 1. \tag{4.9}$$

The Fisher information is rewritten as

$$F(\theta) = F[\hat{\rho}_\theta] = \sum_\mu \frac{\{\text{Tr}[(\partial_\theta \hat{\rho}_\theta)\hat{E}_\mu]\}^2}{\text{Tr}[\hat{\rho}_\theta \hat{E}_\mu]}, \tag{4.10}$$

which apparently depends on a choice of the positive operator-valued measurement. The maximum value of the Fisher information is called the quantum Fisher information [192, 193] and given by

$$F_Q[\hat{\rho}_\theta] = \max_{\hat{E}_\mu} F[\hat{\rho}_\theta] = \sum_{k,l} \frac{2}{p_k + p_l} |\langle k|(\partial_\theta \hat{\rho}_\theta)|l\rangle|^2, \tag{4.11}$$

where $\{p_k\}$ and $\{|k\rangle\}$ are given by the spectral decomposition of the density operator

$$\hat{\rho}_\theta = \sum_k p_k |k\rangle\langle k|. \tag{4.12}$$

Here, the positive operator valued measurement which maximizes the Fisher information satisfies

$$\hat{E}_\mu \{1 - \lambda R_{\hat{\rho}_\theta}^{-1}[\partial_\theta \hat{\rho}_\theta]\}\hat{\rho}_\theta = 0, \tag{4.13}$$

where λ is a real number and $R_{\hat{\rho}_\theta}^{-1}[\cdot]$ is a super-operator defined by

$$R_{\hat{\rho}_\theta}^{-1}[\hat{A}] = \frac{2}{p_k + p_l} \langle k|\hat{A}|l\rangle |k\rangle\langle l|. \tag{4.14}$$

If a probe state is given by a pure state, i.e., $\hat{\rho}_\theta = |\psi_\theta\rangle\langle\psi_\theta|$, the quantum Fisher information can be written as

$$F_Q[\hat{\rho}_\theta] = 4\langle \partial_\theta \psi_\theta|[1 - |\psi_\theta\rangle\langle\psi_\theta|]|\partial_\theta \psi_\theta\rangle, \tag{4.15}$$

(see Appendix A.8, for derivation of the quantum Fisher information). Note that the quantum Fisher information for a mixed state is associated with the Bures metric and that for a pure state is associated with the Fubini-Study metric, which can be understood as the distance in the Hilbert space [192, 193].

Then the convexity and the additivity of the Fisher information show important properties. For a mixed state $\hat{\rho} = p\hat{\rho}^{(1)} + (1-p)\hat{\rho}^{(2)}$, $0 < p < 1$, the convexity of the Fisher information leads to

$$F_Q[\hat{\rho}] \leq pF_Q[\hat{\rho}^{(1)}] + (1-p)F_Q[\hat{\rho}^{(2)}], \tag{4.16}$$

which implies that classical probabilistic mixture never increases the quantum Fisher information. Next, for a product state $\hat{\rho} = \bigotimes_{i=1}^{\nu} \hat{\rho}^{(i)}$, the additivity of the Fisher information leads to

$$F_Q[\hat{\rho}] = \sum_{i=1}^{\nu} F_Q[\hat{\rho}^{(i)}], \tag{4.17}$$

which implies that the quantum Fisher information of classical (product) states can be calculated by summing up the quantum Fisher information of each subsystem.

For a probe state, which satisfies

$$i\frac{\partial \hat{\rho}_\theta}{\partial \theta} = [\hat{A}, \hat{\rho}_\theta], \tag{4.18}$$

where $\hat{A}$ is a certain Hermitian operator, the quantum Fisher information can be rewritten as

$$F_Q[\hat{\rho}_\theta] = 2 \sum_{k,l} \frac{(p_k - p_l)^2}{p_k + p_l} |\langle k|\hat{A}|l\rangle|^2. \tag{4.19}$$

For a pure state, the quantum Fisher information becomes

$$F_Q[\hat{\rho}_\theta] = 4\langle (\Delta \hat{A})^2 \rangle, \tag{4.20}$$

which is quadruple of the variance of $\hat{A}$. Suppose that an Hermitian operator $\hat{A}$ is given by $\hat{A} = \sum_{i=1}^N \hat{A}^{(i)}$, where each $\hat{A}^{(i)}$ acts on each subsystem and its eigenvalue is of the order of $\mathcal{O}(1)$. Then, the additivity of the quantum Fisher information implies that the quantum Fisher information of a classical state is not more that $F_Q \sim N$, which is called the standard quantum limit. In other words, if the quantum Fisher information of a given state is larger than N, then the given state is a non-classical state, i.e., an entangled state. Because the quantum Fisher information is given by the variance of $\hat{A}$, the maximum value of the quantum Fisher information concerning the operator $\hat{A} = \sum_{i=1}^N \hat{A}^{(i)}$ is $F_Q \sim N^2$, which is called the Heisenberg limit. For this kind of the Hermitian operators, a given state is called a macroscopically entangled state if the quantum Fisher information scales with N^2.

4.3 Macroscopic entanglement in collective spin systems

In this section, we consider an ensemble of two-level systems $\{\hat{\boldsymbol{\sigma}}_i\}$. The collective spin operator $\hat{\boldsymbol{J}} = (\hat{J}_x, \hat{J}_y, \hat{J}_z)$ is defined by

$$\hat{\boldsymbol{J}} = \frac{1}{2} \sum_{i=1}^N \hat{\boldsymbol{\sigma}}_i, \tag{4.21}$$

which satisfies the commutation relation of the angular momentum

$$[\hat{J}_\alpha, \hat{J}_\beta] = i\epsilon_{\alpha\beta\gamma}\hat{J}_\gamma, \tag{4.22}$$

where $\epsilon_{\alpha\beta\gamma}$ is the Levi-Civita symbol. The collective rotation operator along an axis $\boldsymbol{n}$ by an angle θ is given by

$$\hat{U}_n = \exp[-i\theta\hat{J}_{\boldsymbol{n}}], \tag{4.23}$$

where $\hat{J}_n$ is the angular momentum operator with the quantization axis along $\boldsymbol{n}$. Here we consider the simultaneous eigenstate $|J;M\rangle$ of $\hat{J}_z$ and $\hat{\boldsymbol{J}}^2$, which satisfies

$$\hat{J}_z|J;M\rangle = M|J;M\rangle, \quad \hat{\boldsymbol{J}}^2|J;M\rangle = J(J+1)|J;M\rangle, \tag{4.24}$$

where spin size J can take $J = N/2, N/2 - 1, \cdots (> 0)$, and M can take $M = -J, -J+1, \cdots, J$. We can also express the collective spin operators by using two bosonic operators, $\hat{a}_1$ and $\hat{a}_2$, as

$$\begin{cases} \hat{J}_x = \dfrac{1}{2}(\hat{a}_1^\dagger \hat{a}_2 + \hat{a}_2^\dagger \hat{a}_1), \\[2mm] \hat{J}_y = \dfrac{1}{2i}(\hat{a}_1^\dagger \hat{a}_2 - \hat{a}_2^\dagger \hat{a}_1), \\[2mm] \hat{J}_z = \dfrac{1}{2}(\hat{a}_1^\dagger \hat{a}_1 - \hat{a}_2^\dagger \hat{a}_2). \end{cases} \tag{4.25}$$

For the bosonic expression, the simultaneous eigenstate of $\hat{J}_z$ and $\hat{\boldsymbol{J}}^2$ is given by

$$|N_1, N_2\rangle = |(N_1 + N_2)/2; (N_1 - N_2)/2\rangle, \tag{4.26}$$

where N_1 (N_2) is number of mode-1 (-2) bosons.

Suppose that a Hamiltonian $\hat{\mathcal{H}}$ is described by using only these collective spin operators, and then the commutation relation

$$[\hat{J}_\alpha, \hat{\boldsymbol{J}}^2] = 0, \quad \alpha = x, y, z, \tag{4.27}$$

leads to the commutation relation

$$[\hat{\mathcal{H}}, \hat{\boldsymbol{J}}^2] = 0, \tag{4.28}$$

which ensures that this system can be block-diagonalized in the eigensectors of $\hat{\boldsymbol{J}}^2$. It means that as long as we consider unitary dynamics, we can discuss properties of the system in a single eigensector.

First we start with separable states. The coherent spin state is a product state, in which all two-level spins point the same direction, and it can be expressed as

$$|\theta, \varphi; N\rangle = \bigotimes_{i=1}^{N} \left[\cos\frac{\theta}{2} |\uparrow\rangle_i + e^{i\varphi} \sin\frac{\theta}{2} |\downarrow\rangle_i \right], \tag{4.29}$$

in the individual spin representation, or equivalently

$$|\theta, \varphi; N\rangle = \sum_{M=-J}^{J} \sqrt{\frac{(2J)!}{(J+M)!(J-M)!}} \left(\cos\frac{\theta}{2}\right)^{J+M} \left(\sin\frac{\theta}{2}\right)^{J-M} e^{i(J-M)\varphi} |J; M\rangle, \tag{4.30}$$

in the collective spin representation [194, 195]. By using the collective rotation operator along the axis that points perpendicular to the coherent spin state, the quantum Fisher information of the coherent spin state achieves the standard quantum limit $F_Q = N$ [196]. It means that the coherent spin state is a classical optimal state for quantum metrology.

Next, we consider an entangled state that can achieve the Heisenberg limit. Here we introduce the NOON state [181]

$$|\text{NOON}\rangle = \frac{1}{\sqrt{2}}(|N, 0\rangle + |0, N\rangle), \tag{4.31}$$

or equivalently

$$|\text{NOON}\rangle = \frac{1}{\sqrt{2}}(|J; J\rangle + |J; -J\rangle). \tag{4.32}$$

Then, by using the collective rotation operator along the z-axis, the quantum Fisher information of the NOON state achieves the Heisenberg limit $F_Q = N^2$ [197]. Therefore, the NOON state is a metrologically useful state and a macroscopically entangled state.

4.4 Bosonic Josephson junctions

In this section, we introduce a bosonic Josephson junction as an example of collective spin systems. Here we consider Bose-Einstein condensation in a single spatial mode with two internal atomic states [182, 198]. The Hamiltonian of this system is given by

$$\hat{\mathcal{H}} = \hat{\mathcal{H}}_1 + \hat{\mathcal{H}}_2 + \hat{\mathcal{H}}_{\text{int}} + \hat{\mathcal{H}}_{\text{coup}}, \tag{4.33}$$

where $\hat{\mathcal{H}}_j$, $j = 1, 2$, represents each condensate of internal atomic states

$$\hat{\mathcal{H}}_j = \int d\boldsymbol{x}\, \hat{\psi}_j^\dagger(\boldsymbol{x}) \left[-\frac{\hbar^2}{2m}\frac{\partial^2}{\partial \boldsymbol{x}^2} + V_j(\boldsymbol{x}) + \frac{4\pi\hbar^2 a_j}{2m} \hat{\psi}_j^\dagger(\boldsymbol{x})\hat{\psi}_j(\boldsymbol{x}) \right] \hat{\psi}_j(\boldsymbol{x}), \tag{4.34}$$

and $\hat{\mathcal{H}}_{\text{int}}$ represents scattering between two condensates

$$\hat{\mathcal{H}}_{\text{int}} = \frac{4\pi\hbar^2 a_{12}}{m} \int d\boldsymbol{x}\, \hat{\psi}_1^\dagger(\boldsymbol{x})\hat{\psi}_1(\boldsymbol{x})\hat{\psi}_2^\dagger(\boldsymbol{x})\hat{\psi}_2(\boldsymbol{x}), \tag{4.35}$$

and $\hat{\mathcal{H}}_{\mathrm{coup}}$ represents coupling of two internal atomic states via laser-induced Raman transitions

$$\hat{\mathcal{H}}_{\mathrm{coup}} = \frac{\hbar\Omega_R}{2} \int d\boldsymbol{x} [\hat{\psi}_1(\boldsymbol{x})\hat{\psi}_2^\dagger(\boldsymbol{x})e^{-i\Delta t} + \hat{\psi}_1^\dagger(\boldsymbol{x})\hat{\psi}_2(\boldsymbol{x})e^{i\Delta t}]. \tag{4.36}$$

Here $\hat{\psi}_j$, $(\hat{\psi}_j^\dagger)$, $j = 1, 2$, is the annihilation (creation) operator of the bosonic field with mass m, V_j is a potential trapping atoms, a_j, $j = 1, 2$, and a_{12} is the scattering length, Ω_R is the Rabi frequency, and Δ is the detuning. Now we rewrite this Hamiltonian (4.33) by using the approximation [182, 198]

$$\hat{\psi}_j(\boldsymbol{x}) \approx \phi_j(\boldsymbol{x})\hat{a}_j, \quad j = 1, 2, \tag{4.37}$$

where $\phi_j(\boldsymbol{x})$, $j = 1, 2$, is the real normalized mode function and $\hat{a}_j$, $j = 1, 2$, is the bosonic operator of each mode. Then, the Hamiltonian (4.33) is rewritten as

$$\hat{\mathcal{H}} \approx \hbar\omega_1\hat{a}_1^\dagger\hat{a}_1 + \hbar\omega_2\hat{a}_2^\dagger\hat{a}_2 + \hbar\chi_1\hat{a}_1^\dagger\hat{a}_1^\dagger\hat{a}_1\hat{a}_1 + \hbar\chi_2\hat{a}_2^\dagger\hat{a}_2^\dagger\hat{a}_2\hat{a}_2 + \hbar\chi_{12}\hat{a}_1^\dagger\hat{a}_1\hat{a}_2^\dagger\hat{a}_2 + \frac{\hbar\Omega}{2}(\hat{a}_1\hat{a}_2^\dagger e^{-i\Delta t} + \hat{a}_1^\dagger\hat{a}_2 e^{i\Delta t}), \tag{4.38}$$

where

$$\hbar\omega_j = \int d\boldsymbol{x}\phi_j(\boldsymbol{x})\left[-\frac{\hbar^2}{2m}\frac{\partial^2}{\partial\boldsymbol{x}^2} + V_j(\boldsymbol{x})\right]\phi_j(\boldsymbol{x}), \quad j = 1, 2, \tag{4.39}$$

$$\hbar\chi_j = \frac{4\pi\hbar^2 a_j}{2m} \int d\boldsymbol{x}\phi_j^4(\boldsymbol{x}), \quad j = 1, 2, \tag{4.40}$$

$$\hbar\chi_{12} = \frac{4\pi\hbar^2 a_{12}}{m} \int d\boldsymbol{x}\phi_1^2(\boldsymbol{x})\phi_2^2(\boldsymbol{x}), \tag{4.41}$$

$$\hbar\Omega = \hbar\Omega_R \int d\boldsymbol{x}\phi_1(\boldsymbol{x})\phi_2(\boldsymbol{x}). \tag{4.42}$$

Then, by using the collective spin expression (4.25) and the number operator $\hat{N} = \hat{a}_1^\dagger\hat{a}_1 + \hat{a}_2^\dagger\hat{a}_2$, we obtain

$$\hat{\mathcal{H}} \approx \hbar\chi\hat{J}_z^2 + \hbar\Omega\cos\Delta\hat{J}_x - \hbar\Omega\sin\Delta\hat{J}_y + \hbar\delta\hat{J}_z + (\hat{N} \text{ and } \hat{N}^2 \text{ terms}), \tag{4.43}$$

where $\chi = \chi_1 + \chi_2 - \chi_{12}$ and $\delta = (\omega_1 - \omega_2) + (\hat{N} - 1)(\chi_1 - \chi_2)$. Because the Hamiltonian commutes with $\hat{N}$ and $\hat{N}^2$, we can discuss in a fixed particle number sector. We also set $\Delta = 0$ and $\delta = 0$, then we obtain the bosonic Josephson junction Hamiltonian [182, 198]

$$\hat{\mathcal{H}} = \hbar\chi\hat{J}_z^2 + \hbar\Omega\hat{J}_x. \tag{4.44}$$

Therefore, we can view bosonic Josephson junctions as collective spin systems. It should be noted that this Hamiltonian is also known as the Lipkin-Meshkov-Glick model [199].

Now, we discuss this model by using the semi-classical approximation [200]. There, we use a number and phase expression of the angular momentum

$$\begin{cases} \hat{J}_x \rightarrow \dfrac{N}{2}\sqrt{1 - z^2}\cos\phi, \\ \hat{J}_z \rightarrow \dfrac{N}{2}z, \end{cases} \tag{4.45}$$

where z and ϕ are classical variables corresponding to position and momentum, respectively. By substituting this expression into the bosonic Josephson junction Hamiltonian (4.44), we obtain

$$\hat{\mathcal{H}} \rightarrow \mathcal{H} = \frac{\hbar\Omega N}{2}\sqrt{1 - z^2}\cos\phi + \frac{\hbar\chi N^2}{4}z^2. \tag{4.46}$$

By expanding $\cos\phi$ around $\phi \approx 0$, we obtain an approximate classical Hamiltonian with quadratic momentum

$$\mathcal{H} \approx -\frac{\hbar\Omega N}{4}\phi\sqrt{1 - z^2}\phi + V(z), \tag{4.47}$$

where $V(z)$ is potential energy

$$V(z) = \frac{\hbar\chi N^2}{4}z^2 + \frac{\hbar\Omega N}{2}\sqrt{1-z^2}. \tag{4.48}$$

Mass of this system depends on position, i.e.,

$$m \propto \frac{1}{\sqrt{1-z^2}}, \tag{4.49}$$

and it ensures that a particle is confined within $z \in [-1, 1]$. Here, z-derivative of the potential is given by

$$\frac{d}{dz}V(z) = \frac{\hbar\chi N^2}{2}z^2 - \frac{\hbar\Omega N}{2}\frac{z}{\sqrt{1-z^2}}, \tag{4.50}$$

and thus classical stationary states satisfying $dV/dz = 0$ are given by

$$z = 0, \pm\sqrt{1-\Lambda^{-2}}, \tag{4.51}$$

where Λ is a characteristic parameter of the bosonic Josephson junction defined by

$$\Lambda = \frac{\chi N}{\Omega}. \tag{4.52}$$

Equation (4.51) implies that a bosonic Josephson junction has only one stationary state $z = 0$ when $\Lambda^{-1} > 1$. This stationary state $z = 0$ is almost similar to the coherent state along x-axis, i.e., the quantum paramagnetic state, and thus a bosonic Josephson junction is in the disordered phase for $\Lambda^{-1} > 1$. For $0 \leq \Lambda^{-1} < 1$, two stationary states $z = \pm\sqrt{1-\Lambda^{-2}}$ appear. However, behavior of these stationary states differs depending on the sign of χ. Indeed, the second derivative of the potential is given by

$$\frac{d^2}{dz^2}V(z) = \frac{\hbar\chi N^2}{2} - \frac{\hbar\Omega N}{2}\frac{1}{(1-z^2)^{3/2}}, \tag{4.53}$$

and thus, for the two stationary states $z = \pm\sqrt{1-\Lambda^{-2}}$, we obtain

$$\frac{d^2}{dz^2}V(z)\bigg|_{z=\pm\sqrt{1-\Lambda^{-2}}} = \frac{\hbar\chi N^2}{2}(1-\Lambda^2). \tag{4.54}$$

Because now we are considering the region $0 \leq \Lambda^{-1} < 1$, i.e., the region $\Lambda > 1$, the second derivative of the potential for two stationary states becomes positive when $\chi < 0$, and negative when $\chi > 0$, or in other words, two stationary states are stable for $\chi < 0$ and unstable for $\chi > 0$. Here we plot the potential (4.48) for $\chi < 0$ in Fig. 4.1. We can find a single stationary state $z = 0$ for $\Lambda^{-1} = 2$, a three-fold degenerate stationary state $z = 0$ for $\Lambda^{-1} = 1$, and an unstable stationary state $z = 0$ and two stable stationary states $z = \pm\sqrt{1-\Lambda^{-2}}$ for $\Lambda^{-1} = 1/2$. The double-well behavior of the potential for $0 \leq \Lambda^{-1} < 1$ with $\chi < 0$ leads to formation of a cat state in the ground state, i.e., a bosonic Josephson junction has a cat state as the ground state in the ordered phase $0 \leq \Lambda^{-1} < 1$ with $\chi < 0$. Furthermore, the ground state of a bosonic Josephson junction with $\Lambda^{-1} = 0$ becomes the NOON state (4.31). It should be noted that the point $\Lambda^{-1} = 1$ is the critical point showing a second order phase transition [183].

A problem is how to realize this cat state in a bosonic Josephson junction. One might think of just cooling down a system in the ordered phase. However, it is known that the energy gap between the ground state and the first excited state is exponentially small, and thus we could not obtain only the ground state, but a superposition of the ground state and the first excited state. Unfortunately, this superposition is enough to kill a cat state. This is because the ground state is a symmetric state of two stationary states and the first excited state is an anti-symmetric state of two stationary states, and thus a superposition of these states causes symmetry breaking [201]. Therefore, the resulting state would no longer a cat state. A candidate to realize this cat state is adiabatic control of a bosonic Josephson
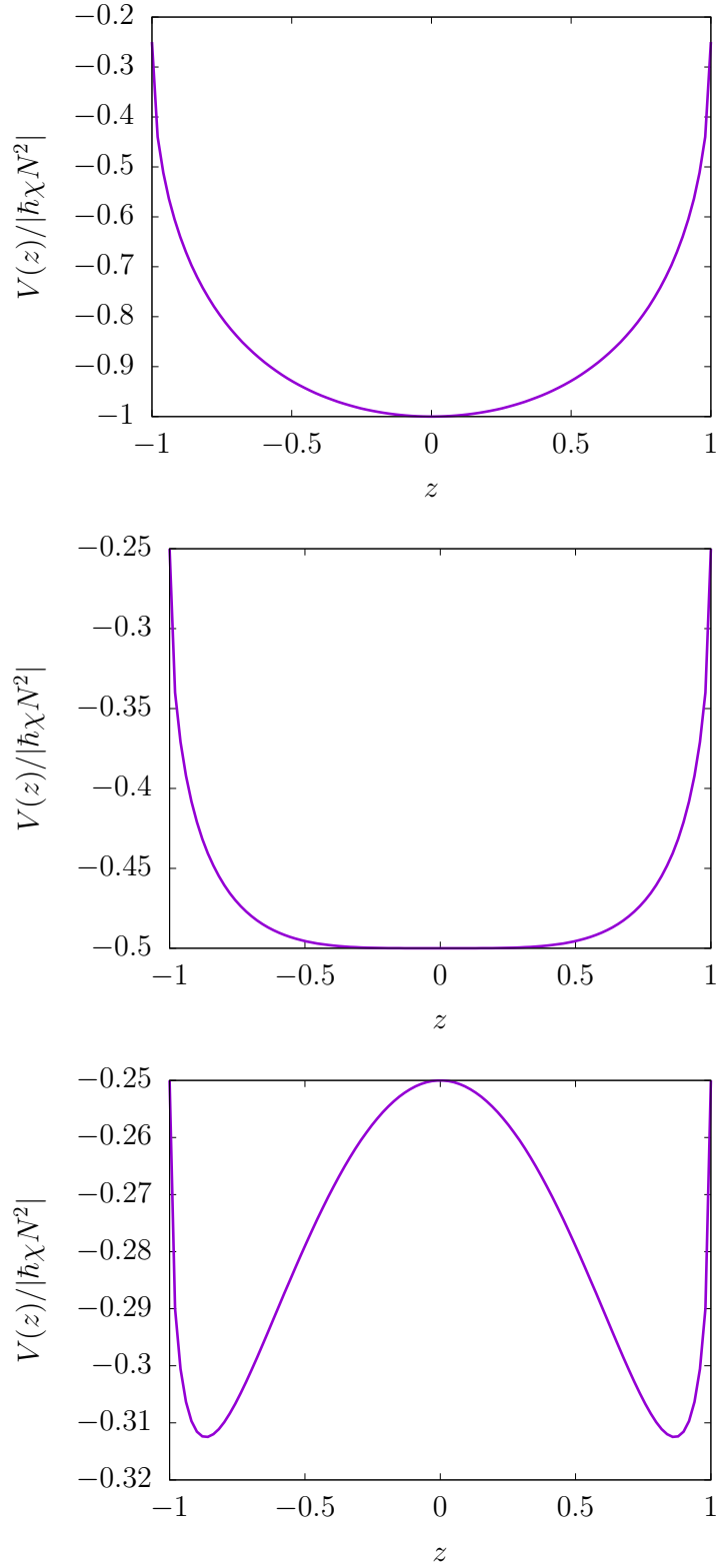
Figure4.1   Potential energy (4.48) of a bosonic Josephson junction. The horizontal axis is position of a particle z representing magnetization and the vertical axis is scaled potential $V/|\hbar\chi N^2|$. The parameter regions are given by (top) $\Lambda^{-1} = 2$, (middle) $\Lambda^{-1} = 1$, and (bottom) $\Lambda^{-1} = 1/2$. This figure is the reuse of the published article [82].

junction [182, 202]. We first prepare the ground state in the disordered phase, where the energy gap between the ground state and the first excited state can be large, or just above the critical point by using $\pi/2$ pulse. Then, we adiabatically change the parameter Λ into the ordered phase. Because the ground state and the first excited sate have different parity and the Hamiltonian of a bosonic Josephson junction (4.44) conserves parity [202], we could obtain the ground state in the ordered phase, i.e., a cat state. A difficulty of this scheme is a long generation time due to the adiabatic theorem. Therefore, it is of great interest to apply shortcuts to adiabaticity.

4.5   Application of shortcuts to adiabaticity

According to Takahashi [115] and Campbell *et al.* [203], in order to derive an approximate counter-diabatic Hamiltonian for the bosonic Josephson junction Hamiltonian (4.44), we introduce the Holstein-Primakoff transformation

$$
\begin{cases}
\hat{S}_+ = \sqrt{2S}\sqrt{1 - \dfrac{\hat{a}^\dagger \hat{a}}{2S}}\,\hat{a}, \\[2mm]
\hat{S}_- = \sqrt{2S}\,\hat{a}^\dagger \sqrt{1 - \dfrac{\hat{a}^\dagger \hat{a}}{2S}}, \\[2mm]
\hat{S}_z = S - \hat{a}^\dagger \hat{a},
\end{cases}
\tag{4.55}
$$

where $\hat{S}_\pm$ is given by

$$
\begin{cases}
\hat{S}_+ = \hat{S}_x + i\hat{S}_y, \\
\hat{S}_- = \hat{S}_x - i\hat{S}_y,
\end{cases}
\tag{4.56}
$$

$\hat{S}_\alpha$, $\alpha = x, y, z$ is the spin operator with spin size $S = N/2$, and $\hat{a}$ ($\hat{a}^\dagger$) is the annihilation (creation) operator. Here, we set the quantization axis to the z-axis, and thus the bosonic operators represent deviations from the coherent spin state along the z-axis. We introduce the rotation operators around the y- and z-axes

$$
\begin{cases}
\hat{U}_y(\phi) = \exp[-i\phi \hat{S}_y], \\
\hat{U}_z(\psi) = \exp[-i\psi \hat{S}_z],
\end{cases}
\tag{4.57}
$$

and then the spin operators are rotated as

$$
\begin{cases}
\hat{S}_x^{(\phi,\psi)} \equiv \hat{U}_z^\dagger(\psi)\hat{U}_y^\dagger(\phi)\hat{S}_x\hat{U}_y(\phi)\hat{U}_z(\psi) = \hat{S}_x \cos\phi\cos\psi - \hat{S}_y \cos\phi\sin\psi + \hat{S}_z \sin\phi, \\
\hat{S}_y^{(\phi,\psi)} \equiv \hat{U}_z^\dagger(\psi)\hat{U}_y^\dagger(\phi)\hat{S}_y\hat{U}_y(\phi)\hat{U}_z(\psi) = \hat{S}_x \sin\psi + \hat{S}_y \cos\psi, \\
\hat{S}_z^{(\phi,\psi)} \equiv \hat{U}_z^\dagger(\psi)\hat{U}_y^\dagger(\phi)\hat{S}_z\hat{U}_y(\phi)\hat{U}_z(\psi) = -\hat{S}_x \sin\phi\cos\psi + \hat{S}_y \sin\phi\sin\psi + \hat{S}_z \cos\phi.
\end{cases}
\tag{4.58}
$$

When a given state is similar to the spin coherent state, the Holstein-Primakoff transformation can be approximated as

$$
\begin{cases}
\hat{S}_x \approx \dfrac{\sqrt{2S}}{2}(\hat{a} + \hat{a}^\dagger), \\[2mm]
\hat{S}_y \approx \dfrac{\sqrt{2S}}{2i}(\hat{a} - \hat{a}^\dagger), \\[2mm]
\hat{S}_z = S - \hat{a}^\dagger \hat{a},
\end{cases}
\tag{4.59}
$$

which is an approximation up to the order of $\mathcal{O}(N)$.

For the bosonic Josephson junction Hamiltonian (4.44), the quantization axes are along the x-axis for the disordered phase and along the axes rotated by $\pm\phi$ from the x-axis in the x-z plane for the ordered phase, where ϕ is given by $\cos\phi = \Omega/\chi N$ from the classical analysis. Therefore, for the bosonic

Josephson junction Hamiltonian, the Holstein-Primakoff transformation should be given by

$$\begin{cases} \hat{J}_x = \hat{S}_x^{(\pi/2,\pi/2)} = \hat{S}_z, \\ \hat{J}_y = \hat{S}_y^{(\pi/2,\pi/2)} = \hat{S}_x, \\ \hat{J}_z = \hat{S}_z^{(\pi/2,\pi/2)} = \hat{S}_y, \end{cases} \tag{4.60}$$

for the disordered phase, and

$$\begin{cases} \hat{J}_x = \hat{U}_x^\dagger(\pm\phi)\hat{S}_x^{(\pi/2,\pi/2)}\hat{U}_x(\pm\phi) = \pm\hat{S}_y\sin\phi + \hat{S}_z\cos\phi, \\ \hat{J}_y = \hat{U}_x^\dagger(\pm\phi)\hat{S}_y^{(\pi/2,\pi/2)}\hat{U}_x(\pm\phi) = \hat{S}_x, \\ \hat{J}_z = \hat{U}_x^\dagger(\pm\phi)\hat{S}_z^{(\pi/2,\pi/2)}\hat{U}_x(\pm\phi) = \hat{S}_y\cos\phi \mp \hat{S}_z\sin\phi, \end{cases} \tag{4.61}$$

for the ordered phase. Then, the bosonic Josephson junction Hamiltonian is approximately transformed as

$$\hat{\mathcal{H}} \approx \left(\frac{\hbar\chi N}{2} - \hbar\Omega\right)\hat{a}^\dagger\hat{a} - \frac{\hbar\chi N}{4}(\hat{a}^2 + \hat{a}^{\dagger 2}) + \text{(c-numbers)}, \tag{4.62}$$

for the disordered phase, and

$$\hat{\mathcal{H}} \approx \left[\frac{\hbar\Omega}{2}\left(\frac{\Omega}{\chi N}\right) - \hbar\chi N\right]\hat{a}^\dagger\hat{a} - \frac{\hbar\Omega}{4}\left(\frac{\Omega}{\chi N}\right)(\hat{a}^2 + \hat{a}^{\dagger 2}) + \text{(c-numbers \& higher orders)}, \tag{4.63}$$

for the ordered phase. Both expressions of the bosonic Josephson junction Hamiltonian have the similar form

$$\hat{\mathcal{H}} = A\hat{a}^\dagger\hat{a} + B(\hat{a}^2 + \hat{a}^{\dagger 2}), \tag{4.64}$$

and thus, by introducing the Bogoliubov transformation

$$\begin{pmatrix} \hat{b} \\ \hat{b}^\dagger \end{pmatrix} = \begin{pmatrix} \cosh\frac{\theta}{2} & \sinh\frac{\theta}{2} \\ \sinh\frac{\theta}{2} & \cosh\frac{\theta}{2} \end{pmatrix} \begin{pmatrix} \hat{a} \\ \hat{a}^\dagger \end{pmatrix}, \tag{4.65}$$

where $\hat{b}$ ($\hat{b}^\dagger$) is the annihilation (creation) operator of the Bogoliubov boson, these Hamiltonian can be diagonalized as

$$\hat{\mathcal{H}} = \sqrt{A^2 - 4B^2}\hat{b}^\dagger\hat{b} + \text{(c-numbers)}. \tag{4.66}$$

Here, we set $\tanh\theta = 2B/A$. Therefore, the bosonic Josephson junction Hamiltonian can approximately be rewritten as

$$\hat{\mathcal{H}} \approx \hbar\omega\hat{b}^\dagger\hat{b}, \tag{4.67}$$

where the energy is given by

$$\hbar\omega = \hbar\sqrt{\Omega(\Omega - \chi N)}, \tag{4.68}$$

for the disordered phase, and

$$\hbar\omega = \hbar\sqrt{(\chi N)^2 - \Omega^2}, \tag{4.69}$$

for the ordered phase. The counter-diabatic Hamiltonian for this Hamiltonian is given by Eq. (1.93). By inversely transforming the counter-diabatic Hamiltonian for a harmonic oscillator (1.93), we obtain an approximate counter-diabatic Hamiltonian for bosonic Josephson junctions

$$\hat{\mathcal{H}}^{\text{cd}} = \hbar f(\hat{J}_y\hat{J}_z + \hat{J}_z\hat{J}_y), \tag{4.70}$$

where f is given by

$$\hbar f = -\frac{\hbar[\dot{\Omega}(\Omega - \chi N) + \Omega(\dot{\Omega} - \dot{\chi}N)]}{4N\Omega(\Omega - \chi N)}, \tag{4.71}$$

for the disordered phase, and

$$\hbar f = -\frac{\hbar[(\chi N)(\dot{\chi} N) - \Omega \dot{\Omega}]}{2N[(\chi N)^2 - \Omega^2]}, \tag{4.72}$$

for the ordered phase. Apparently, these counter-diabatic fields show divergence at the critical point $\Lambda^{-1} = 1$, and thus we cannot apply these counter-diabatic terms to create a cat state. Note that the form of this counter-diabatic Hamiltonian is known as the two-axis counter-twisting Hamiltonian, which was theoretically studied in the context of spin squeezing [204], and this counter-diabatic Hamiltonian can be expressed as

$$\hat{\mathcal{H}}^{\mathrm{cd}} = \frac{\hbar f}{2}[e^{-i\frac{\pi}{2}}(\hat{a}_1^\dagger \hat{a}_1^\dagger \hat{a}_1 \hat{a}_2 + \hat{a}_2^\dagger \hat{a}_2^\dagger \hat{a}_2 \hat{a}_1) + e^{i\frac{\pi}{2}}(\hat{a}_1^\dagger \hat{a}_2^\dagger \hat{a}_2 \hat{a}_2 + \hat{a}_2^\dagger \hat{a}_1^\dagger \hat{a}_1 \hat{a}_1)], \tag{4.73}$$

in the bosonic operator expression.

In the next chapter, we will discuss a way to avoid this divergence and show generation of a cat state in a bosonic Josephson junction via a shortcut.

Chapter 5

Shortcuts to adiabaticity for bosonic Josephson junctions

In this chapter, we consider shortcuts to adiabaticity for bosonic Josephson junctions across the critical point and generation of macroscopic entanglement. In Sec. 5.1, we construct counter-diabatic terms for bosonic Josephson junctions by taking finite-size corrections via $1/N$ expansion of the Holstein-Primakoff transformation. In Sec. 5.2, we discuss generation of macroscopically entangled states in bosonic Josephson junctions. We summarize our method and results in Sec. 5.3. Note that this chapter is based on a series of the articles by the present author [82, 109].

5.1 Counter-diabatic driving

We consider the bosonic Josephson junction Hamiltonian

$$\hat{\mathcal{H}} = \hbar\chi\hat{J}_z^2 + \hbar\Omega\hat{J}_x, \tag{5.1}$$

and assume $\chi < 0$ and $\Omega \leq 0$. As mentioned in Sec. 4.4, the phase of this system is characterized by the parameter

$$\Lambda = \frac{\chi N}{\Omega}. \tag{5.2}$$

In the disordered phase, $\Lambda^{-1} > 1$, all $(2J+1)$ eigenstates of the bosonic Josephson junction Hamiltonian are separated from each other, and thus the counter-diabatic terms are constructed by using the non-degenerate formalism. However, in the ordered phase, $0 \leq \Lambda^{-1} < 1$, eigenstates have two-fold degeneracies in the thermodynamic limit (only the highest energy eigenstate has no degeneracy if the total number of atoms N is given by even), and thus the counter-diabatic terms should be constructed by using the degenerate formalism. Indeed, the construction of the counter-diabatic terms in Sec. 4.5 are based on the Holstein-Primakoff transformation and the harmonic approximation, which means that we consider the thermodynamic limit. In these situations, the degenerate ground states are given by the ground states of each harmonic well, whereas originally the degenerate ground states are given by the symmetric and the anti-symmetric states. Then, the counter-diabatic terms should be given by the summation of the counter-diabatic terms constructed in each well

$$\hat{\mathcal{H}}^{\mathrm{cd}} \approx \sum_{\mu=\pm} \hat{\mathcal{H}}_\mu^{\mathrm{cd}}, \tag{5.3}$$

where $\hat{\mathcal{H}}_\mu^{\mathrm{cd}}$ is the counter-diabatic terms for each well. Similarly, classical-approximate counter-diabatic terms discussed in Sec. 3.2 also take the form (5.3). This is because to consider the mean-field approximation leads to decomposition of the symmetric state into two symmetry-broken states. We first show

that the classical-approximate counter-diabatic terms do not make sense in the present process. For simplicity, we discuss in the collective spin representation, but it is straightforward to discuss in individual spin representation. The mean-field approximation in the bosonic Josephson junction Hamiltonian leads to the mean-field Hamiltonian

$$\hat{\mathcal{H}}_{\mathrm{MF}} = 2\hbar\chi M_z \hat{J}_z + \hbar\Omega \hat{J}_x, \tag{5.4}$$

where $M_z = \langle \hat{J}_z \rangle$ and we ignore constant terms. Then the classical-approximate counter-diabatic Hamiltonian is given by

$$\hat{\mathcal{H}}_{\mathrm{MF}}^{\mathrm{cd}} = \hbar f \hat{J}_y, \tag{5.5}$$

where

$$f = \frac{2\chi M_z \dot{\Omega} - 2(\dot{\chi} M_z + \chi \dot{M}_z)\Omega}{(2\chi M_z)^2 + \Omega^2}. \tag{5.6}$$

We find that for the other symmetry-broken state $-M_z$ the counter-diabatic term has negative sign, and thus Eq. (5.3) vanishes. Therefore, the present classical-approximate counter-diabatic terms cannot be used in the present scheme, while it make sense for fast control of symmetry-broken states.

In order to avoid these difficulties, we introduce the finite-size corrections. Here we again consider the Holstein-Primakoff transformation but expand up to the third order of the bosonic operators

$$\begin{cases} \hat{S}_x \approx \dfrac{\sqrt{2S}}{2}(\hat{a} + \hat{a}^\dagger) - \dfrac{1}{4\sqrt{2S}}(\hat{a}^\dagger \hat{a}\hat{a} + \hat{a}^\dagger \hat{a}^\dagger \hat{a}), \\[2mm] \hat{S}_y \approx \dfrac{\sqrt{2S}}{2i}(\hat{a} - \hat{a}^\dagger) - \dfrac{1}{4i\sqrt{2S}}(\hat{a}^\dagger \hat{a}\hat{a} - \hat{a}^\dagger \hat{a}^\dagger \hat{a}), \\[2mm] \hat{S}_z \approx S - \hat{a}^\dagger \hat{a}. \end{cases} \tag{5.7}$$

From the rotation of quantization axes, the angular momentum operators of bosonic Josephson junctions are given by

$$\begin{cases} \hat{J}_x = \hat{S}_x^{(\pi/2, \pi/2)} = \hat{S}_z, \\ \hat{J}_y = \hat{S}_y^{(\pi/2, \pi/2)} = \hat{S}_x, \\ \hat{J}_z = \hat{S}_z^{(\pi/2, \pi/2)} = \hat{S}_y, \end{cases} \tag{5.8}$$

for the disordered phase, and

$$\begin{cases} \hat{J}_x = \hat{U}_x^\dagger(\pm\phi)\hat{S}_x^{(\pi/2, \pi/2)}\hat{U}_x(\pm\phi) = \pm\hat{S}_y \sin\phi + \hat{S}_z \cos\phi, \\ \hat{J}_y = \hat{U}_x^\dagger(\pm\phi)\hat{S}_y^{(\pi/2, \pi/2)}\hat{U}_x(\pm\phi) = \hat{S}_x, \\ \hat{J}_z = \hat{U}_x^\dagger(\pm\phi)\hat{S}_z^{(\pi/2, \pi/2)}\hat{U}_x(\pm\phi) = \hat{S}_y \cos\phi \mp \hat{S}_z \sin\phi, \end{cases} \tag{5.9}$$

for the ordered phase. By using the normal ordering and the harmonic approximation, the bosonic Josephson junction Hamiltonian can be rewritten as

$$\hat{\mathcal{H}} \approx \left[\frac{\hbar\chi N}{2}\left(1 - \frac{1}{N}\right) - \hbar\Omega\right]\hat{a}^\dagger \hat{a} - \frac{\hbar\chi N}{4}\left(1 - \frac{1}{2N}\right)(\hat{a}^2 + \hat{a}^{\dagger 2}) + (\text{c-numbers \& higher orders}), \tag{5.10}$$

for the disordered phase, and

$$\begin{aligned} \hat{\mathcal{H}} \approx &\left[\frac{\hbar\Omega}{2}\left(\frac{\Omega}{\chi N}\right)\left(1 - \frac{3}{N}\right) - \hbar\chi N\left(1 - \frac{1}{N}\right)\right]\hat{a}^\dagger \hat{a} - \frac{\hbar\Omega}{4}\left(\frac{\Omega}{\chi N}\right)\left(1 - \frac{1}{2N}\right)(\hat{a}^2 + \hat{a}^{\dagger 2}) \\ &\mp \frac{i\hbar\Omega}{2\sqrt{N}}\sqrt{1 - \left(\frac{\Omega}{\chi N}\right)^2}(\hat{a} - \hat{a}^\dagger) + (\text{c-numbers \& higher orders}), \end{aligned} \tag{5.11}$$

for the ordered phase. Here we assume $\cos\phi = \Lambda^{-1}$, which holds in the thermodynamic limit, whereas it also changes due to the finite-size corrections. However, this can be justified as follows. We introduce small deviation of the quantization axis $\Delta\phi$, and then

$$\cos(\phi + \Delta\phi) = \cos\phi\cos\Delta\phi - \sin\phi\sin\Delta\phi \approx \cos\phi - \Delta\phi\sin\phi + \mathcal{O}(\Delta\phi^2). \tag{5.12}$$

Adiabaticity of this system becomes bad around the critical point, where $\phi \approx 0$. Therefore, we could approximate as $\cos(\phi + \Delta\phi) \approx \cos\phi$. For the ordered phase, we introduce displacement in the bosonic operators

$$\begin{cases} \hat{a} = \hat{a}' + iA_\pm, \\ \hat{a}^\dagger = \hat{a}'^\dagger - iA_\pm, \end{cases} \tag{5.13}$$

where $A_\pm$ is the real number given by

$$A_\pm = \pm\frac{1}{2\sqrt{N}}\frac{\Omega\sqrt{(\chi N)^2 - \Omega^2}}{(\chi N)^2(1 - \frac{1}{N}) - \Omega^2(1 - \frac{7}{4N})}. \tag{5.14}$$

Then the Hamiltonian can be rewritten as

$$\hat{\mathcal{H}} \approx \left[\frac{\hbar\Omega}{2}\left(\frac{\Omega}{\chi N}\right)\left(1 - \frac{3}{N}\right) - \hbar\chi N\left(1 - \frac{1}{N}\right)\right]\hat{a}'^\dagger\hat{a}' - \frac{\hbar\Omega}{4}\left(\frac{\Omega}{\chi N}\right)\left(1 - \frac{1}{2N}\right)(\hat{a}'^2 + \hat{a}'^{\dagger 2}) \tag{5.15}$$
$$+ \text{(c-numbers \& higher orders)}.$$

We repeat the derivation of the counter-diabatic terms as discussed in Sec. 4.5, i.e., by using the Bogoliubov transformation and the counter-diabatic terms for a harmonic oscillator, we obtain

$$\hat{\mathcal{H}}^{\text{cd}} \approx \hbar f(\hat{J}_y\hat{J}_z + \hat{J}_z\hat{J}_y), \tag{5.16}$$

where the strength of the counter-diabatic terms is given by

$$f = \frac{[\frac{\chi N}{2}(\frac{1}{N} - \frac{3}{4N^2}) - \Omega(1 - \frac{1}{N})]\frac{\dot{\chi}N}{2} + [\frac{\chi N}{2}(1 - \frac{1}{N}) - \Omega]\dot{\Omega}}{2N\{[\frac{\chi N}{2}(1 - \frac{1}{N}) - \Omega]^2 - [(\frac{\chi N}{2})(1 - \frac{1}{2N})]^2\}}, \tag{5.17}$$

in the disordered phase, and

$$f = -\frac{[\chi N(1 - \frac{1}{N})^2 + \frac{\Omega}{2}(\frac{\Omega}{\chi N})(1 - \frac{1}{N})(1 - \frac{3}{N}) + \frac{5\Omega}{4}(\frac{\Omega}{\chi N})^3(\frac{1}{N} - \frac{7}{4N^2})]\dot{\chi}N}{N\{[\frac{\Omega}{2}(\frac{\Omega}{\chi N})(1 - \frac{3}{N}) - \chi N(1 - \frac{1}{N})]^2 - [\frac{\Omega}{2}(\frac{\Omega}{\chi N})(1 - \frac{1}{2N})]^2\}}$$
$$+ \frac{[\frac{5\Omega}{2}(\frac{\Omega}{\chi N})^2(\frac{1}{N} - \frac{7}{4N^2}) + \Omega(1 - \frac{1}{N})(1 - \frac{3}{N})]\dot{\Omega}}{N\{[\frac{\Omega}{2}(\frac{\Omega}{\chi N})(1 - \frac{3}{N}) - \chi N(1 - \frac{1}{N})]^2 - [\frac{\Omega}{2}(\frac{\Omega}{\chi N})(1 - \frac{1}{2N})]^2\}}, \tag{5.18}$$

in the ordered phase.

Hereafter, for simplicity, we consider the time-independent nonlinear interaction χ and the time-dependent coupling $\Omega = \Omega(t)$. In particular, we consider a polynomial schedule

$$\Lambda^{-1} = 48s^5 - 120s^4 + 100s^3 - 30s^2 + 2, \quad s = t/t_f. \tag{5.19}$$

This schedule is determined from the boundary conditions

$$\begin{cases} \Lambda^{-1}|_{t=0} = 2, \quad \Lambda^{-1}|_{t=t_f/2} = 1, \quad \Lambda^{-1}|_{t=t_f} = 0, \\ \dot{\Lambda}^{-1}|_{t=0} = \dot{\Lambda}^{-1}|_{t=t_f/2} = \dot{\Lambda}^{-1}|_{t=t_f} = 0. \end{cases} \tag{5.20}$$

Here we plot the strength of the counter-diabatic terms (5.17) and (5.18) in Fig. 5.1. With and without the counter-diabatic Hamiltonian (5.16), we will simulate the bosonic Josephson junction Hamiltonian (5.1) and discuss about generation of cat states in the next section.

48
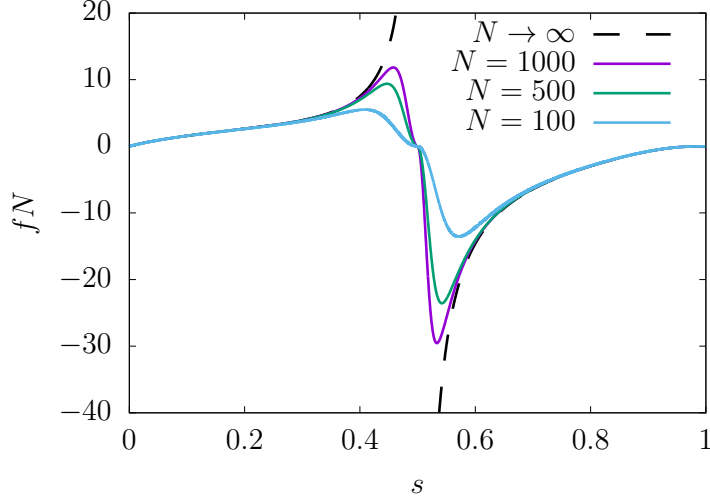
Figure5.1 Strength of the counter-diabatic fields for $N = 100, 500, 1000,$ and ∞. The horizontal axis is normalized time $s = t/t_f$ and the vertical axis is the strength of the counter-diabatic fields. Here, we set $\chi N t_f = 2$. This figure is the reuse of the published article [82].

5.2   Macroscopic entanglement generation

First we investigate the distribution of populations on the energy eigenstates. The final Hamiltonian commutes with the angular momentum operator $\hat{J}_z$, and thus populations on the energy eigenstates are given by $|\langle m|\Psi(t_f)\rangle|^2$, where $|m\rangle$ is the eigenvector of $\hat{J}_z$ satisfying $\hat{J}_z|m\rangle = m|m\rangle$. If generation is perfectly adiabatic, it results in the NOON state, and thus we obtain $|\langle \pm J|\Psi(t_f)\rangle|^2 = 1/2$ and otherwise zero. We simulate generation processes with and without counter-diabatic terms, and depict the distributions for $N = 1000$ and $\chi N t_f = 2$ in Fig. 5.2. We can find a two-peak structure in the case of counter-diabatic driving in contrast to a single-peak structure in the case of adiabatic driving. From the bosonic Josephson junction Hamiltonian, we know that energy eigenvalues are small when $|m|$ is large, and thus apparently counter-diabatic driving leads to a lower energy state.

As mentioned in Sec. 1.1, adiabatic control of a quantum state can be regarded as confinement around classical fixed points, and thus we do not have to consider turning off a Hamiltonian. Indeed, we simulate the case, where the Hamiltonian is set to be the final Hamiltonian after a creation process, and depict time evolution of the distribution up to the time $s = t/t_f = 2$ for $N = 1000$ and $\chi N t_f = 2$ in Fig. 5.3. We can find that the system obviously stop its dynamics after the creation time $s = t/t_f = 1$. Therefore, we do not have to care about timing to stop the generation process and to transfer to a next step.

We are also interested in how our shortcuts protocol can accelerate adiabatic time evolution. In order to assess speedup, we introduce the residual energy

$$E_{\mathrm{res}} = E(t_f) - E_{\mathrm{GS}}, \tag{5.21}$$

where $E(t_f)$ is the energy of generated states

$$E(t_f) = \langle \Psi(t_f)|\hat{\mathcal{H}}(t_f)|\Psi(t_f)\rangle, \tag{5.22}$$

and E_{GS} is the ground state energy of the final Hamiltonian, i.e., the energy of the NOON state under the final Hamiltonian

$$E_{\mathrm{GS}} = \langle \mathrm{NOON}|\hat{\mathcal{H}}(t_f)|\mathrm{NOON}\rangle = \hbar\chi J^2 = \frac{\hbar\chi N^2}{4}. \tag{5.23}$$

49
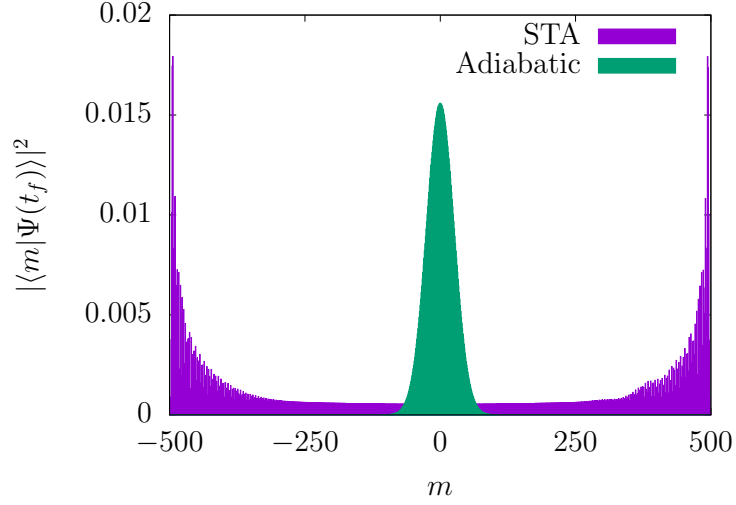
Figure5.2 Distributions of the populations at the final time $\chi N t_f = 2$ for $N = 1000$. The horizontal axis is eigenvalues and the vertical axis is populations of associated eigenstates. The purple histogram denoted as "STA" represents a state generated by the shortcuts protocol and the green histogram denoted as "Adiabatic" is a state generated by the naive adiabatic protocol. This figure is the reuse of the published article [82].
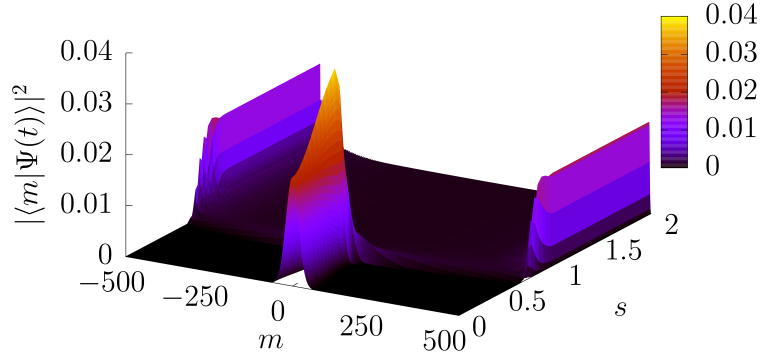
Figure5.3 Time evolution of the distribution of the eigenstate populations for $N = 1000$ and $\chi N t_f = 2$. This figure is the reuse of the published article [82].

We simulate both adiabatic and shortcuts-to-adiabatic processes with various generation time, and plot in Fig. 5.4. One can find that our shortcuts protocol can improve the naive adiabatic protocol up to $\chi N t_f \sim 30$. However, if $\chi N t_f$ is lager than ~ 30, then our shortcuts protocol leads to even worse results.

Now we will confirm if the generated state is a macroscopically entangled state or not. In order to study it, we calculate the quantum Fisher information of the generated state. As mentioned in Sec. 4.2, if the quantum Fisher information of the generated state is larger than N, then the generated state is at least entangled. Furthermore, we can conclude that the generated state is a macroscopically entangled
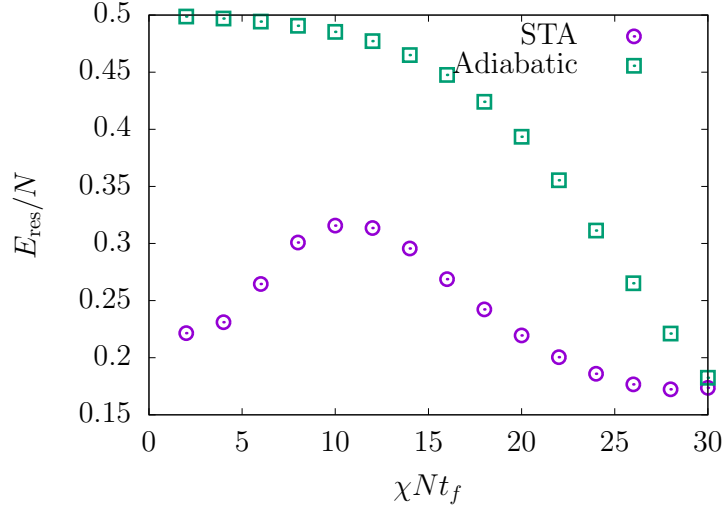
Figure5.4　Residual energy of generated states for $N = 1000$. The horizontal axis is generation time $\chi N t_f$ and the vertical axis is the residual energy. The purple circles denoted as "STA" represent the residual energy of states generated by the shortcuts protocol and the green squares denoted as "Adiabatic" represent the residual energy of states generated by the naive adiabatic protocol. This figure is the reuse of the published article [82].

state if the quantum Fisher information scales by N^2. Because adiabatic and shortcuts-to-adiabatic schemes can achieve the NOON state if the generation is perfectly adiabatic, and thus it is expected that we can obtain large quantum Fisher information by utilizing the similar interferometric scheme to the case of the NOON state [197]. Therefore, we consider the following probe state

$$|\psi_\theta\rangle = \exp[-i\theta \hat{J}_z]|\Psi(t_f)\rangle, \tag{5.24}$$

where θ is unknown parameter that we want to estimate and $|\Psi(t_f)\rangle$ is the generated state. Then, the quantum Fisher information is given by

$$F_Q[\hat{\rho}_\theta] = 4\langle (\Delta \hat{J}_z)^2 \rangle. \tag{5.25}$$

We plot the quantum Fisher information for $N = 100$, $N = 500$, and $N = 1000$ with $\theta = 0$ and $\chi N t_f = 2$ in Fig. 5.5. The results show that the quantum Fisher information nearly scales by N^2, slightly below the Heisenberg limit. Therefore, we can conclude that the generated state is a macroscopically entangled state. It would be worthy to be mentioned that the quantum Fisher information of the generated state is larger than the maximum quantum Fisher information of the Dicke state [205–207], which can be realized in the ground state of the present Hamiltonian with a positive non-linear interaction [208].

5.3　Summary

In this chapter, we discussed shortcuts to adiabaticity for bosonic Josephson junctions across the critical point. There, we took finite-size corrections into account by using $1/N$ expansion in the Holstein-Primakoff transformation. We found that the resulting counter-diabatic terms can be finite even at the critical point if we choose appropriate time-dependence of the parameter Λ in contrast to the divergence in the previous work, where the counter-diabatic terms were constructed in the thermodynamic limit [115, 203].

We attempted generating macroscopically entangled states in bosonic Josephson junctions by using our method. We found two peaks in the distribution of eigenstate populations for a quite fast generation time, with which the system cannot follow change of the Hamiltonian if we consider the naive adiabatic
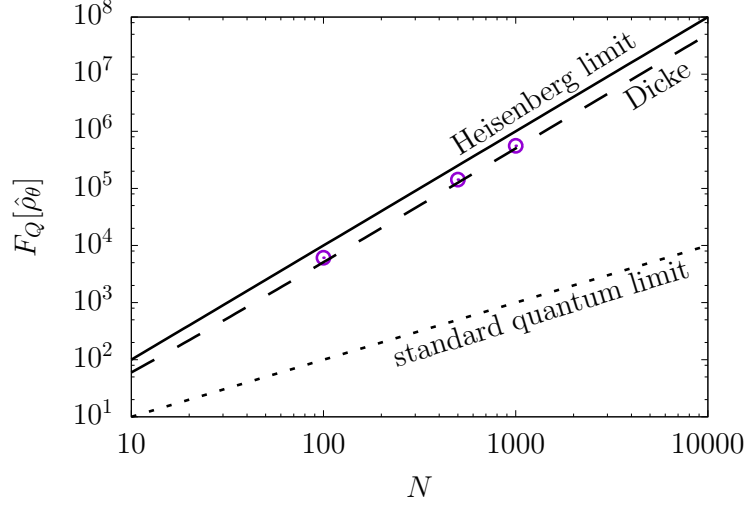
Figure5.5 Quantum Fisher information of states generated by the shortcuts protocol for $N = 100$, 500, and 1000. The horizontal axis is number of atoms and the vertical axis is the quantum Fisher information of generated states. As supplements, we also plot the Heisenberg limit by the solid line, the maximum quantum Fisher information of the Dicke state by the dashed line, and the standard quantum limit by the dotted line. Here, we set $\chi N t_f = 2$. This figure is the reuse of the published article [82].

generation protocol. Because the counter-diabatic terms disappear at the end of the generation process and the final Hamiltonian is similar to that of the adiabatic scheme, the system nearly stops its dynamics after generation. Indeed, we confirmed this dynamics. We also studied how our method can accelerate adiabatic time evolution. The numerical result of the residual energy indicated that our method can improve adiabaticity if the generation time is shorter than $\chi N t_f \sim 30$. We also investigated the quantum Fisher information in order to confirm if the generated state is a macroscopically entangled state or not. The result clearly indicated macroscopic entanglement in the generated state.

Chapter 6

Summary, discussion, and perspectives

In this thesis, we studied shortcuts to adiabaticity for many-body systems. In particular, we investigated counter-diabatic driving [19–21], which is one of the representative methods of shortcuts to adiabaticity [18]. In counter-diabatic driving, we construct counter-diabatic terms by using knowledge of energy eigenstates in quantum mechanics [19–21] or of volume of equal energy surfaces in phase space in classical mechanics [26]. Counter-diabatic terms cancel out diabatic changes, and thus we can obtain adiabatic time evolution within a short time, whereas dynamics is actually non-adiabatic. One of the difficulties in application of shortcuts to adiabaticity to many-body systems is the requirement of knowledge of energy eigenstates or of volume of equal energy surfaces. Even if one could obtain those knowledge and construct counter-diabatic terms, it is also difficult to implement required control because counter-diabatic terms for many-body systems generally consist of non-local and many-body interactions.

For generic classical spin systems, we found that counter-diabatic terms can be constructed by analogy of those for a two-level system [30]. This is because any state of a classical spin system can be described by a product state of two-level systems. The counter-diabatic terms are given by additional time-dependent external fields, and thus we can in principle implement in experiments. We showed that the counter-diabatic terms enable us to conserve the angle between each spin and the associated effective field during time evolution. Therefore, by setting the initial state in a stationary state, i.e., a state whose angles between spins and associated effective fields are zero, we can track the instantaneous stationary state that originates from the initial stationary state. Note that we cannot track an instantaneous stationary state if criticality happens, i.e., if bifurcation or collapse of the instantaneous stationary state takes place. We demonstrated this property by using a simple model.

As one of the applications of our method, we considered a classical model of quantum annealing. However, we found that a number of instances showing criticality rapidly increases along with the system size. Although our scheme is one of the classical algorithms of quantum annealing, this result might indicate difficulties of quantum annealing for large systems. We also considered to improve performance of our method by choosing different paths [133]. Here we utilized inhomogeneous driving [141–151]. We clearly showed decrease of a number of failure due to criticality, whereas the rate of decrease is not so efficient for large systems.

It should be noted that some proposals of shortcuts to adiabaticity for quantum annealing were also presented concurrently with our work. Özgüler *et al.* proposed a single-particle and cluster approximation in counter-diabatic driving [90]. There, they ignored interactions and constructed counter-diabatic terms by only using local fields, or took interactions into account by clustering some spins. However, the former case failed in obtaining the ground state for strong interactions and the latter case slightly improved results but it required many-body interaction terms. Hartmann and Lechner considered to make use of the variational approach of counter-diabatic driving for lattice gauge quantum annealing [91]. There, information of interactions were slightly took into account and they found improvements by comparing with naive quantum annealing, but probability to find the ground state was not so large. One would be interested in the comparison between our method and other methods. In the single-particle and cluster approximation approach, the probability to find the ground state tends to smaller than 0.1 for $N \sim 10$ when the strength of interactions is comparable to that of local fields, whereas it is close to 1 in the

negligibly small interaction limit. In the variational approach, the probability to find the ground state is around 0.93 for $N = 3$ and 0.59 for $N = 6$. Our method gives the probability to find the ground state more than 0.99 for $N = 36$, and thus it seems better than others, whereas different models have been studied in these work. Direct comparison in an identical model should be studied in the future.

One would wonder the relationship between our method and other methods of quantum annealing. In genuine quantum annealing, the adiabatic theorem and the existence of the energy gap between the ground state and the first excited state ensure that we can obtain the ground state of a given problem Hamiltonian if we take an enough long time. However, for classical dynamics, it depends on instances whether we can obtain the ground state or not. That is, we can obtain the ground state of a given problem Hamiltonian if the ground state of a driver Hamiltonian and the ground state of the problem Hamiltonian are connected by a path of an instantaneous stationary state at each time. Otherwise, it results in one of the metastable states due to a first order transition, or in precession dynamics due to criticality. Therefore, quantum annealing seems different depending on whether we consider genuine quantum dynamics or classical dynamics. However, for instances that cannot be solved by classical dynamics, first order transitions or criticality would also appear in genuine quantum dynamics unless it has strong quantum fluctuations or large entanglement. It means that exponentially small energy gaps appear in duration of quantum annealing. Therefore, by even genuine quantum annealing, such problems cannot be solved efficiently. It should be noted that quantum annealers and usual classical algorithms also have thermal fluctuations. They could sometimes resolve a part of hard instances, but these would be just lucky hits.

How to resolve such hard instances is still an open problem. For classical dynamics, we need to find a path leading to the ground state of a given problem with avoiding first order transitions and criticality. It is a future work to study if there is an efficient method to find such a path. For quantum dynamics, we need strong quantum fluctuations or large entanglement in order to resolve difficulties that can be found in the classical limit. We should study which of driver Hamiltonians can induce strong quantum fluctuations and if there is large entanglement in the future. It is also important to study if such strong quantum fluctuations and large entanglement really play an important role to resolve such difficulties.

Furthermore, for bosonic Josephson junctions, we constructed approximate counter-diabatic terms [82]. Here we utilized the Holstein-Primakoff transformation and the harmonic approximation as proposed in the previous works [115, 203], but we took finite size corrections into account in order to avoid divergence at the critical point. As the result of finite size corrections, we obtained finite and continuous counter-diabatic terms. The form of counter-diabatic terms is nothing but the two-axis counter-twisting interaction [204]. Although the two-axis counter-twisting interaction has not been realized in experiments yet, many experimentalists are trying to realize it and it would realize in near future. By applying approximate counter-diabatic terms, we found that a bosonic Josephson junction forms two peaks within a short time. We also calculated the residual energy of generated states both with and without counter-diabatic terms, which showed suppression of diabatic transitions by counter-diabatic terms. Furthermore, we calculated the quantum Fisher information of generated states with counter-diabatic terms within a short time. The result clearly showed that generated states are actually cat states.

We could not discuss experimental implementation of our scheme. This is because the two-axis counter-twisting interaction has not been realized in experiments yet and we do not know possible energy scale of it. It should be discussed in the future. We also wonder if our generation scheme is robust with respect to various errors and noises or not. For example, one of the main difficulties in generating cat states in atomic systems is particle losses [184]. Speedup of generation could minimize bad influence of particle losses, but there is still a possibility that interplay of non-linear interactions and particle losses leads to destruction of cat states [209]. This actually happens in generation of a phase cat state by using the one-axis twisting interaction. This point should also be studied in the future.

It is also of great interest to consider schemes without the two-axis counter-twisting interaction. For such schemes, we could consider quantum adiabatic brachistochrone in our method. There, we optimize the strength of the one-axis twisting interaction χ and of the Rabi coupling Ω so that counter-diabatic terms become small. This actually ensures good adiabaticity because small counter-diabatic terms imply that a reference Hamiltonian is already nearly adiabatic. This scheme would be already possible to

implement in experiments by using the state of the art techniques.

AppendixA

Detailed calculations and proofs

A.1 Adiabatic transformation

In this section, we explain how to construct adiabatic transformation $\hat{U}_A(t)$.

By using a basic property of the projection operator

$$\hat{P}_n^2(\boldsymbol{\lambda}; t) = \hat{P}_n(\boldsymbol{\lambda}; t), \tag{A.1}$$

we can show that the following equation

$$\hat{P}_n(\boldsymbol{\lambda}; t) \left(\frac{d}{dt} \hat{P}_n(\boldsymbol{\lambda}; t) \right) \hat{P}_n(\boldsymbol{\lambda}; t) = 0, \tag{A.2}$$

holds. We introduce an operator

$$\hat{A}_n(t) = i\hbar \left[\frac{d}{dt} \hat{P}_n(\boldsymbol{\lambda}; t), \hat{P}_n(\boldsymbol{\lambda}; t) \right], \tag{A.3}$$

which satisfies

$$i\hbar \frac{d}{dt} \hat{P}_n(\boldsymbol{\lambda}; t) = [\hat{A}_n(t), \hat{P}_n(\boldsymbol{\lambda}; t)]. \tag{A.4}$$

Now we consider a differential equation

$$i\hbar \frac{d}{dt} \hat{X}(t) = \hat{A}_n(t) \hat{X}(t). \tag{A.5}$$

The solution of this differential equation can be written as

$$\hat{X}(t) = \hat{V}_n(t) \hat{X}(0). \tag{A.6}$$

Here $\hat{V}_n(t)$ satisfies

$$i\hbar \frac{d}{dt} \hat{V}_n(t) = \hat{A}_n(t) \hat{V}_n(t), \quad \hat{V}_n(0) = 1, \tag{A.7}$$

and thus $\hat{V}_n(t)$ is a unitary operator because $\hat{A}_n(t)$ is an Hermitian operator. By using Eq. (A.4), we can show that an operator

$$\hat{W}_n(t) = \hat{P}_n(\boldsymbol{\lambda}; t) \hat{V}_n(t), \tag{A.8}$$

is also a solution of Eq. (A.5), and thus

$$i\hbar \frac{d}{dt} \hat{W}_n(t) = \hat{A}_n(t) \hat{W}_n(t), \quad \hat{W}_n(0) = \hat{P}_n(\boldsymbol{\lambda}; 0), \tag{A.9}$$

holds. Equation (A.6) implies

$$\hat{W}_n(t) = \hat{V}_n(t) \hat{W}_n(0), \tag{A.10}$$

and thus we obtain

$$\hat{P}_n(\boldsymbol{\lambda};t) = \hat{V}_n(t)\hat{P}_n(\boldsymbol{\lambda};0)\hat{V}_n^\dagger(t), \tag{A.11}$$

or equivalently

$$\hat{P}_n(\boldsymbol{\lambda};t) = \hat{W}_n(t)\hat{P}_n(\boldsymbol{\lambda};0)\hat{W}_n^\dagger(t). \tag{A.12}$$

Note that $\hat{W}_n(t)$ is not unitary. Indeed, Eqs. (A.8) and (A.10) lead to

$$\hat{W}_n^\dagger(t)\hat{W}_n(t) = \hat{P}_n(\boldsymbol{\lambda};0), \quad \hat{W}_n(t)\hat{W}_n^\dagger(t) = \hat{P}_n(\boldsymbol{\lambda};t). \tag{A.13}$$

However, Eqs. (A.8) and (A.10) also imply the orthogonal property

$$\hat{W}_n^\dagger(t)\hat{W}_m(t) = 0, \quad \hat{W}_n(t)\hat{W}_m^\dagger(t) = 0, \tag{A.14}$$

for $n \neq m$, and thus an operator

$$\hat{U}_A(t) = \sum_n \hat{W}_n(t), \quad \hat{U}_A(0) = 1, \tag{A.15}$$

is unitary and satisfies

$$\hat{P}_n(\boldsymbol{\lambda};t) = \hat{U}_A(t)\hat{P}_n(\boldsymbol{\lambda};0)\hat{U}_A^\dagger(t), \tag{A.16}$$

for all n. Therefore, $\hat{U}_A(t)$ is an adiabatic transformation.

A.2   Adiabatic theorem

In this section, we prove the adiabatic theorem.

First, we introduce the resolvent of the Hamiltonian

$$\hat{R}_{\hat{\mathcal{H}}}[\epsilon] = \frac{1}{\hat{\mathcal{H}}(\boldsymbol{\lambda};t) - \epsilon(\boldsymbol{\lambda};t)} = \sum_n \frac{1}{E_n(\boldsymbol{\lambda};t) - \epsilon(\boldsymbol{\lambda};t)}\hat{P}_n(\boldsymbol{\lambda};t), \tag{A.17}$$

where $\epsilon(\boldsymbol{\lambda};t)$ is a complex number on parameter space. We define the reduced resolvent for the nth energy eigenvalue $E_n(\boldsymbol{\lambda};t)$ of the Hamiltonian $\hat{\mathcal{H}}(\boldsymbol{\lambda};t)$ by

$$\hat{S}_{\hat{\mathcal{H}}}^{(n)}[\epsilon] = \hat{R}_{\hat{\mathcal{H}}}[\epsilon] - \frac{1}{E_n(\boldsymbol{\lambda};t) - \epsilon(\boldsymbol{\lambda};t)}\hat{P}_n(\boldsymbol{\lambda};t) = \sum_{\substack{m \\ (m \neq n)}} \frac{1}{E_m(\boldsymbol{\lambda};t) - \epsilon(\boldsymbol{\lambda};t)}\hat{P}_m(\boldsymbol{\lambda};t), \tag{A.18}$$

which satisfies

$$[\hat{\mathcal{H}}(\boldsymbol{\lambda};t) - \epsilon(\boldsymbol{\lambda};t)]\hat{S}_{\hat{\mathcal{H}}}^{(n)}[\epsilon] = 1 - \hat{P}_n(\boldsymbol{\lambda};t). \tag{A.19}$$

Now we introduce an unitary operator

$$\hat{U}_D^{(n)}(t) = \exp\left[\frac{i}{\hbar}\int_0^t dt' E_n(\boldsymbol{\lambda};t')\right]\hat{U}_D(t), \tag{A.20}$$

and then

$$i\hbar\frac{d}{dt}[\hat{U}_D^{(n)\dagger}(t)\hat{W}_n(t)] = -\left(i\hbar\frac{d}{dt}\hat{U}_D^{(n)\dagger}(t)\right)\hat{S}_{\hat{\mathcal{H}}}^{(n)}[E_n]\left(i\hbar\frac{d}{dt}\hat{W}_n(t)\right), \tag{A.21}$$

holds. Here, we use

$$i\hbar\frac{d}{dt}\hat{U}_D^{(n)\dagger}(t) = -\hat{U}_D^{(n)\dagger}(t)(\hat{\mathcal{H}}(\boldsymbol{\lambda};t) - E_n(\boldsymbol{\lambda};t)), \tag{A.22}$$

and

$$i\hbar\frac{d}{dt}\hat{W}_n(t) = (1 - \hat{P}_n(\boldsymbol{\lambda};t))\left(i\hbar\frac{d}{dt}\hat{W}_n(t)\right) = (\hat{\mathcal{H}}(\boldsymbol{\lambda};t) - E_n(\boldsymbol{\lambda};t))\hat{S}_{\hat{\mathcal{H}}}^{(n)}[E_n]\left(i\hbar\frac{d}{dt}\hat{W}_n(t)\right). \tag{A.23}$$

By integrating Eq. (A.21), we obtain

$$
\hat{U}_D^{(n)\dagger}(t)\hat{W}_n(t) - \hat{P}_n(0) = -\left[\hat{U}_D^{(n)\dagger}(t')\hat{S}_{\hat{\mathcal{H}}}^{(n)}[E_n]\left(i\hbar\frac{d}{dt'}\hat{W}_n(t')\right)\right]
$$
$$
+ \int_0^t dt' \hat{U}_D^{(n)\dagger}(t')\frac{d}{dt'}\left[\hat{S}_{\hat{\mathcal{H}}}^{(n)}[E_n]\left(i\hbar\frac{d}{dt'}\hat{W}_n(t')\right)\right]. \tag{A.24}
$$

By using the following facts; $\hat{U}_D^{(n)}(t)$ is unitary (order of $\mathcal{O}(1)$), $\hat{S}_{\hat{\mathcal{H}}}^{(n)}[E_n]$ is a function of $\boldsymbol{\lambda}$ rather than that of t and is finite (order of $\mathcal{O}(\Delta E^{-1})$ where ΔE is an energy gap) if there is no crossing, and $(d/dt)\hat{W}_n(t)$ is proportional to $d\boldsymbol{\lambda}/dt$, we can find that dominant contributions in the right-hand side of Eq. (A.24) is proportional to $d\boldsymbol{\lambda}/dt$. Therefore, the relation

$$
[\hat{U}_D(t) - \hat{U}_A'(t)]\hat{P}_n(0) = \mathcal{O}(d\boldsymbol{\lambda}/dt), \tag{A.25}
$$

for all n, where $\hat{U}_A'(t)$ is

$$
\hat{U}_A'(t) = \sum_n \exp\left[-\frac{i}{\hbar}\int_0^t dt' E_n(\boldsymbol{\lambda};t')\right]\hat{W}_n(t), \tag{A.26}
$$

holds. Here, $\hat{U}_A'(t)$ is also adiabatic transformation, and thus Eq. (A.25) proves the adiabatic theorem.

A.3   Adiabatic condition

In order to quantify deviation of dynamical transformation from adiabatic transformation, we introduce the following operator

$$
\hat{\eta}^{(n)}(t) = \hat{P}_n(\boldsymbol{\lambda};0)\hat{U}_D^\dagger(t)(1-\hat{P}_n(\boldsymbol{\lambda};t))\hat{U}_D(t)\hat{P}_n(\boldsymbol{\lambda};0), \tag{A.27}
$$

for each n. This operator is vanishingly small when time evolution is almost adiabatic. By using adiabatic transformation (A.26), this operator can be rewritten as

$$
\hat{\eta}^{(n)}(t) = \hat{P}_n(\boldsymbol{\lambda};0)\hat{U}_D^\dagger(t)\hat{U}_A'(t)(1-\hat{P}_n(\boldsymbol{\lambda};0))\hat{U}_A'^\dagger(t)\hat{U}_D(t)\hat{P}_n(\boldsymbol{\lambda};0). \tag{A.28}
$$

Now we calculate $\hat{U}_A'^\dagger(t)\hat{U}_D(t)$. Time derivative of $\hat{U}_A'^\dagger(t)\hat{U}_D(t)$ is given by

$$
i\hbar\frac{d}{dt}(\hat{U}_A'^\dagger(t)\hat{U}_D(t)) = -\sum_{\substack{n,m \\ (n\neq m)}} \exp\left[\frac{i}{\hbar}\int_0^t dt'(E_m(\boldsymbol{\lambda};t') - E_n(\boldsymbol{\lambda};t'))\right]
$$
$$
\times \hat{W}_m^\dagger(t)\left(i\hbar\frac{d}{dt}\hat{P}_n(\boldsymbol{\lambda};t)\right)\hat{W}_n(t)(\hat{U}_A'^\dagger(t)\hat{U}_D(t)). \tag{A.29}
$$

By defining the following operator

$$
\hat{F}(t) = \sum_{\substack{n,m \\ (n\neq m)}} \exp\left[\frac{i}{\hbar}\int_0^t dt'(E_m(\boldsymbol{\lambda};t') - E_n(\boldsymbol{\lambda};t'))\right]\hat{W}_m^\dagger(t)\left(i\hbar\frac{d}{dt}\hat{P}_n(\boldsymbol{\lambda};t)\right)\hat{W}_n(t), \tag{A.30}
$$

Eq. (A.29) can be formally solved as

$$
\hat{U}_A'^\dagger(t)\hat{U}_D(t) = 1 - \frac{1}{i\hbar}\int_0^t dt'\hat{F}(t') + \left(\frac{1}{i\hbar}\right)^2\int_0^t dt'\int_0^{t'} dt''\hat{F}(t')\hat{F}(t'') - \cdots. \tag{A.31}
$$

When a system is almost adiabatic, dynamical transformation $\hat{U}_D(t)$ should be similar to adiabatic transformation $\hat{U}_A'(t)$, and thus Eq. (A.31) should be almost unity and $\hat{F}(t)$ should be small. Therefore, Eq. (A.31) approximately becomes

$$
\hat{U}_A^\dagger(t)\hat{U}_D(t) \approx 1 - \frac{1}{i\hbar}\int_0^t dt'\hat{F}(t'). \tag{A.32}
$$

Because

$$\hat{P}_n(\boldsymbol{\lambda};0)\hat{F}(t)\hat{P}_n(\boldsymbol{\lambda};0) = 0, \tag{A.33}$$

holds, and thus Eq. (A.28) can be rewritten as

$$\hat{\eta}^{(n)}(t) = \frac{1}{\hbar^2}\hat{P}_n(\boldsymbol{\lambda};0)\left(\int_0^t dt'\hat{F}(t')\right)^2\hat{P}_n(\boldsymbol{\lambda};0). \tag{A.34}$$

Because we assumed that a system is almost adiabatic, we can also assume that $E_m(\boldsymbol{\lambda};t) - E_n(\boldsymbol{\lambda};t)$ and $\hat{W}_m(t)(i\hbar(d/dt)\hat{P}_n(\boldsymbol{\lambda};t))\hat{W}_n(t)$ vary slowly in time, and thus time integral of $\hat{F}(t)$ approximately becomes

$$\int_0^t dt'\hat{F}(t') \approx \sum_{\substack{n,m \\ (n\neq m)}} \frac{\exp\left[\frac{i}{\hbar}\int_0^t dt'(E_m(\boldsymbol{\lambda};t') - E_n(\boldsymbol{\lambda};t'))\right]}{\frac{i}{\hbar}(E_m(\boldsymbol{\lambda};t) - E_n(\boldsymbol{\lambda};t))}\hat{W}_m^\dagger(t)\left(i\hbar\frac{d}{dt}\hat{P}_n(\boldsymbol{\lambda};t)\right)\hat{W}_n(t). \tag{A.35}$$

Then, Eq. (A.34) can be rewritten as

$$\hat{\eta}^{(n)}(t) \approx \hbar^2\sum_{\substack{m \\ (m\neq n)}} \frac{\hat{W}_n^\dagger(t)\left(\frac{d}{dt}\hat{P}_m(\boldsymbol{\lambda};t)\right)^2\hat{W}_n(t)}{(E_m(\boldsymbol{\lambda};t) - E_n(\boldsymbol{\lambda};t))^2}, \tag{A.36}$$

We assume that the projection operator is given by

$$\hat{P}_n(\boldsymbol{\lambda};t) = |n(\boldsymbol{\lambda};t)\rangle\langle n(\boldsymbol{\lambda};t)|, \tag{A.37}$$

and then we can evaluate $\hat{\eta}^{(n)}(t)$ as

$$\langle\hat{\eta}^{(n)}(t)\rangle \equiv \langle n(\boldsymbol{\lambda};0)|\hat{\eta}^{(n)}(t)|n(\boldsymbol{\lambda};0)\rangle \approx \hbar^2\sum_{\substack{m \\ (m\neq n)}}\frac{\left|\frac{d\boldsymbol{\lambda}}{dt}\cdot\langle n(\boldsymbol{\lambda};t)|\partial_{\boldsymbol{\lambda}}m(\boldsymbol{\lambda};t)\rangle\right|^2}{(E_m(\boldsymbol{\lambda};t) - E_n(\boldsymbol{\lambda};t))^2}. \tag{A.38}$$

It leads to the adiabatic condition

$$\hbar\left|\frac{d\boldsymbol{\lambda}}{dt}\cdot\frac{\langle n(\boldsymbol{\lambda};t)|\partial_{\boldsymbol{\lambda}}m(\boldsymbol{\lambda};t)\rangle}{E_m(\boldsymbol{\lambda};t) - E_n(\boldsymbol{\lambda};t)}\right| \ll 1, \quad \text{for all } m(\neq n), \tag{A.39}$$

or equivalently

$$\hbar\left|\frac{d\boldsymbol{\lambda}}{dt}\cdot\frac{\langle n(\boldsymbol{\lambda};t)|(\partial_{\boldsymbol{\lambda}}\hat{\mathcal{H}}(\boldsymbol{\lambda};t))|m(\boldsymbol{\lambda};t)\rangle}{(E_m(\boldsymbol{\lambda};t) - E_n(\boldsymbol{\lambda};t))^2}\right| \ll 1, \quad \text{for all } m(\neq n). \tag{A.40}$$

A.4 Counter-diabatic Hamiltonian for degenerate systems

We consider time derivative of adiabatic transformation for degenerate systems

$$\begin{aligned}
i\hbar\frac{d}{dt}\hat{U}_A(t) = &\hat{\mathcal{H}}(\boldsymbol{\lambda};t)\hat{U}_A(t) \\
&+ \sum_n\exp\left[-\frac{i}{\hbar}\int_0^t dt'E_n(\boldsymbol{\lambda};t')\right]\sum_{\mu,\nu}\left[i\hbar\frac{dc_\mu^{(n)}}{dt}c_\nu^{(n)*}(0)|n,\mu(\boldsymbol{\lambda};t)\rangle\langle n,\nu(\boldsymbol{\lambda};t)|\right. \\
&\left. + c_\mu^{(n)}(t)c_\nu^{(n)*}(0)\left(i\hbar\frac{d}{dt}|n,\mu(\boldsymbol{\lambda};t)\rangle\right)\langle n,\nu(\boldsymbol{\lambda};0)|\right].
\end{aligned} \tag{A.41}$$

Here, the second terms are calculated as

$$\sum_{\mu,\nu} i\hbar \frac{dc_\mu^{(n)}}{dt} c_\nu^{(n)*}(0)|n,\mu(\boldsymbol{\lambda};t)\rangle\langle n,\nu(\boldsymbol{\lambda};0)| = -\sum_{\mu,\nu,\kappa} \langle n,\mu(\boldsymbol{\lambda};t)| \left(i\hbar \frac{d}{dt}|n,\kappa(\boldsymbol{\lambda};t)\rangle \right)$$
$$\times c_\kappa^{(n)}(t) c_\nu^{(n)*}(0)|n,\mu(\boldsymbol{\lambda};t)\rangle\langle n,\nu(\boldsymbol{\lambda};0)|$$
$$= -\sum_{\mu,\iota} |n,\mu(\boldsymbol{\lambda};t)\rangle\langle n,\mu(\boldsymbol{\lambda};t)| \left(i\hbar \frac{d}{dt}|n,\iota(\boldsymbol{\lambda};t)\rangle \right) \langle n,\iota(\boldsymbol{\lambda};t)|$$
$$\times \sum_{\kappa,\nu} c_\kappa^{(n)}(t) c_\nu^{(n)*}(0)|n,\kappa(\boldsymbol{\lambda};t)\rangle\langle n,\nu(\boldsymbol{\lambda};0)|, \tag{A.42}$$

and

$$\sum_{\mu,\nu} c_\mu^{(n)}(t) c_\nu^{(n)*}(0) \left(i\hbar \frac{d}{dt}|n,\mu(\boldsymbol{\lambda};t)\rangle \right) \langle n,\nu(\boldsymbol{\lambda};0)| = \sum_\mu \left(i\hbar \frac{d}{dt}|n,\mu(\boldsymbol{\lambda};t)\rangle \right) \langle n,\mu(\boldsymbol{\lambda};t)|$$
$$\times \sum_{\nu,\kappa} c_\kappa^{(n)}(t) c_\nu^{(n)*}(0)|n,\kappa(\boldsymbol{\lambda};t)\rangle\langle n,\nu(\boldsymbol{\lambda};0)|. \tag{A.43}$$

Then, Eq. (A.41) becomes

$$i\hbar \frac{d}{dt}\hat{U}_A(t) = \hat{\mathcal{H}}(\boldsymbol{\lambda};t)\hat{U}_A(t) + \hat{\mathcal{H}}^{\mathrm{cd}}(t)\hat{U}_A(t), \tag{A.44}$$

where $\hat{\mathcal{H}}^{\mathrm{cd}}(t)$ is given by

$$\hat{\mathcal{H}}^{\mathrm{cd}}(t) = i\hbar \frac{d\boldsymbol{\lambda}}{dt} \cdot \sum_n \sum_\mu \left[1 - \sum_\nu |n,\nu(\boldsymbol{\lambda};t)\rangle\langle n,\nu(\boldsymbol{\lambda};t)| \right] |\partial_{\boldsymbol{\lambda}}n,\mu(\boldsymbol{\lambda};t)\rangle\langle n,\mu(\boldsymbol{\lambda};t)|, \tag{A.45}$$

and thus the total Hamiltonian is given by

$$\hat{\mathcal{H}}^{\mathrm{tot}}(t) = \hat{\mathcal{H}}(\boldsymbol{\lambda};t) + \hat{\mathcal{H}}^{\mathrm{cd}}(t). \tag{A.46}$$

A.5 Lewis-Riesenfeld theory

In this section we review the theoretical framework of the Lewis-Riesenfeld theory [35]. We consider a system governed by a time-dependent Hamiltonian $\hat{\mathcal{H}}(t)$. The Lewis-Riesenfeld invariant of this system is given by a Hermitian operator $\hat{F}(t)$ satisfying

$$i\hbar \frac{\partial \hat{F}}{\partial t} = [\hat{\mathcal{H}}(t), \hat{F}(t)]. \tag{A.47}$$

The Lewis-Riesenfeld invariant is also called the dynamical invariant because it maintains a solution of the Schrödinger equation, i.e., a solution $|\Psi(t)\rangle$ of the Schrödinger equation

$$i\hbar \frac{\partial}{\partial t}|\Psi(t)\rangle = \hat{\mathcal{H}}(t)|\Psi(t)\rangle, \tag{A.48}$$

remains in a solution

$$i\hbar \frac{\partial}{\partial t}(\hat{F}(t)|\Psi(t)\rangle) = \hat{\mathcal{H}}(t)(\hat{F}(t)|\Psi(t)\rangle). \tag{A.49}$$

It can be easily confirmed by using Eq. (A.47). We consider the spectrum decomposition of the Lewis-Riesenfeld invariant

$$\hat{F}(t) = \sum_n \lambda_n |\phi_n(t)\rangle\langle\phi_n(t)|, \tag{A.50}$$

60

then the eigenvalue λ_n becomes a time-independent real number. Here, λ_n is real because $\hat{F}(t)$ is Hermitian, and time-independence can be confirmed as follows. By differentiating the following equality

$$\hat{F}(t)|\phi_n(t)\rangle = \lambda_n|\phi_n(t)\rangle, \tag{A.51}$$

by time t, we obtain

$$\langle\phi_m(t)|\frac{\partial\hat{F}}{\partial t}|\phi_n(t)\rangle = (\lambda_n - \lambda_m)\langle\phi_m(t)|\partial_t\phi_n(t)\rangle + \dot{\lambda}_n\delta_{nm}. \tag{A.52}$$

On the other hand, by using Eq. (A.47), we obtain

$$i\hbar\langle\phi_m(t)|\frac{\partial\hat{F}}{\partial t}|\phi_n(t)\rangle = (\lambda_n - \lambda_m)\langle\phi_m(t)|\hat{\mathcal{H}}(t)|\phi_n(t)\rangle. \tag{A.53}$$

Then, Eqs. (A.52) and (A.53) lead to

$$\dot{\lambda}_n = \langle\phi_n(t)|\frac{\partial\hat{F}}{\partial t}|\phi_n(t)\rangle = 0. \tag{A.54}$$

Therefore, the eigenvalues of the Lewis-Riesenfeld invariant are time-independent.

In addition, for $\lambda_n \neq \lambda_m$, Eqs. (A.52) and (A.53) also lead to

$$i\hbar\langle\phi_m(t)|\partial_t\phi_n(t)\rangle = \langle\phi_m(t)|\hat{\mathcal{H}}(t)|\phi_n(t)\rangle. \tag{A.55}$$

If this equation also holds for $\lambda_n = \lambda_m$, then the eigenvectors of the Lewis-Riesenfeld invariant $\{|\phi_n(t)\rangle\}$ becomes the solutions of the Schrödinger equation. Here we introduce the gauge transformation

$$|\psi_n(t)\rangle = e^{i\alpha_n(t)}|\phi_n(t)\rangle, \tag{A.56}$$

where $\alpha_n(t)$ is a time-dependent real number. Note that $|\psi_n(t)\rangle$ is also the eigenvector of the Lewis-Riesenfeld invariant, and thus it also satisfies Eq. (A.55). We assume that $|\psi_n(t)\rangle$ satisfies

$$i\hbar\langle\psi_n(t)|\partial_t\psi_n(t)\rangle = \langle\psi_n(t)|\hat{\mathcal{H}}(t)|\psi_n(t)\rangle, \tag{A.57}$$

then $\alpha_n(t)$ must satisfy

$$\hbar\dot{\alpha}_n(t) = \langle\phi_n(t)|\left(i\hbar\frac{\partial}{\partial t} - \hat{\mathcal{H}}(t)\right)|\phi_n(t)\rangle. \tag{A.58}$$

This phase factor is called the Lewis-Riesenfeld phase. With this phase, $|\psi_n(t)\rangle$ becomes a solution of the Schrödinger equation, i.e., the solution of the Schrödigner equation can be written as

$$|\Psi(t)\rangle = \sum_n c_n|\psi_n(t)\rangle = \sum_n c_n e^{i\alpha_n(t)}|\phi_n(t)\rangle, \tag{A.59}$$

where c_n is a time-independent coefficient.

A.6   Cramér-Rao bound

For a given probability distribution $P(\mu|\theta)$, from the normalization condition

$$\sum_\mu P(\mu|\theta) = 1, \tag{A.60}$$

we obtain

$$\sum_\mu \partial_\theta P(\mu|\theta) = 0. \tag{A.61}$$

Then, the following equality holds

$$(\partial_\theta \bar{\Theta})^2 = \left[\sum_\mu \partial_\theta P(\mu|\theta) \Theta(\mu) \right]^2$$
$$= \left\{ \sum_\mu \partial_\theta P(\mu|\theta)[\Theta(\mu) - \bar{\Theta}] \right\}^2 . \tag{A.62}$$

Here, we utilized the fact that $\bar{\Theta}$ is μ-independent and Eq. (A.61). In addition, by using

$$\partial_\theta P(\mu|\theta) = P(\mu|\theta)[\partial_\theta \log P(\mu|\theta)], \tag{A.63}$$

Eq. (A.62) can be rewritten as

$$(\partial_\theta \bar{\Theta})^2 = \left\{ \sum_\mu P(\mu|\theta)[\partial_\theta \log P(\mu|\theta)][\Theta(\mu) - \bar{\Theta}] \right\}^2 . \tag{A.64}$$

The right hand side of this equation can be understood as the inner product of $[\partial_\theta \log P(\mu|\theta)]$ and $[\Theta(\mu) - \bar{\Theta}]$ with the weight function $P(\mu|\theta)$, and thus the Cauchy-Schwarz inequality implies

$$(\partial_\theta \bar{\Theta})^2 \leq \left\{ \sum_\mu P(\mu|\theta)[\partial_\theta \log P(\mu|\theta)]^2 \right\} \left\{ \sum_\mu P(\mu|\theta)[\Theta(\mu) - \bar{\Theta}]^2 \right\} . \tag{A.65}$$

Therefore, by introducing the Fisher information

$$F(\theta) = \sum_\mu P(\mu|\theta)[\partial_\theta \log P(\mu|\theta)]^2 = \sum_\mu \frac{[\partial_\theta P(\mu|\theta)]^2}{P(\mu|\theta)}, \tag{A.66}$$

and by assuming a locally unbiased estimator, we obtain the Cramér-Rao bound

$$\Delta\Theta \geq \frac{1}{\sqrt{F(\theta)}}. \tag{A.67}$$

It should be noted that the equality of the Cauchy-Schwarz inequality holds when two vectors are linear-dependent, i.e., the equality of the Cramér-Rao bound is satisfied when the equality

$$\partial_\theta \log P(\mu|\theta) = \lambda[\Theta(\mu) - \bar{\Theta}], \tag{A.68}$$

with a certain real λ, holds for all μ.

A.7 Fisher information

Here we show two representative properties of the Fisher information $F(\theta) = F[P(\mu|\theta)]$. The first property is the convexity of the Fisher information. For a mixture of probability distributions

$$P(\mu|\theta) = pP^{(1)}(\mu|\theta) + (1-p)P^{(2)}(\mu|\theta), \quad 0 < p < 1, \tag{A.69}$$

the convexity of the Fisher information implies

$$F[P(\mu|\theta)] \leq pF[P^{(1)}(\mu|\theta)] + (1-p)F[P^{(2)}(\mu|\theta)]. \tag{A.70}$$

Now we will show this property by contradiction, i.e., we assume

$$F[pP^{(1)}(\mu|\theta) + (1-p)P^{(2)}(\mu|\theta)] > pF[P^{(1)}(\mu|\theta)] + (1-p)F[P^{(2)}(\mu|\theta)]. \tag{A.71}$$

From the definition of the Fisher information (A.66), this inequality holds if the following inequality

$$\frac{[p\partial_\theta P^{(1)}(\mu|\theta) + (1-p)\partial_\theta P^{(2)}(\mu|\theta)]^2}{pP^{(1)}(\mu|\theta) + (1-p)P^{(2)}(\mu|\theta)} > p\frac{[\partial_\theta P^{(1)}(\mu|\theta)]^2}{P(\mu|\theta)} + (1-p)\frac{[\partial_\theta P^{(2)}(\mu|\theta)]^2}{P^{(2)}(\mu|\theta)}, \tag{A.72}$$

holds. However this inequality implies

$$0 > p(1-p)\{\partial_\theta[P^{(1)}(\mu|\theta)P^{(2)}(\mu|\theta)]\}^2, \tag{A.73}$$

and thus this is contradiction. Therefore, the assumption (A.71) was wrong, and thus the convexity of the Fisher information (A.70) holds.

The other property is the additivity of the Fisher information. For a set of ν measurements and its probability distribution

$$P(\mu|\theta) = \prod_{i=1}^{\nu} P^{(i)}(\mu_i|\theta), \quad \mu = \{\mu_1, \mu_2, \cdots, \mu_\nu\}, \tag{A.74}$$

the additivity of the Fisher information implies

$$F[P(\mu|\theta)] = \sum_{i=1}^{\nu} F[P^{(i)}(\mu_i|\theta)]. \tag{A.75}$$

By using the definition of the Fisher information (A.66) and Eq. (A.61), we can easily show this property as

$$\begin{aligned}
F[P(\mu|\theta)] &= \sum_\mu P(\mu|\theta)[\partial_\theta \log P(\mu|\theta)]^2 \\
&= \sum_\mu \prod_{i=1}^{\nu} P^{(i)}(\mu_i|\theta) \left[\sum_{j=1}^{\nu} \partial_\theta \log P^{(j)}(\mu_j|\theta)\right]^2 \\
&= \sum_{j=1}^{\nu} \sum_{\mu_j} P^{(j)}(\mu_j|\theta)[\partial_\theta \log P^{(j)}(\mu_j|\theta)]^2 + \sum_{\substack{j,k=1 \\ (j\neq k)}}^{\nu} \sum_{\mu_j, \mu_k} [\partial_\theta P^{(j)}(\mu_j|\theta)][\partial_\theta P^{(k)}(\mu_k|\theta)] \\
&= \sum_{j=1}^{\nu} F[P^{(j)}(\mu_j|\theta)].
\end{aligned} \tag{A.76}$$

A.8 Quantum Fisher information

In quantum mechanics, for a given probe state $\hat{\rho}_\theta$ and given positive operator valued measurement $\{\hat{E}_\mu\}$, the probability distribution is given by

$$P(\mu|\theta) = \text{Tr}[\hat{\rho}_\theta \hat{E}_\mu], \tag{A.77}$$

and thus the Fisher information is given by

$$F(\theta) = F[\hat{\rho}_\theta] = \sum_\mu \frac{\{\text{Tr}[\partial_\theta \hat{\rho}_\theta \hat{E}_\mu]\}^2}{\text{Tr}[\hat{\rho}_\theta \hat{E}_\mu]}. \tag{A.78}$$

In this section, we derive the quantum Fisher information, which is the maximum of the Fisher information,

$$F_Q[\hat{\rho}_\theta] = \max_{\{\hat{E}_\mu\}} F[\hat{\rho}_\theta]. \tag{A.79}$$

In order to that, we introduce the following super-operator

$$R_{\hat{\rho}_\theta}[\hat{A}] = \frac{1}{2}(\hat{\rho}_\theta \hat{A} + \hat{A}\hat{\rho}_\theta), \tag{A.80}$$

where $\hat{A}$ is an Hermitian operator. By introducing the spectrum decomposition of the density operator

$$\hat{\rho}_\theta = \sum_k p_k |k\rangle\langle k|, \tag{A.81}$$

this super-operator can be rewritten as

$$R_{\hat{\rho}_\theta}[\hat{A}] = \frac{1}{2} \sum_{k,l} (p_k + p_l)\langle k|\hat{A}|l\rangle |k\rangle\langle l|. \tag{A.82}$$

We also introduce the inverse mapping

$$R_{\hat{\rho}_\theta}^{-1}[\hat{A}] = \sum_{k,l} \frac{2}{p_k + p_l}\langle k|\hat{A}|l\rangle |k\rangle\langle l|, \tag{A.83}$$

which satisfies $(R_{\hat{\rho}_\theta}^{-1} \circ R_{\hat{\rho}_\theta})[\hat{A}] = \hat{A}$. Then the following equality holds

$$\mathrm{Tr}[\hat{A}\hat{B}] = \mathrm{ReTr}(\hat{\rho}_\theta \hat{A} R_{\hat{\rho}_\theta}^{-1}[\hat{B}]). \tag{A.84}$$

By using this equality, the Fisher information can be rewritten as

$$\begin{aligned}
F[\hat{\rho}_\theta] &= \sum_\mu \frac{1}{\mathrm{Tr}[\hat{\rho}_\theta \hat{E}_\mu]} [\mathrm{ReTr}(\hat{\rho}_\theta \hat{E}_\mu R_{\hat{\rho}_\theta}^{-1}[\partial_\theta \hat{\rho}_\theta])]^2 \\
&\leq \sum_\mu \frac{1}{\mathrm{Tr}[\hat{\rho}_\theta \hat{E}_\mu]} |\mathrm{Tr}(\hat{\rho}_\theta \hat{E}_\mu R_{\hat{\rho}_\theta}^{-1}[\partial_\theta \hat{\rho}_\theta])|^2 \\
&= \sum_\mu \left| \mathrm{Tr}\left[\frac{\hat{\rho}_\theta^{1/2}\hat{E}_\mu^{1/2}}{\sqrt{\mathrm{Tr}[\hat{\rho}_\theta \hat{E}_\mu]}} \hat{E}_\mu^{1/2} R_{\hat{\rho}_\theta}^{-1}[\partial_\theta \hat{\rho}_\theta]\hat{\rho}_\theta^{1/2} \right] \right|^2.
\end{aligned} \tag{A.85}$$

Here the equality holds if

$$\mathrm{ImTr}(\hat{\rho}_\theta \hat{E}_\mu R_{\hat{\rho}_\theta}^{-1}[\partial_\theta \hat{\rho}_\theta]) = 0. \tag{A.86}$$

By using the Cauchy-Schwarz inequality, the Fisher information can further be rewritten as

$$\begin{aligned}
F[\hat{\rho}_\theta] &\leq \sum_\mu \mathrm{Tr}[|\hat{E}_\mu^{1/2} R_{\hat{\rho}_\theta}^{-1}[\partial_\theta \hat{\rho}_\theta]\hat{\rho}_\theta^{1/2}|^2] \\
&= \sum_\mu \mathrm{Tr}[\hat{\rho}_\theta R_{\hat{\rho}_\theta}^{-1}[\partial_\theta \hat{\rho}_\theta]\hat{E}_\mu R_{\hat{\rho}_\theta}^{-1}[\partial_\theta \hat{\rho}_\theta]] \\
&= \mathrm{Tr}[\hat{\rho}_\theta (R_{\hat{\rho}_\theta}^{-1}[\partial_\theta \hat{\rho}_\theta])^2].
\end{aligned} \tag{A.87}$$

Here the equality holds if

$$\hat{E}_\mu^{1/2}\hat{\rho}_\theta^{1/2} = \lambda \hat{E}_\mu^{1/2} R_{\hat{\rho}_\theta}^{-1}[\partial_\theta \hat{\rho}_\theta]\hat{\rho}_\theta^{1/2}, \tag{A.88}$$

with certain complex number λ. Note that these two conditions (A.86) and (A.88) are equivalent to the condition

$$\hat{E}_\mu\hat{\rho}_\theta = \lambda \hat{E}_\mu R_{\hat{\rho}_\theta}^{-1}[\partial_\theta \hat{\rho}_\theta]\hat{\rho}_\theta, \tag{A.89}$$

with certain real number λ. Then such positive operator valued measurement $\{\hat{E}_\mu\}$ satisfying the condition (A.89) maximizes the Fisher information, i.e., the quantum Fisher information is given by

$$F_Q[\hat{\rho}_\theta] = \text{Tr}[\hat{\rho}_\theta (R_{\hat{\rho}_\theta}^{-1}[\partial_\theta \hat{\rho}_\theta])^2].\tag{A.90}$$

Here, for a mixed state (A.81), the quantum Fisher information becomes

$$F_Q[\hat{\rho}_\theta] = \sum_{k,l} \frac{2}{p_k + p_l} |\langle k|(\partial_\theta \hat{\rho}_\theta)|l\rangle|^2,\tag{A.91}$$

and for a pure state $\hat{\rho}_\theta = |\psi_\theta\rangle\langle\psi_\theta|$, the quantum Fisher information reads

$$F_Q[\hat{\rho}_\theta] = 4\langle\partial_\theta \psi_\theta|(1 - |\psi_\theta\rangle\langle\psi_\theta|)|\partial_\theta \psi_\theta\rangle.\tag{A.92}$$

AppendixB

Algorithms

B.1 Markov chain Monte Carlo method

In this section, we introduce the Markov chain Monte Carlo method, which can be used in both simulated quantum annealing (path integral Monte Carlo method in quantum annealing) and simulated annealing.

We denote a state as $\boldsymbol{s}$ and consider a probability distribution $P(\boldsymbol{s}; t)$ at time t. We assume that the probability distribution at time $t + \Delta t$ is determined only by using the probability distribution at time t. Such process is called the Markov chain. For a given time interval Δt, we assume that the transition probability from the state $\boldsymbol{s}'$ to the state $\boldsymbol{s}$ is given by $w(\boldsymbol{s}|\boldsymbol{s}')$. Then, the Markov chain is described by the master equation

$$P(\boldsymbol{s}; t + \Delta t) = \sum_{\boldsymbol{s}'} w(\boldsymbol{s}|\boldsymbol{s}')\Delta t P(\boldsymbol{s}'; t). \tag{B.1}$$

Note that the transition probability remaining in the same state $w(\boldsymbol{s}|\boldsymbol{s})$ is given by

$$w(\boldsymbol{s}|\boldsymbol{s})\Delta t = 1 - \sum_{\substack{\boldsymbol{s}' \\ (\boldsymbol{s}' \neq \boldsymbol{s})}} w(\boldsymbol{s}'|\boldsymbol{s})\Delta t. \tag{B.2}$$

To update a state according to this transition probability is called the Markov chain Monte Carlo method. From the definition of the probability distribution

$$\sum_{\boldsymbol{s}} P(\boldsymbol{s}; t) = 1, \tag{B.3}$$

the condition

$$\sum_{\boldsymbol{s}, \boldsymbol{s}'} w(\boldsymbol{s}|\boldsymbol{s}')\Delta t P(\boldsymbol{s}'; t) = 1, \tag{B.4}$$

must be satisfied. We consider the case, in which the probability distribution is equilibrated in the infinite time limit

$$P_\infty(\boldsymbol{s}) = \lim_{t \to \infty} P(\boldsymbol{s}; t), \tag{B.5}$$

(for the detailed conditions to equilibrate, see, e.g., [210]). From Eq. (B.1) in the infinite time limit, the equilibrated probability distribution satisfies

$$P_\infty(\boldsymbol{s}) = \sum_{\boldsymbol{s}'} w(\boldsymbol{s}|\boldsymbol{s}')\Delta t P_\infty(\boldsymbol{s}'), \tag{B.6}$$

or equivalently, by using Eq. (B.2),

$$\sum_{\substack{\boldsymbol{s}' \\ (\boldsymbol{s}' \neq \boldsymbol{s})}} w(\boldsymbol{s}'|\boldsymbol{s})P_\infty(\boldsymbol{s}) = \sum_{\substack{\boldsymbol{s}' \\ (\boldsymbol{s}' \neq \boldsymbol{s})}} w(\boldsymbol{s}|\boldsymbol{s}')P_\infty(\boldsymbol{s}'), \tag{B.7}$$

is satisfied. This condition is called the balance condition. The transition probability $w(\boldsymbol{s}|\boldsymbol{s}')$ satisfying the balance condition is not unique. The following detailed balance condition

$$w(\boldsymbol{s}'|\boldsymbol{s})P_\infty(\boldsymbol{s}) = w(\boldsymbol{s}|\boldsymbol{s}')P_\infty(\boldsymbol{s}'), \tag{B.8}$$

which satisfies the balance condition, is often imposed. Note that the transition probability $w(\boldsymbol{s}|\boldsymbol{s}')$ satisfying the detailed balance condition is not still unique.

We assume that the equilibrated probability distribution is given by the Gibbs-Boltzmann distribution

$$P_{\mathrm{GB}}(\boldsymbol{s}) = \frac{1}{Z}\exp[-\beta\mathcal{H}(\boldsymbol{s})], \tag{B.9}$$

where β is the inverse temperature and $\mathcal{H}(\boldsymbol{s})$ is the classical Hamiltonian. Then, the detailed balance condition leads to

$$\frac{w(\boldsymbol{s}'|\boldsymbol{s})}{w(\boldsymbol{s}|\boldsymbol{s}')} = \frac{P_{\mathrm{GB}}(\boldsymbol{s}')}{P_{\mathrm{GB}}(\boldsymbol{s})} = \exp\{-\beta[\mathcal{H}(\boldsymbol{s}') - \mathcal{H}(\boldsymbol{s})]\}. \tag{B.10}$$

Here, we show two examples, which satisfy the condition (B.10). The first example is called the heat bath method, in which the transition probability is given by

$$w(\boldsymbol{s}|\boldsymbol{s}') = \frac{e^{-\beta\mathcal{H}(\boldsymbol{s})}}{e^{-\beta\mathcal{H}(\boldsymbol{s})} + e^{-\beta\mathcal{H}(\boldsymbol{s}')}}. \tag{B.11}$$

The second example is called the Metropolis method, in which the transition probability is given by

$$w(\boldsymbol{s}|\boldsymbol{s}') = \begin{cases} e^{-\beta[\mathcal{H}(\boldsymbol{s}) - \mathcal{H}(\boldsymbol{s}')]} & \text{for} \quad \mathcal{H}(\boldsymbol{s}) - \mathcal{H}(\boldsymbol{s}') \geq 0, \\ 1 & \text{otherwise.} \end{cases} \tag{B.12}$$

With these transition probabilities, the Markov chain Monte Carlo method leads to equilibration of a system. It should be noted that simulated annealing is a method to gradually decrease (increase) the temperature (inverse temperature β) with equilibrating by using the Markov chain Monte Carlo method.

B.2 Maximum flow and minimum cut theorem

In this section, we introduce the maximum flow and minimum cut algorithm, which enables us to obtain the exact ground state and its energy of the random field Ising model [211].

First, we define the maximum flow problem. We consider a capacitated network, which is a directed network with non-negative capacities. That is, for a given graph $G = (\mathcal{N}, \mathcal{A})$, where $\mathcal{N}$ is a set of nodes and $\mathcal{A}$ is a set of arcs, we distinguish arcs $(i, j) \in \mathcal{A}$ and $(j, i) \in \mathcal{A}$, and each arc $(i, j) \in \mathcal{A}$ accompanies a non-negative capacity u_{ij}. The arc adjacency list is defined by

$$A(i) = \{(i, j)|(i, j) \in \mathcal{A}\}, \tag{B.13}$$

i.e., the set of all arcs emitted from a given node $i \in \mathcal{N}$. We specialize two nodes in $\mathcal{N}$, i.e., the source node $s \in \mathcal{N}$ and the sink node $t \in \mathcal{N}$. A flow in the network G is defined by a set of non-negative numbers x_{ij} bounded by

$$0 \leq x_{ij} \leq u_{ij}, \tag{B.14}$$

and satisfying the mass balance constraint

$$\sum_{\{j|(i,j)\in A\}} x_{ij} - \sum_{\{j|(j,i)\in A\}} x_{ji} = \begin{cases} +v & \text{for} \quad i = s, \\ -v & \text{for} \quad i = t, \\ 0 & \text{otherwise.} \end{cases} \tag{B.15}$$
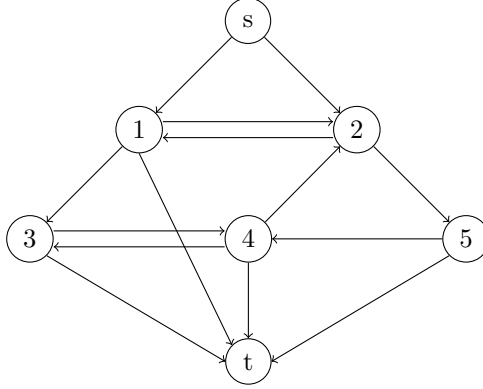
FigureB.1 Schematic picture of a capacitated network with the source and the sink nodes. Here we have the set of seven nodes represented by the circles and the set of fourteen directed arcs represented by the arrows. Each arc accompanies its capacity of a flow. The maximum flow problem is to determine the maximum amount of the flow that streams from the source node to the sink node without increase and decrease its amount during streaming.

The maximum flow problem is to find the maximum value of v. In order to solve this problem, we introduce the concept of the residual network. The residual capacity is defined as the maximum value of flows, which can be additionally sent from a node i to a node j, and thus it is given by

$$r_{ij} = (u_{ij} - x_{ij}) + x_{ji}. \tag{B.16}$$

The residual network is a capacitated network whose capacities are given by the positive residual capacities. We also introduce an augmenting path, which is a directed path from the source node s to the sink node t in the residual network. The capacity of an augmenting path is defined by the minimum residual capacity of arcs in this path. It is obvious that a flow is not maximum if there exist augmenting paths, i.e., we can add as much flows as capacities of augmenting paths. Therefore, if one finds an augmenting path, one have to add a flow along this augmenting path as much as the capacity of this augmenting path in order to solve the maximum flow problem.

Next, we define the minimum cut problem and associate the maximum flow problem with it. A cut is defined by a partition of a set of nodes into two subsets, i.e., we divide $\mathcal{N}$ into S and $\bar{S} = \mathcal{N} \backslash S$. We express this cut as $[S, \bar{S}]$. In particular, if $s \in S$ and $t \in \bar{S}$, we call $[S, \bar{S}]$ an s-t-cut. Arcs $(i, j) \in \mathcal{A}$ with $i \in S$ and $j \in \bar{S}$ are called the forward arcs and those with $j \in S$ and $i \in \bar{S}$ are called the backward arcs. We denote the set of all forward arcs as $(S, \bar{S})$. The capacity of an s-t-cut is defined as

$$u[S, \bar{S}] = \sum_{(i,j) \in (S,\bar{S})} u_{ij}. \tag{B.17}$$

The minimum cut problem is to find an s-t-cut, which minimizes the capacity of it. Here, the summation of the mass balance constraint (B.15) over the all nodes in S leads to

$$\sum_{i \in S} \left\{ \sum_{\{j|(i,j) \in A(i)\}} x_{ij} - \sum_{\{j|(j,i) \in A(i)\}} x_{ji} \right\} = v, \tag{B.18}$$

and its left-hand side can be rewritten as

$$\sum_{i \in S} \left\{ \sum_{\{j|(i,j) \in A(i)\}} x_{ij} - \sum_{\{j|(j,i) \in A(i)\}} x_{ji} \right\} = \sum_{(i,j) \in (S,\bar{S})} x_{ij} - \sum_{(j,i) \in (\bar{S},S)} x_{ji}. \tag{B.19}$$

68

Because $x_{ji} \geq 0$ and $x_{ij} \leq u_{ij}$, it holds

$$v \leq \sum_{(i,j) \in (S, \bar{S})} u_{ij} = u[S, \bar{S}]. \tag{B.20}$$

From this equation, if we find a flow which is equal to the capacity of a cut, then this flow is the maximum flow and this cut is the minimum cut, i.e., the maximum flow problem and the minimum cut problem is equivalent, and thus this problem is called the maximum flow and minimum cut problem. If $r_{ij} = 0$ for all $(i, j) \in (S, \bar{S})$, i.e., there is no augmenting path in the residual network, Eq. (B.16) leads to $x_{ij} = u_{ij} + x_{ji}$, and thus Eq. (B.14) leads to $x_{ij} = u_{ij}$ for $(i, j) \in (S, \bar{S})$ and $x_{ji} = 0$ for $(j, i) \in (\bar{S}, S)$. Therefore, Eqs. (B.18) and (B.19) lead to the equality in Eq. (B.20), i.e., the maximum flow and minimum cut problem is solved (for details and more efficient algorithm, see, e.g., [211]).

Finally we associate the problem to find the ground state of the random field Ising model with the maximum flow and minimum cut problem. The Hamiltonian of the random field Ising model is given by

$$\mathcal{H} = -\sum_{(i,j)} J_{ij} \sigma_i \sigma_j - \sum_i h_i \sigma_i, \tag{B.21}$$

where σ_i is the Ising spin, J_{ij} is non-negative (ferromagnetic) interaction and h_i is a random magnetic field. Here, we add the source node s and the sink node t, and put fixed Ising spins

$$\begin{cases} \sigma_s = +1, \\ \sigma_t = -1. \end{cases} \tag{B.22}$$

We also introduce the interactions

$$J_{si} = \begin{cases} h_i, & \text{for} \quad h_i \geq 0, \\ 0, & \text{for} \quad h_i < 0, \end{cases} \tag{B.23}$$

and

$$J_{it} = \begin{cases} |h_i|, & \text{for} \quad h_i < 0, \\ 0, & \text{for} \quad h_i \geq 0. \end{cases} \tag{B.24}$$

Then the Hamiltonian can be viewed as the random bond Ising model

$$\mathcal{H} = -\sum_{(i,j)} J_{ij} \sigma_i \sigma_j, \tag{B.25}$$

with non-negative random interactions J_{ij} and two boundary conditions (B.22). We introduce the following cut $S = \{i \in \mathcal{N} | \sigma_i = +1\}$ and $\bar{S} = \mathcal{N} \backslash S = \{i \in \mathcal{N} | \sigma_i = -1\}$. Then, for a given spin configuration $\{\sigma_i\}$, the energy of the system is given by

$$\begin{aligned} E &= -\sum_{\{(i,j)|i,j \in S\}} J_{ij} - \sum_{\{(i,j)|i,j \in \bar{S}\}} J_{ij} + \sum_{(i,j) \in (S,\bar{S})} J_{ij} \\ &= -\sum_{(i,j)} J_{ij} + 2 \sum_{(i,j) \in (S,\bar{S})} J_{ij}. \end{aligned} \tag{B.26}$$

Because the first term takes a fixed value, the problem to find the ground state (energy) is rewritten as the problem to minimize the second term. This problem is nothing but the minimum cut problem, and thus we can exactly solve this problem.

Bibliography

[1] A. Acín, I. Bloch, H. Buhrman, T. Calarco, C. Eichler, J. Eisert, D. Esteve, N. Gisin, S. J. Glaser, F. Jelezko, S. Kuhr, M. Lewenstein, M. F. Riedel, P. O. Schmidt, R. Thew, A. Wallraff, I. Walmsley, and F. K. Wilhelm: The quantum technologies roadmap: a European community view, *New Journal of Physics* **20** 080201 (2018).

[2] J. Preskill: Quantum Computing in the NISQ era and beyond, *Quantum* **2** 79 (2018).

[3] M. W. Johnson, M. H. S. Amin, S. Gildert, T. Lanting, F. Hamze, N. Dickson, R. Harris, A. J. Berkley, J. Johansson, P. Bunyk, E. M. Chapple, C. Enderud, J. P. Hilton, K. Karimi, E. Ladizinsky, N. Ladizinsky, T. Oh, I. Perminov, C. Rich, M. C. Thom, E. Tolkacheva, C. J. S. Truncik, S. Uchaikin, J. Wang, B. Wilson, and G. Rose: Quantum annealing with manufactured spins, *Nature* **473** 194 (2011).

[4] S. Boixo, T. F. Rønnow, S. V. Isakov, Z. Wang, D. Wecker, D. A. Lidar, J. M. Martinis, and M. Troyer: Evidence for quantum annealing with more than one hundred qubits, *Nature Physics* **10** 218 (2014).

[5] T. Kadowaki and H. Nishimori: Quantum annealing in the transverse Ising model, *Physical Review E* **58** 5355 (1998).

[6] D. Venturelli, D. J. J. Marchand, and G. Rojo: Quantum Annealing Implementation of Job-Shop Scheduling (2015); arXiv:1506.08479.

[7] F. Neukart, G. Compostella, C. Seidel, D. von Dollen, S. Yarkoni, and B. Parney: Traffic Flow Optimization Using a Quantum Annealer, *Frontiers in ICT* **4** 29 (2017).

[8] T. Stollenwerk, B. O'Gorman, D. Venturelli, S. Mandrà, O. Rodionova, H. K. Ng, B. Sridhar, E. G. Rieffel, and R. Biswas: Quantum Annealing Applied to De-Conflicting Optimal Trajectories for Air Traffic Management (2017); arXiv:1711.04889.

[9] R. Harris, Y. Sato, A. J. Berkley, M. Reis, F. Altomare, M. H. Amin, K. Boothby, P. Bunyk, C. Deng, C. Enderud, S. Huang, E. Hoskinson, M. W. Johnson, E. Ladizinsky, N. Ladizinsky, T. Lanting, R. Li, T. Medina, R. Molavi, R. Neufeld, T. Oh, I. Pavlov, I. Perminov, G. Poulin-Lamarre, C. Rich, A. Smirnov, L. Swenson, N. Tsai, M. Volkmann, J. Whittaker, and J. Yao: Phase transitions in a programmable quantum spin glass simulator., *Science* **361** 162 (2018).

[10] A. D. King, J. Carrasquilla, J. Raymond, I. Ozfidan, E. Andriyash, A. Berkley, M. Reis, T. Lanting, R. Harris, F. Altomare, K. Boothby, P. I. Bunyk, C. Enderud, A. Fréchette, E. Hoskinson, N. Ladizinsky, T. Oh, G. Poulin-Lamarre, C. Rich, Y. Sato, A. Y. Smirnov, L. J. Swenson, M. H. Volkmann, J. Whittaker, J. Yao, E. Ladizinsky, M. W. Johnson, J. Hilton, and M. H. Amin: Observation of topological phenomena in a programmable lattice of 1,800 qubits, *Nature* **560** 456 (2018).

[11] V. Giovannetti, S. Lloyd, and L. Maccone: Advances in quantum metrology, *Nature Photonics* **5** 222 (2011).

[12] C. Degen, F. Reinhard, and P. Cappellaro: Quantum sensing, *Reviews of Modern Physics* **89** 035002 (2017).

[13] L. Pezzè, A. Smerzi, M. K. Oberthaler, R. Schmied, and P. Treutlein: Quantum metrology with nonclassical states of atomic ensembles, *Reviews of Modern Physics* **90** 035005 (2018).

[14] V. Giovannetti, S. Lloyd, and L. Maccone: Quantum-enhanced measurements: beating the standard quantum limit., *Science* **306** 1330 (2004).

[15] V. Giovannetti, S. Lloyd, and L. Maccone: Quantum Metrology, *Physical Review Letters* **96** 010401 (2006).

[16] L. Pezzé and A. Smerzi: Entanglement, Nonlinear Dynamics, and the Heisenberg Limit, *Physical*

Review Letters **102** 100401 (2009).

[17] T. Kato: On the Adiabatic Theorem of Quantum Mechanics, *Journal of the Physical Society of Japan* **5** 435 (1950).

[18] E. Torrontegui, S. Ibáñez, S. Martínez-Garaot, M. Modugno, A. del Campo, D. Guéry-Odelin, A. Ruschhaupt, X. Chen, and J. G. Muga: Shortcuts to Adiabaticity, *Advances In Atomic, Molecular, and Optical Physics* **62** 117 (2013).

[19] M. Demirplak and S. A. Rice: Adiabatic Population Transfer with Control Fields, *The Journal of Physical Chemistry A* **107** 9937 (2003).

[20] M. Demirplak and S. A. Rice: Assisted Adiabatic Passage Revisited, *The Journal of Physical Chemistry B* **109** 6838 (2005).

[21] M. V. Berry: Transitionless quantum driving, *Journal of Physics A: Mathematical and Theoretical* **42** 365303 (2009).

[22] X. Chen, I. Lizuain, A. Ruschhaupt, D. Guéry-Odelin, and J. G. Muga: Shortcut to Adiabatic Passage in Two- and Three-Level Atoms, *Physical Review Letters* **105** 123003 (2010).

[23] J. G. Muga, X. Chen, S. Ibáñez, I. Lizuain, and A. Ruschhaupt: Transitionless quantum drivings for the harmonic oscillator, *Journal of Physics B: Atomic, Molecular and Optical Physics* **43** 085509 (2010).

[24] A. del Campo, M. M. Rams, and W. H. Zurek: Assisted Finite-Rate Adiabatic Passage Across a Quantum Critical Point: Exact Solution for the Quantum Ising Model, *Physical Review Letters* **109** 115703 (2012).

[25] D. Sels and A. Polkovnikov: Minimizing irreversible losses in quantum systems by local counterdiabatic driving., *Proceedings of the National Academy of Sciences of the United States of America* **114** E3909 (2017).

[26] C. Jarzynski: Generating shortcuts to adiabaticity in quantum and classical dynamics, *Physical Review A* **88** 040101 (2013).

[27] A. del Campo: Shortcuts to Adiabaticity by Counterdiabatic Driving, *Physical Review Letters* **111** 100502 (2013).

[28] S. Deffner, C. Jarzynski, and A. del Campo: Classical and Quantum Shortcuts to Adiabaticity for Scale-Invariant Driving, *Physical Review X* **4** 021013 (2014).

[29] M. Okuyama and K. Takahashi: From Classical Nonlinear Integrable Systems to Quantum Shortcuts to Adiabaticity, *Physical Review Letters* **117** 070401 (2016).

[30] T. Hatomura and T. Mori: Shortcuts to adiabatic classical spin dynamics mimicking quantum annealing, *Physical Review E* **98** 032136 (2018).

[31] C. Jarzynski: Geometric Phases and Anholonomy for a Class of Chaotic Classical Systems, *Physical Review Letters* **74** 1732 (1995).

[32] A. Emmanouilidou, X.-G. Zhao, P. Ao, and Q. Niu: Steering an Eigenstate to a Destination, *Physical Review Letters* **85** 1626 (2000).

[33] F. Wegner: Flow equations and normal ordering: a survey, *Journal of Physics A: Mathematical and General* **39** 8221 (2006).

[34] X. Chen, A. Ruschhaupt, S. Schmidt, A. del Campo, D. Guéry-Odelin, and J. G. Muga: Fast Optimal Frictionless Atom Cooling in Harmonic Traps: Shortcut to Adiabaticity, *Physical Review Letters* **104** 063002 (2010).

[35] H. R. Lewis and W. B. Riesenfeld: An Exact Quantum Theory of the Time-Dependent Harmonic Oscillator and of a Charged Particle in a Time-Dependent Electromagnetic Field, *Journal of Mathematical Physics* **10** 1458 (1969).

[36] X. Chen, E. Torrontegui, and J. G. Muga: Lewis-Riesenfeld invariants and transitionless quantum driving, *Physical Review A* **83** 062116 (2011).

[37] S. Masuda and K. Nakamura: Fast-forward problem in quantum mechanics, *Physical Review A* **78** 062108 (2008).

[38] S. Masuda and K. Nakamura: Fast-forward of adiabatic dynamics in quantum mechanics, *Proceedings of the Royal Society A: Mathematical, Physical and Engineering Sciences* **466** 1135 (2010).

[39] S. Masuda and K. Nakamura: Acceleration of adiabatic quantum dynamics in electromagnetic fields, *Physical Review A* **84** 043434 (2011).

71

[40] S. Masuda: Acceleration of adiabatic transport of interacting particles and rapid manipulations of a dilute Bose gas in the ground state, *Physical Review A* **86** 063624 (2012).

[41] A. T. Rezakhani, W.-J. Kuo, A. Hamma, D. A. Lidar, and P. Zanardi: Quantum Adiabatic Brachistochrone, *Physical Review Letters* **103** 080502 (2009).

[42] A. T. Rezakhani, D. F. Abasto, D. A. Lidar, and P. Zanardi: Intrinsic geometry of quantum adiabatic evolution and quantum phase transitions, *Physical Review A* **82** 012321 (2010).

[43] A. Carlini, A. Hosoya, T. Koike, and Y. Okudaira: Time-Optimal Quantum Evolution, *Physical Review Letters* **96** 060503 (2006).

[44] A. Carlini, A. Hosoya, T. Koike, and Y. Okudaira: Time-optimal unitary operations, *Physical Review A* **75** 042308 (2007).

[45] L. S. Pontryagin: *Mathematical Theory of Optimal Processes* (Interscience Publishers, New York, 1962).

[46] X. Chen and J. G. Muga: Engineering of fast population transfer in three-level systems, *Physical Review A* **86** 033405 (2012).

[47] A. Ruschhaupt, X. Chen, D. Alonso, and J. G. Muga: Optimally robust shortcuts to population inversion in two-level quantum systems, *New Journal of Physics* **14** 093040 (2012).

[48] Y. Ban, X. Chen, E. Y. Sherman, and J. G. Muga: Fast and Robust Spin Manipulation in a Quantum Dot by Electric Fields, *Physical Review Letters* **109** 206602 (2012).

[49] U. Güngördü, Y. Wan, M. A. Fasihi, and M. Nakahara: Dynamical invariants for quantum control of four-level systems, *Physical Review A* **86** 062312 (2012).

[50] T.-Y. Lin, F.-C. Hsiao, Y.-W. Jhang, C. Hu, and S.-Y. Tseng: Mode conversion using optical analogy of shortcut to adiabatic passage in engineered multimode waveguides, *Optics Express* **20** 24085 (2012).

[51] S.-Y. Tseng and X. Chen: Engineering of fast mode conversion in multimode waveguides, *Optics Letters* **37** 5118 (2012).

[52] M. G. Bason, M. Viteau, N. Malossi, P. Huillery, E. Arimondo, D. Ciampini, R. Fazio, V. Giovannetti, R. Mannella, and O. Morsch: High-fidelity quantum driving, *Nature Physics* **8** 147 (2012).

[53] J. Zhang, J. H. Shim, I. Niemeyer, T. Taniguchi, T. Teraji, H. Abe, S. Onoda, T. Yamamoto, T. Ohshima, J. Isoya, and D. Suter: Experimental Implementation of Assisted Quantum Adiabatic Passage in a Single Spin, *Physical Review Letters* **110** 240501 (2013).

[54] J. G. Muga, X. Chen, A. Ruschhaupt, and D. Guéry-Odelin: Frictionless dynamics of Bose-Einstein condensates under fast trap variations, *Journal of Physics B: Atomic, Molecular and Optical Physics* **42** 241001 (2009).

[55] X. Chen and J. G. Muga: Transient energy excitation in shortcuts to adiabaticity for the time-dependent harmonic oscillator, *Physical Review A* **82** 053403 (2010).

[56] J.-F. Schaff, X.-L. Song, P. Vignolo, and G. Labeyrie: Fast optimal transition between two equilibrium states, *Physical Review A* **82** 033430 (2010).

[57] J.-F. Schaff, X.-L. Song, P. Capuzzi, P. Vignolo, and G. Labeyrie: Shortcut to adiabaticity for an interacting Bose-Einstein condensate, *Europhysics Letters* **93** 23001 (2011).

[58] J.-F. Schaff, P. Capuzzi, G. Labeyrie, and P. Vignolo: Shortcuts to adiabaticity for trapped ultracold gases, *New Journal of Physics* **13** 113017 (2011).

[59] A. del Campo: Frictionless quantum quenches in ultracold gases: A quantum-dynamical microscope, *Physical Review A* **84** 031606 (2011).

[60] A. del Campo: Fast frictionless dynamics as a toolbox for low-dimensional Bose-Einstein condensates, *Europhysics Letters* **96** 60005 (2011).

[61] A. del Campo and M. G. Boshier: Shortcuts to adiabaticity in a time-dependent box, *Scientific Reports* **2** 648 (2012).

[62] E. Torrontegui, S. Martínez-Garaot, A. Ruschhaupt, and J. G. Muga: Shortcuts to adiabaticity: Fast-forward approach, *Physical Review A* **86** 013601 (2012).

[63] E. Torrontegui, X. Chen, M. Modugno, A. Ruschhaupt, D. Guéry-Odelin, and J. G. Muga: Fast transitionless expansion of cold atoms in optical Gaussian-beam traps, *Physical Review A* **85** 033605 (2012).

[64] D. Stefanatos and J.-S. Li: Frictionless decompression in minimum time of Bose-Einstein conden-

sates in the Thomas-Fermi regime, *Physical Review A* **86** 063602 (2012).

[65] P. Salamon, K. H. Hoffmann, Y. Rezek, and R. Kosloff: Maximum work in minimum time from a conservative quantum system, *Physical Chemistry Chemical Physics* **11** 1027 (2009).

[66] Y. Rezek, P. Salamon, K. H. Hoffmann, and R. Kosloff: The quantum refrigerator: The quest for absolute zero, *Europhysics Letters* **85** 30008 (2009).

[67] R. Kosloff and T. Feldmann: Optimal performance of reciprocating demagnetization quantum refrigerators, *Physical Review E* **82** 011134 (2010).

[68] K. H. Hoffmann, P. Salamon, Y. Rezek, and R. Kosloff: Time-optimal controls for frictionless cooling in harmonic traps, *Europhysics Letters* **96** 60015 (2011).

[69] A. Levy and R. Kosloff: Quantum Absorption Refrigerator, *Physical Review Letters* **108** 070604 (2012).

[70] T. Feldmann and R. Kosloff: Short time cycles of purely quantum refrigerators, *Physical Review E* **85** 051114 (2012).

[71] Y. Zheng, S. Campbell, G. De Chiara, and D. Poletti: Cost of counterdiabatic driving and work output, *Physical Review A* **94** 042132 (2016).

[72] S. Campbell and S. Deffner: Trade-Off Between Speed and Cost in Shortcuts to Adiabaticity, *Physical Review Letters* **118** 100601 (2017).

[73] K. Funo, J.-N. Zhang, C. Chatou, K. Kim, M. Ueda, and A. del Campo: Universal Work Fluctuations During Shortcuts to Adiabaticity by Counterdiabatic Driving, *Physical Review Letters* **118** 100602 (2017).

[74] E. Torrontegui, S. Ibáñez, X. Chen, A. Ruschhaupt, D. Guéry-Odelin, and J. G. Muga: Fast atomic transport without vibrational heating, *Physical Review A* **83** 013415 (2011).

[75] X. Chen, E. Torrontegui, D. Stefanatos, J.-S. Li, and J. G. Muga: Optimal trajectories for efficient atomic transport without final excitation, *Physical Review A* **84** 043415 (2011).

[76] E. Torrontegui, X. Chen, M. Modugno, S. Schmidt, A. Ruschhaupt, and J. G. Muga: Fast transport of Bose-Einstein condensates, *New Journal of Physics* **14** 013031 (2012).

[77] S. An, D. Lv, A. del Campo, and K. Kim: Shortcuts to adiabaticity by counterdiabatic driving for trapped-ion displacement in phase space, *Nature Communications* **7** 12999 (2016).

[78] G. Ness, C. Shkedrov, Y. Florshaim, and Y. Sagi: Realistic shortcuts to adiabaticity in optical transfer, *New Journal of Physics* **20** 095002 (2018).

[79] E. Torrontegui, S. Martínez-Garaot, M. Modugno, X. Chen, and J. G. Muga: Engineering fast and stable splitting of matter waves, *Physical Review A* **87** 033630 (2013).

[80] B. Juliá-Díaz, E. Torrontegui, J. Martorell, J. G. Muga, and A. Polls: Fast generation of spin-squeezed states in bosonic Josephson junctions, *Physical Review A* **86** 063623 (2012).

[81] A. Yuste, B. Juliá-Díaz, E. Torrontegui, J. Martorell, J. G. Muga, and A. Polls: Shortcut to adiabaticity in internal bosonic Josephson junctions, *Physical Review A* **88** 043647 (2013).

[82] T. Hatomura: Shortcuts to adiabatic cat-state generation in bosonic Josephson junctions, *New Journal of Physics* **20** 015010 (2018).

[83] M. Sarandy, E. Duzzioni, and R. Serra: Quantum computation in continuous time using dynamic invariants, *Physics Letters A* **375** 3343 (2011).

[84] K. Takahashi: Hamiltonian engineering for adiabatic quantum computation: Lessons from shortcuts to adiabaticity (2018); arXiv:1808.07177.

[85] A. C. Santos and M. S. Sarandy: Superadiabatic Controlled Evolutions and Universal Quantum Computation, *Scientific Reports* **5** 15775 (2015).

[86] I. B. Coulamy, A. C. Santos, I. Hen, and M. S. Sarandy: Energetic Cost of Superadiabatic Quantum Computation, *Frontiers in ICT* **3** 19 (2016).

[87] J. L. Wu and S. L. Su: Universal speeded-up adiabatic geometric quantum computation in three-level systems via counterdiabatic driving (2018); arXiv:1811.07566.

[88] T. Wang, Z. Zhang, L. Xiang, Z. Jia, P. Duan, Z. Zong, Z. Sun, Z. Dong, J. Wu, Y. Yin, and G. Guo: Experimental realization of a fast controlled-Z gate via a shortcut-to-adiabaticity (2018); arXiv:1811.08096.

[89] K. Takahashi: Shortcuts to adiabaticity for quantum annealing, *Physical Review A* **95** 012309 (2017).

[90] A. B. Özgüler, R. Joynt, and M. G. Vavilov: Steering Random Spin Systems to Speed up the Quantum Adiabatic Algorithm (2018); arXiv:1804.01180.

[91] A. Hartmann and W. Lechner: Rapid counter-diabatic sweeps in lattice gauge adiabatic quantum computing (2018); arXiv:1807.02053.

[92] S. Choi, R. Onofrio, and B. Sundaram: Optimized sympathetic cooling of atomic mixtures via fast adiabatic strategies, *Physical Review A* **84** 051601 (2011).

[93] S. Choi, R. Onofrio, and B. Sundaram: Squeezing and robustness of frictionless cooling strategies, *Physical Review A* **86** 043436 (2012).

[94] S. Ibáñez, X. Chen, E. Torrontegui, J. G. Muga, and A. Ruschhaupt: Multiple Schrödinger Pictures and Dynamics in Shortcuts to Adiabaticity, *Physical Review Letters* **109** 100403 (2012).

[95] K. Takahashi: How fast and robust is the quantum adiabatic passage?, *Journal of Physics A: Mathematical and Theoretical* **46** 315304 (2013).

[96] K. Takahashi: Fast-forward scaling in a finite-dimensional Hilbert space, *Physical Review A* **89** 042113 (2014).

[97] B. Damski: Counterdiabatic driving of the quantum Ising model, *Journal of Statistical Mechanics: Theory and Experiment* **2014** P12019 (2014).

[98] T. Opatrný and K. Mølmer: Partial suppression of nonadiabatic transitions, *New Journal of Physics* **16** 015025 (2014).

[99] S. Martínez-Garaot, E. Torrontegui, X. Chen, and J. G. Muga: Shortcuts to adiabaticity in three-level systems using Lie transforms, *Physical Review A* **89** 053408 (2014).

[100] K. Takahashi: Unitary deformations of counterdiabatic driving, *Physical Review A* **91** 042115 (2015).

[101] V. Mukherjee, S. Montangero, and R. Fazio: Local shortcut to adiabaticity for quantum many-body systems, *Physical Review A* **93** 062108 (2016).

[102] S. Masuda, U. Güngördü, X. Chen, T. Ohmi, and M. Nakahara: Fast control of topological vortex formation in Bose-Einstein condensates by counterdiabatic driving, *Physical Review A* **93** 013626 (2016).

[103] A. Patra and C. Jarzynski: Classical and Quantum Shortcuts to Adiabaticity in a Tilted Piston, *The Journal of Physical Chemistry B* **121** 3403 (2017).

[104] M. Okuyama and K. Takahashi: Quantum-Classical Correspondence of Shortcuts to Adiabaticity, *Journal of the Physical Society of Japan* **86** 043002 (2017).

[105] K. Takahashi: Shortcuts to adiabaticity applied to nonequilibrium entropy production: an information geometry viewpoint, *New Journal of Physics* **19** 115007 (2017).

[106] K. Nishimura and K. Takahashi: Counterdiabatic Hamiltonians for multistate Landau-Zener problem, *SciPost Physics* **5** 029 (2018).

[107] X. Zhou, S. Jin, and J. Schmiedmayer: Shortcut loading a Bose-Einstein condensate into an optical lattice, *New Journal of Physics* **20** 055005 (2018).

[108] F. Petiziol, B. Dive, F. Mintert, and S. Wimberger: Fast adiabatic evolution by oscillating initial Hamiltonians, *Physical Review A* **98** 043436 (2018).

[109] T. Hatomura: Shortcuts to adiabaticity in the infinite-range ising model by mean-field counter-diabatic driving, *Journal of the Physical Society of Japan* **86** 094002 (2017).

[110] A. Messiah: *Quantum Mechanics* (Dover Publications, 1999).

[111] M. V. Berry: Quantal Phase Factors Accompanying Adiabatic Changes, *Proceedings of the Royal Society A: Mathematical, Physical and Engineering Sciences* **392** 45 (1984).

[112] B. Simon: Holonomy, the Quantum Adiabatic Theorem, and Berry's Phase, *Physical Review Letters* **51** 2167 (1983).

[113] F. Wilczek and A. Zee: Appearance of Gauge Structure in Simple Dynamical Systems, *Physical Review Letters* **52** 2111 (1984).

[114] A. C. Santos and M. S. Sarandy: Generalized shortcuts to adiabaticity and enhanced robustness against decoherence, *Journal of Physics A: Mathematical and Theoretical* **51** 025301 (2018).

[115] K. Takahashi: Transitionless quantum driving for spin systems, *Physical Review E* **87** 062117 (2013).

[116] B. Apolloni, C. Carvalho, and D. de Falco: Quantum stochastic optimization, *Stochastic Processes*

and their Applications **33** 233 (1989).

[117] R. L. Somorjai: Novel approach for computing the global minimum of proteins. 1. General concepts, methods, and approximations, *The Journal of Physical Chemistry* **95** 4141 (1991).

[118] P. Amara, D. Hsu, and J. E. Straub: Global energy minimum searches using an approximate solution of the imaginary time Schroedinger equation, *The Journal of Physical Chemistry* **97** 6715 (1993).

[119] A. Finnila, M. Gomez, C. Sebenik, C. Stenson, and J. Doll: Quantum annealing: A new method for minimizing multidimensional functions, *Chemical Physics Letters* **219** 343 (1994).

[120] J. Brooke, D. Bitko, T. Rosenbaum, Aeppli, and G. Aeppli: Quantum annealing of a disordered magnet, *Science* **284** 779 (1999).

[121] J. Brooke, T. F. Rosenbaum, and G. Aeppli: Tunable quantum tunnelling of magnetic domain walls, *Nature* **413** 610 (2001).

[122] E. Farhi, J. Goldstone, S. Gutmann, and M. Sipser: Quantum Computation by Adiabatic Evolution (2000); arXiv:0001106.

[123] E. Farhi, J. Goldstone, S. Gutmann, J. Lapan, A. Lundgren, and D. Preda: A Quantum Adiabatic Evolution Algorithm Applied to Random Instances of an NP-Complete Problem, *Science* **292** 472 (2001).

[124] D. Aharonov, W. van Dam, J. Kempe, Z. Landau, S. Lloyd, and O. Regev: Adiabatic Quantum Computation is Equivalent to Standard Quantum Computation, *SIAM Journal on Computing* **37** 166 (2007).

[125] S. Boixo, T. Albash, F. M. Spedalieri, N. Chancellor, and D. A. Lidar: Experimental signature of programmable quantum annealing, *Nature Communications* **4** 2067 (2013).

[126] T. Lanting, A. Przybysz, A. Smirnov, F. Spedalieri, M. Amin, A. Berkley, R. Harris, F. Altomare, S. Boixo, P. Bunyk, N. Dickson, C. Enderud, J. Hilton, E. Hoskinson, M. Johnson, E. Ladizinsky, N. Ladizinsky, R. Neufeld, T. Oh, I. Perminov, C. Rich, M. Thom, E. Tolkacheva, S. Uchaikin, A. Wilson, and G. Rose: Entanglement in a Quantum Annealing Processor, *Physical Review X* **4** 021041 (2014).

[127] J. A. Smolin and G. Smith: Classical signature of quantum annealing, *Frontiers in Physics* **2** 52 (2014).

[128] L. Wang, T. F. Rønnow, S. Boixo, S. V. Isakov, Z. Wang, D. Wecker, D. A. Lidar, J. M. Martinis, and M. Troyer: Comment on: "Classical signature of quantum annealing" (2013); arXiv:1305.5837.

[129] S. W. Shin, G. Smith, J. A. Smolin, and U. Vazirani: How "Quantum" is the D-Wave Machine? (2014); arXiv:1401.7087.

[130] T. Albash, T. Rønnow, M. Troyer, and D. Lidar: Reexamining classical and quantum models for the D-Wave One processor, *The European Physical Journal Special Topics* **224** 111 (2015).

[131] G. E. Santoro, R. Martonák, E. Tosatti, and R. Car: Theory of quantum annealing of an Ising spin glass., *Science* **295** 2427 (2002).

[132] R. Martonák, G. E. Santoro, and E. Tosatti: Quantum annealing by the path-integral Monte Carlo method: The two-dimensional random Ising model, *Physical Review B* **66** 094203 (2002).

[133] E. Farhi, J. Goldstone, and S. Gutmann: Quantum Adiabatic Evolution Algorithms with Different Paths (2002); arXiv:0208135.

[134] Y. Seki and H. Nishimori: Quantum annealing with antiferromagnetic fluctuations, *Physical Review E* **85** 051112 (2012).

[135] B. Seoane and H. Nishimori: Many-body transverse interactions in the quantum annealing of the p-spin ferromagnet, *Journal of Physics A: Mathematical and Theoretical* **45** 435301 (2012).

[136] E. Crosson, E. Farhi, C. Y.-Y. Lin, H.-H. Lin, and P. Shor: Different Strategies for Optimization Using the Quantum Adiabatic Algorithm (2014); arXiv:1401.7320.

[137] Y. Seki and H. Nishimori: Quantum annealing with antiferromagnetic transverse interactions for the Hopfield model, *Journal of Physics A: Mathematical and Theoretical* **48** 335301 (2015).

[138] H. Nishimori and K. Takada: Exponential Enhancement of the Efficiency of Quantum Annealing by Non-Stoquastic Hamiltonians, *Frontiers in ICT* **4** 2 (2017).

[139] L. Hormozi, E. W. Brown, G. Carleo, and M. Troyer: Nonstoquastic Hamiltonians and quantum annealing of an Ising spin glass, *Physical Review B* **95** 184416 (2017).

[140] S. Bravyi, D. P. Divincenzo, R. Oliveira, and B. M. Terhal: The complexity of stoquastic local Hamiltonian problems, *Quantum Information & Computation* **8** 361 (2001).

[141] E. Farhi, J. Goldston, D. Gosset, S. Gutmann, H. B. Meyer, and P. Shor: Quantum adiabatic algorithms, small gaps, and different paths, *Quantum Information & Computation* **11** 181 (2001).

[142] W. H. Zurek and U. Dorner: Phase transition in space: how far does a symmetry bend before it breaks?, *Philosophical transactions. Series A, Mathematical, physical, and engineering sciences* **366** 2953 (2008).

[143] J. Dziarmaga and M. M. Rams: Dynamics of an inhomogeneous quantum phase transition, *New Journal of Physics* **12** 055007 (2010).

[144] N. G. Dickson and M. H. S. Amin: Does Adiabatic Quantum Optimization Fail for NP-Complete Problems?, *Physical Review Letters* **106** 050502 (2011).

[145] N. G. Dickson and M. H. Amin: Algorithmic approach to adiabatic quantum optimization, *Physical Review A* **85** 032303 (2012).

[146] M. M. Rams, M. Mohseni, and A. del Campo: Inhomogeneous quasi-adiabatic driving of quantum critical dynamics in weakly disordered spin chains, *New Journal of Physics* **18** 123034 (2016).

[147] T. Lanting, A. D. King, B. Evert, and E. Hoskinson: Experimental demonstration of perturbative anticrossing mitigation using nonuniform driver Hamiltonians, *Physical Review A* **96** 042322 (2017).

[148] J. I. Adame and P. L. McMahon: Inhomogeneous driving in quantum annealers can result in orders-of-magnitude improvements in performance (2018); arXiv:1806.11091.

[149] M. Mohseni, J. Strumpfer, and M. M. Rams: Engineering non-equilibrium quantum phase transitions via causally gapped Hamiltonians, *New Journal of Physics* **20** 105002 (2018).

[150] Y. Susa, Y. Yamashiro, M. Yamamoto, and H. Nishimori: Exponential Speedup of Quantum Annealing by Inhomogeneous Driving of the Transverse Field, *Journal of the Physical Society of Japan* **87** 023002 (2018).

[151] Y. Susa, Y. Yamashiro, M. Yamamoto, I. Hen, D. A. Lidar, and H. Nishimori: Quantum annealing of the p -spin model under inhomogeneous transverse field driving, *Physical Review A* **98** 042326 (2018).

[152] V. Choi: Minor-embedding in adiabatic quantum computation: II. Minor-universal graph design, *Quantum Information Processing* **10** 343 (2011).

[153] K. Husimi: Statistical mechanics of condensation, In H. Yukawa (ed), *Proceedings of the International Conference of Theoretical Physics*, pp. 531–533 (Science Council of Japan, Tokyo, 1953).

[154] H. N. V. Temperley: The Mayer Theory of Condensation Tested Against a Simple Model of the Imperfect Gas, *Proceedings of the Physical Society. Section A* **67** 233 (1954).

[155] S. Suzuki, J. Inoue, and B. K. Chakrabarti: *Quantum Ising Phases and Transitions in Transverse Isin Models* (Springer-Verlag, Berlin Heidelberg, 2013) 2nd ed.

[156] E. C. Stoner and E. P. Wohlfarth: A Mechanism of Magnetic Hysteresis in Heterogeneous Alloys, *Philosophical Transactions of the Royal Society A: Mathematical, Physical and Engineering Sciences* **240** 599 (1948).

[157] W. Wernsdorfer, E. B. Orozco, B. Barbara, K. Hasselbach, A. Benoit, D. Mailly, B. Doudin, J. Meier, J. E. Wegrowe, J.-P. Ansermet, N. Demoncy, H. Pascard, N. Demoncy, A. Loiseau, L. Francois, N. Duxin, and M. P. Pileni: Mesoscopic effects in magnetism: Submicron to nanometer size single particle measurements, *Journal of Applied Physics* **81** 5543 (1998).

[158] A. Einstein, B. Podolsky, and N. Rosen: Can Quantum-Mechanical Description of Physical Reality Be Considered Complete?, *Physical Review* **47** 777 (1935).

[159] A. Aspect, J. Dalibard, and G. Roger: Experimental Test of Bell's Inequalities Using Time- Varying Analyzers, *Physical Review Letters* **49** 1804 (1982).

[160] C. H. Bennett, G. Brassard, C. Crépeau, R. Jozsa, A. Peres, and W. K. Wootters: Teleporting an unknown quantum state via dual classical and Einstein-Podolsky-Rosen channels, *Physical Review Letters* **70** 1895 (1993).

[161] H.-J. Briegel, W. Dür, J. I. Cirac, and P. Zoller: Quantum Repeaters: The Role of Imperfect Local Operations in Quantum Communication, *Physical Review Letters* **81** 5932 (1998).

[162] D. Gottesman and I. L. Chuang: Demonstrating the viability of universal quantum computation using teleportation and single-qubit operations, *Nature* **402** 390 (1999).

[163] E. Schrödinger: Die gegenwärtige Situation in der Quantenmechanik, *Die Naturwissenschaften* **23** 807 (1935).

[164] E. Schrödinger: Die gegenwärtige Situation in der Quantenmechanik, *Die Naturwissenschaften* **23** 823 (1935).

[165] E. Schrödinger: Die gegenwärtige Situation in der Quantenmechanik, *Die Naturwissenschaften* **23** 844 (1935).

[166] A. J. Leggett and A. Garg: Quantum mechanics versus macroscopic realism: Is the flux there when nobody looks?, *Physical Review Letters* **54** 857 (1985).

[167] W. H. Zurek: Decoherence, einselection, and the quantum origins of the classical, *Reviews of Modern Physics* **75** 715 (2003).

[168] G. C. Knee, K. Kakuyanagi, M.-C. Yeh, Y. Matsuzaki, H. Toida, H. Yamaguchi, S. Saito, A. J. Leggett, and W. J. Munro: A strict experimental test of macroscopic realism in a superconducting flux qubit, *Nature Communications* **7** 13253 (2016).

[169] C. Monroe, D. M. Meekhof, B. E. King, and D. J. Wineland: A "Schrodinger Cat" Superposition State of an Atom, *Science* **272** 1131 (1996).

[170] M. Brune, E. Hagley, J. Dreyer, X. Maître, A. Maali, C. Wunderlich, J. M. Raimond, and S. Haroche: Observing the Progressive Decoherence of the "Meter" in a Quantum Measurement, *Physical Review Letters* **77** 4887 (1996).

[171] J. R. Friedman, V. Patel, W. Chen, S. K. Tolpygo, and J. E. Lukens: Quantum superposition of distinct macroscopic states, *Nature* **406** 43 (2000).

[172] A. Ourjoumtsev, H. Jeong, R. Tualle-Brouri, and P. Grangier: Generation of optical 'Schrödinger cats' from photon number states, *Nature* **448** 784 (2007).

[173] B. Vlastakis, G. Kirchmair, Z. Leghtas, S. E. Nigg, L. Frunzio, S. M. Girvin, M. Mirrahimi, M. H. Devoret, and R. J. Schoelkopf: Deterministically encoding quantum information using 100-photon Schrödinger cat states., *Science* **342** 607 (2013).

[174] C. Wang, Y. Y. Gao, P. Reinhold, R. W. Heeres, N. Ofek, K. Chou, C. Axline, M. Reagor, J. Blumoff, K. M. Sliwa, L. Frunzio, S. M. Girvin, L. Jiang, M. Mirrahimi, M. H. Devoret, and R. J. Schoelkopf: A Schrödinger cat living in two boxes., *Science* **352** 1087 (2016).

[175] W.-B. Gao, C.-Y. Lu, X.-C. Yao, P. Xu, O. Gühne, A. Goebel, Y.-A. Chen, C.-Z. Peng, Z.-B. Chen, and J.-W. Pan: Experimental demonstration of a hyper-entangled ten-qubit Schrödinger cat state, *Nature Physics* **6** 331 (2010).

[176] J. A. Jones, S. D. Karlen, J. Fitzsimons, A. Ardavan, S. C. Benjamin, G. A. D. Briggs, and J. J. L. Morton: Magnetic field sensing beyond the standard quantum limit using 10-spin NOON states., *Science* **324** 1166 (2009).

[177] S. Simmons, J. A. Jones, S. D. Karlen, A. Ardavan, and J. J. L. Morton: Magnetic field sensors using 13-spin cat states, *Physical Review A* **82** 022330 (2010).

[178] C. A. Sackett, D. Kielpinski, B. E. King, C. Langer, V. Meyer, C. J. Myatt, M. Rowe, Q. A. Turchette, W. M. Itano, D. J. Wineland, and C. Monroe: Experimental entanglement of four particles, *Nature* **404** 256 (2000).

[179] D. Leibfried, E. Knill, S. Seidelin, J. Britton, R. B. Blakestad, J. Chiaverini, D. B. Hume, W. M. Itano, J. D. Jost, C. Langer, R. Ozeri, R. Reichle, and D. J. Wineland: Creation of a six-atom 'Schrödinger cat' state, *Nature* **438** 639 (2005).

[180] T. Monz, P. Schindler, J. T. Barreiro, M. Chwalla, D. Nigg, W. A. Coish, M. Harlander, W. Hänsel, M. Hennrich, and R. Blatt: 14-Qubit Entanglement: Creation and Coherence, *Physical Review Letters* **106** 130506 (2011).

[181] H. Lee, P. Kok, and J. P. Dowling: A quantum Rosetta stone for interferometry, *Journal of Modern Optics* **49** 2325 (2002).

[182] J. I. Cirac, M. Lewenstein, K. Mølmer, and P. Zoller: Quantum superposition states of Bose-Einstein condensates, *Physical Review A* **57** 1208 (1998).

[183] R. Botet, R. Jullien, and P. Pfeuty: Size Scaling for Infinitely Coordinated Systems, *Physical Review Letters* **49** 478 (1982).

[184] Y. Li, Y. Castin, and A. Sinatra: Optimum Spin Squeezing in Bose-Einstein Condensates with Particle Losses, *Physical Review Letters* **100** 210401 (2008).

[185] R. A. Fisher: On the Mathematical Foundations of Theoretical Statistics, *Philosophical Transactions of the Royal Society A: Mathematical, Physical and Engineering Sciences* **222** 309 (1922).

[186] R. A. Fisher: Theory of Statistical Estimation, *Mathematical Proceedings of the Cambridge Philosophical Society* **22** 700 (1925).

[187] M. Fréchet: Sur l'extension de certaines evaluations statistiques au cas de petits echantillons, *Revue de l'Institut International de Statistique / Review of the International Statistical Institute* **11** 182 (1943).

[188] C. R. Rao: Information and the accuracy attainable in the estimation of statistical parameters, *Bulletin of the Calcutta Mathematical Society* **37** 81 (1945).

[189] H. Cramér: *Mathematical Methods of Statistics* (Princeton University Press, Princeton, NJ, 1946).

[190] M. Cohen: The Fisher information and convexity (Corresp.), *IEEE Transactions on Information Theory* **14** 591 (1968).

[191] L. Pezzè and A. Smerzi: Quantum theory of phase estimation, In G. M. Tino and M. A. Kasevich (eds), *Proceedings of the International School of Physics "Enrico Fermi"*, 2014, pp. 691 – 741.

[192] S. L. Braunstein and C. M. Caves: Statistical distance and the geometry of quantum states, *Physical Review Letters* **72** 3439 (1994).

[193] S. L. Braunstein, C. M. Caves, and G. Milburn: Generalized Uncertainty Relations: Theory, Examples, and Lorentz Invariance, *Annals of Physics* **247** 135 (1996).

[194] J. M. Radcliffe: Some properties of coherent spin states, *Journal of Physics A: General Physics* **4** 313 (1971).

[195] F. T. Arecchi, E. Courtens, R. Gilmore, and H. Thomas: Atomic Coherent States in Quantum Optics, *Physical Review A* **6** 2211 (1972).

[196] W. M. Itano, J. C. Bergquist, J. J. Bollinger, J. M. Gilligan, D. J. Heinzen, F. L. Moore, M. G. Raizen, and D. J. Wineland: Quantum projection noise: Population fluctuations in two-level systems, *Physical Review A* **47** 3554 (1993).

[197] J. J. . Bollinger, W. M. Itano, D. J. Wineland, and D. J. Heinzen: Optimal frequency measurements with maximally correlated states, *Physical Review A* **54** R4649 (1996).

[198] M. J. Steel and M. J. Collett: Quantum state of two trapped Bose-Einstein condensates with a Josephson coupling, *Physical Review A* **57** 2920 (1998).

[199] H. Lipkin, N. Meshkov, and A. Glick: Validity of many-body approximation methods for a solvable model: (I). Exact solutions and perturbation theory, *Nuclear Physics* **62** 188 (1965).

[200] V. S. Shchesnovich and M. Trippenbach: Fock-space WKB method for the boson Josephson model describing a Bose-Einstein condensate trapped in a double-well potential, *Physical Review A* **78** 023611 (2008).

[201] T. Koma and H. Tasaki: Symmetry breaking and finite-size effects in quantum many-body systems, *Journal of Statistical Physics* **76** 745 (1994).

[202] E. Yukawa, G. J. Milburn, and K. Nemoto: Fast macroscopic-superposition-state generation by coherent driving, *Physical Review A* **97** 013820 (2018).

[203] S. Campbell, G. De Chiara, M. Paternostro, G. M. Palma, and R. Fazio: Shortcut to Adiabaticity in the Lipkin-Meshkov-Glick Model, *Physical Review Letters* **114** 177206 (2015).

[204] M. Kitagawa and M. Ueda: Squeezed spin states, *Physical Review A* **47** 5138 (1993).

[205] R. H. Dicke: Coherence in Spontaneous Radiation Processes, *Physical Review* **93** 99 (1954).

[206] M. J. Holland and K. Burnett: Interferometric detection of optical phase shifts at the Heisenberg limit, *Physical Review Letters* **71** 1355 (1993).

[207] B. C. Sanders and G. J. Milburn: Optimal Quantum Measurements for Phase Estimation, *Physical Review Letters* **75** 2944 (1995).

[208] R. W. Spekkens and J. E. Sipe: Spatial fragmentation of a Bose-Einstein condensate in a double-well potential, *Physical Review A* **59** 3868 (1999).

[209] K. Pawłowski, M. Fadel, P. Treutlein, Y. Castin, and A. Sinatra: Mesoscopic quantum superpositions in bimodal Bose-Einstein condensates: Decoherence and strategies to counteract it, *Physical Review A* **95** 063609 (2017).

[210] H. Nishimori and G. Ortiz: *Elements of phase transitions and critical phenomena* (Oxford University Press, 2015).

[211] H. Rieger: Frustrated systems: Ground state properties via combinatorial optimization, In J. Kertész and I. Kondor (eds), *Advances in Computer Simulation*, pp. 122–158 (Springer Berlin Heidelberg, 1998).